Chemical Engineering Journal 532 (2026) 174189

Contents lists available at ScienceDirect

Chemical Engineering Journal

journal homepage: www.elsevier.com/locate/cej

Toward the efficient utilization of solar energy for hydrogen production through photocatalytic reforming: A literature and patent review☆

Marica Muscetta [a,*], Hebah S. Jarusheh [b], Gareth Williams [c], Kazi M. Alam [d], Karthik Shankar [d], Giovanni Palmisano [b], Sergio Vernuccio [e,*]

[a] Dipartimento di Ingegneria Chimica, dei Materiali e della Produzione Industriale, Università di Napoli Federico II, Napoli, Italy
[b] Department of Chemical and Petroleum Engineering, Research and Innovation Center on CO_2 and H_2, Khalifa University of Science and Technology, P.O. Box 127788, Abu Dhabi, United Arab Emirates
[c] School of Mathematical and Physical Sciences, University of Sheffield, United Kingdom
[d] Department of Electrical and Computer Engineering, University of Alberta, Edmonton, AB, T6G 1H9, Canada
[e] School of Chemistry and Chemical Engineering, University of Southampton, United Kingdom

ARTICLE INFO

Keywords:
Advanced oxidation processes
Photocatalysis
Photoreforming
Hydrogen
Wastewater
Photocatalytic reactors

ABSTRACT

The increasing global energy demand and urgent need to curb greenhouse gas emissions have intensified efforts to develop solar-driven hydrogen production technologies. Photocatalytic reforming of organic substrates – including biomass-derived compounds, organic species, and wastewater – has emerged as a promising route capable of simultaneously generating hydrogen and degrading pollutants. Recent advances have led to substantial improvements in photocatalyst performance, with reported hydrogen evolution rates ranging from below 1 mmol/g_{cat}·h for non-metal-doped semiconductors to over 50 mmol/g_{cat}·h for optimized dye-sensitized and heterojunction systems, and up to 112 mmol/g_{cat}·h for functionalized COF nanosheets. Apparent quantum yields span a similar breadth, from modest values below 1% to over 80% in state-of-the-art organic frameworks. Wastewater valorization studies demonstrate both environmental and energetic benefits, achieving hydrogen productivities up to 6.5 mmol/L in solar pilot plants and pollutant removal efficiencies exceeding 90% for dyes and pharmaceuticals. Techno-economic analyses indicate that integrated hydrogen–wastewater systems can reduce levelized hydrogen costs, with some configurations achieving internal rates of return above 10% and hydrogen yields approaching 800 L H_2 per kg of organic removed. This review integrates scientific literature with international patent trends, providing a unified assessment of photocatalyst development, sacrificial agent strategies, and photoreactor design innovations. Building on these insights, the review delineates a forward-looking roadmap that prioritizes photocatalyst performance, wastewater matrices, scalable reactor architectures, and techno-economic integration as key research and engineering directions required to translate photocatalytic reforming from laboratory studies to commercially viable, large-scale hydrogen production.

1. Introduction and general overview of the published material

As a direct consequence of global population growth and industrialization, recent decades have witnessed an unprecedented increase in energy consumption [1,2]. Despite their depletion, fossil fuels continue to lead global energy supply as the most widely employed energy sources, producing greenhouse gases such as carbon dioxide and nitrous oxide [3]. Furthermore, fossil fuels are expected to dominate the energy sector at least until 2050, due to an increase in global energy demand of 1.3% to 2040 [4]. To meet the United Nations Net-Zero goal by 2050, research and development efforts should focus on the advancement of clean technologies for energy production from renewable sources, addressing both environmental concerns and the global energy crisis [5,6].

Hydrogen is considered one of the most promising alternative energy sources, due to its significantly higher gravimetric energy density (albeit with a low volumetric energy density) at room temperature – approximately three times that of gasoline – and its high-octane number (> 130) [7,8]. Moreover, H_2-based energy is increasingly recognized as a clean alternative to carbon-based fuels, since its direct combustion emits

☆ This article is part of a Special issue entitled: 'EAAOP-7' published in Chemical Engineering Journal.

* Corresponding authors.
E-mail addresses: marica.muscetta@unina.it (M. Muscetta), s.vernuccio@soton.ac.uk (S. Vernuccio).

https://doi.org/10.1016/j.cej.2026.174189
Received 19 November 2025; Received in revised form 27 January 2026; Accepted 13 February 2026
Available online 15 February 2026

neither greenhouse gases nor air pollutants [9]. Currently, approximately 50% of global H_2 production is derived from steam reforming of natural gas (predominantly methane [10]), by far the dominant method for large-scale hydrogen generation worldwide. Steam reforming requires high temperatures and moderate pressures and is therefore energy intensive. Methane pyrolysis has emerged as a low carbon emission technology to produce large quantities of hydrogen from natural gas, yet the technology is still relatively new, and its advantages and limitations are not yet fully understood [11,12]. However, due to the recent development of hydrogen fuel cells, which are an essential component of the transition to clean energy, there has been an increase in the yearly demand for hydrogen gas as an alternative fuel [9]. Recent research has focused on developing environmentally friendly and pollution-free hydrogen from renewables such as biomass, solar, and wind energy [13–15]. Given the geographical limitations of geothermal energy and the inconsistent availability of biomass, solar power is considered to have the greatest potential among renewable energy sources [16]. Over recent decades, multiple solar-driven hydrogen production technologies have been developed, each characterized by distinct operating principles, maturity levels, and technological challenges. These approaches can be broadly classified into: (1) photocatalytic and photoelectrochemical (PEC) water splitting, where semiconductor materials directly convert solar energy into chemical energy; (2) photovoltaic-electrochemical water splitting, which couple solar electricity generation with conventional electrolysis; (3) solar thermochemical water splitting, based on high-temperature redox cycles; (4) photothermal catalytic processes that exploit solar heat and light synergistically; and (5) photobiological H_2 generation using microorganism and enzymatic reaction pathways [17–21].

Among these technologies, water electrolysis powered by renewable electricity is currently the most technologically mature, with several commercial electrolyzers suitable for large-scale applications. The rapid maturation of photovoltaic technologies over the past two decades, characterized by improved efficiencies, and long-term operational stability, has positioned photovoltaic-electrochemical water splitting as the most commercially advanced solar-driven hydrogen production technology to date. Nevertheless, the widespread adoption of electrolysis remains limited by high capital costs and energy efficiency constraints, highlighting the need for further reduction in electricity consumption and system costs [22–24]. In contrast, direct solar-driven routes – particularly photocatalytic and PEC processes – offer the conceptual advantage of bypassing intermediate electrical conversion step, potentially enabling simpler and more cost-effective systems.

In 1972, Fujishima and Honda reported the first heterogeneous photocatalytic H_2 production through water splitting (see Fig. 1). Heterogeneous photocatalysis utilizes a semiconductor as a catalyst and light harvester. Five years later, Krich et al. (1979) published the first homogeneous photocatalytic H_2 production using triethanolamine (TEOA) [25]. In this sense, photocatalytic generation of H_2 from organic solutions provides a complementary and renewable approach for simultaneous H_2 production and wastewater remediation.

Photocatalytic transformations typically involve several elementary steps, beginning with the absorption of photons by the photocatalyst. When the photon has sufficient energy to bridge the band gap of the material, valence band electrons can be transported to the conduction band resulting in the generation of electron-hole pairs. These mobile electrons and holes carry negative and positive charges and can participate in redox reactions.

However, practical difficulties arise in accurately determining the number of absorbed photons or reacted electrons due to the scattering and reflection of light. To address this, the use of the term "apparent quantum yield" (AQY) is recommended by IUPAC, calculated as follows Eq. (1):

$$AQY = \frac{Number\ of\ H_2\ molecules\ released}{Number\ of\ incident\ photons} \quad (1)$$

A more precise measure of the potential of a photocatalytic system is the Solar-to-Hydrogen (STH) conversion efficiency, which can be calculated using Eq. (2):

$$STH\ (\%) = \frac{Energy\ of\ generated\ H_2}{Energy\ of\ incident\ solar\ light} \bullet 100 \quad (2)$$

As evidence of the growing attention toward photocatalytic hydrogen production, Fig. 2 (a) shows the percentage of scientific documents containing the string "photocatal* hydrogen production" over the total number of papers including the string "photocatal*" in the title, according to Web of Science. The asterisks represent any group of characters that might follow "photocatal" e.g. "ysis", "yst", and are used to broaden the search. The figure illustrates that over 25% of the scientific literature in the broad field of photocatalysis is currently focused on hydrogen production as a specific application.

Numerous recent review articles [26–40] have addressed hydrogen production via photocatalytic reforming, highlighting substantial progress in catalyst design and reaction engineering. In particular, Toe et al. have reviewed the strategies used to improve the selectivity of photoreforming of organic waste into high-value chemicals and deliver highly selective photocatalysts [26]. Chang et al. have recently reviewed

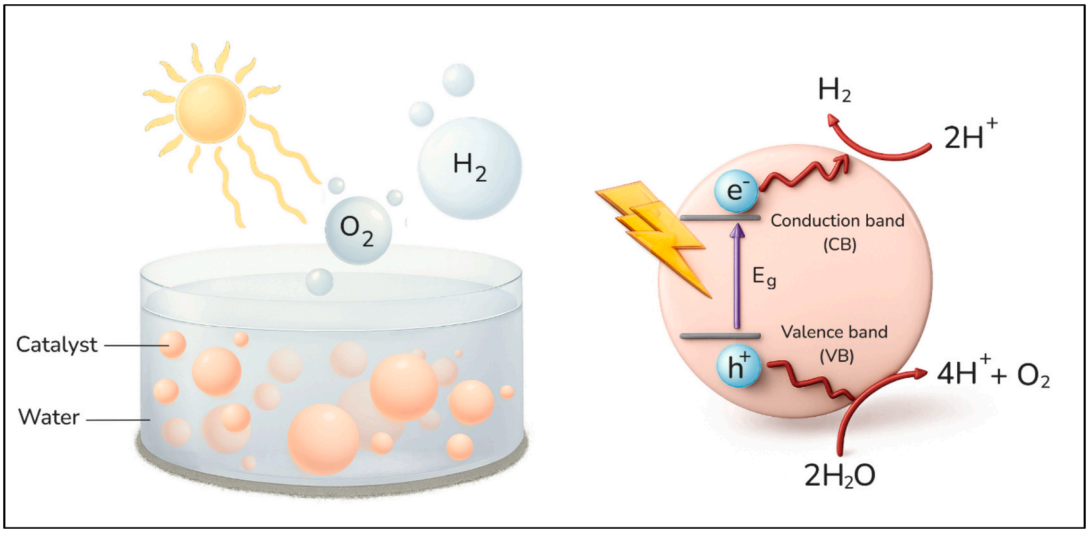

Fig. 1. Schematic illustration of photocatalytic H_2 production process and mechanism of photocatalytic water splitting.

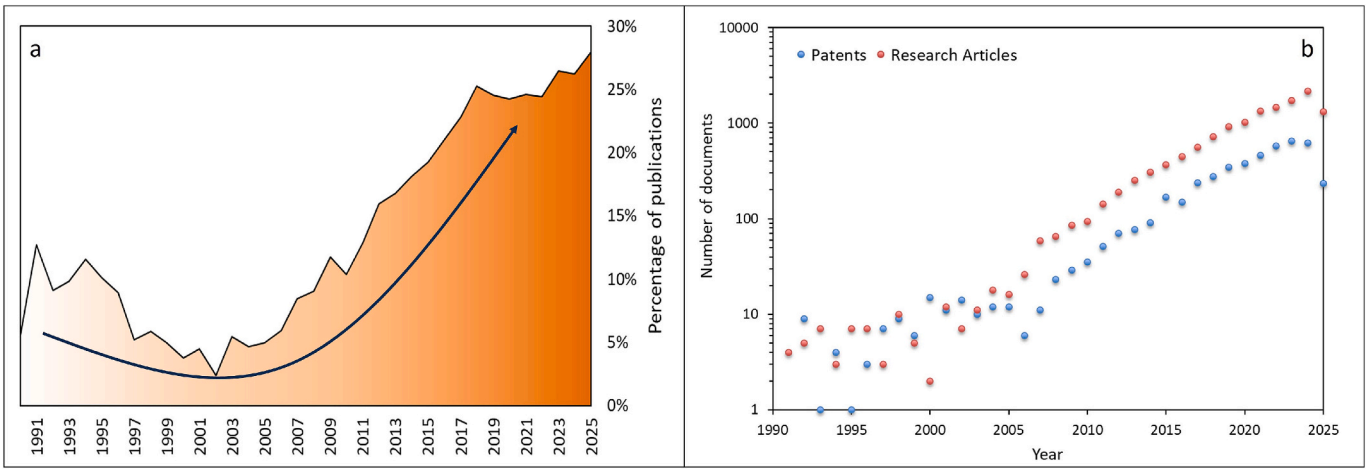

Fig. 2. (a) Trend of scientific publications on photocatalytic hydrogen production as a portion of total publications on photocatalysis (1990–2025) according to Web of Science. (b) Annual trend in scientific publications and technological patents (1990–2025).

the different photocatalytic materials used for methanol photoreforming from the perspective of the reaction mechanism [27]. Li et al. provided a detailed review of S-scheme heterojunction photocatalysts for hydrogen production [28]. The literature presents review articles concentrating on the use of specific sacrificial agents in photoreforming processes, such as biomass-derived feedstocks [29–33], lignocellulosic biomass [34], and waste polymers [35]. Additionally, several review papers have explored specific photocatalytic systems and architectures, including hierarchically porous photocatalysts [36], plasmonic nanocatalysts [37], carbon nitride-based materials [38], and organic-inorganic hybrid photocatalysts [39]. Several investigations have examined the role of tailored sacrificial agents in photocatalytic reforming, with particular attention to biomass-derived substrates [30–34], lignocellulosic resources [35], and waste polymer streams [36]. These studies collectively highlight photocatalytic reforming as a promising platform for converting waste materials into hydrogen and value-added chemicals, in line with circular economy principles. Nevertheless, a comprehensive evaluation of scalability and real-world applicability remains largely absent from the existing literature findings. A very recent review highlighted the key technical and economic challenges hindering large-scale implementation and discussed emerging strategies to improve efficiency, stability, and cost-effectiveness for practical deployment; the authors observed critical challenges in photocatalyst durability under prolonged and realistic operating conditions, consistency of catalytic performance upon scale-up, solar-to-hydrogen conversion efficiency under outdoor irradiation, and the design of scalable, cost-effective photocatalytic reactors [40,41]. Recent efforts aimed at advancing practical implementation have focused on the development of chemically and photochemically stable, low-cost photocatalysts, and the adoption of immobilized catalyst configurations and continuous-flow reactor concepts to facilitate catalyst handling and enhance scalability. A rigorous and critical analysis of these factors is crucial to narrow the gap between proof-of-concept studies and industrially relevant applications and to realistically assess the potential of photocatalytic reforming as a viable and sustainable route for hydrogen production.

While the existing body of reviews in the literature provides valuable insight into hydrogen production from photoreforming, a critical gap remains in addressing the barrier that hinders the industrial-scale implementation of these technologies. Beyond the academic domain, patents serve as a critical indicator of technological maturity and commercial potential. In these regards, Fig. 2 **(b)** presents a comparative temporal analysis of the annual number of patents filed and research articles published annually in the field of photocatalytic hydrogen production between 1990 and 2025. Patent data and research article data were obtained from Espacenet and from Web of Science, respectively, using the search string "photocat* hydrogen production" applied to titles or abstracts. Both datasets reveal a clear upward trajectory, with exponential growth observed from 2005 onward. The parallel growth of these two indicators underscores the dynamic interplay between scientific discovery and innovation, highlighting how fundamental research is increasingly driving the development of practical solutions for sustainable hydrogen production. While the existing body of reviews in the literature provides valuable insight into hydrogen production from photoreforming, a critical gap remains in addressing the barrier that hinders the industrial-scale implementation of these technologies.

This review article aims to bridge the gap between academic research and technological innovation by integrating a critical analysis of both the scientific literature and patent landscape, focusing on assessing the efficiency of photoreforming technologies in the context of hydrogen production. To our knowledge, only one review paper since 2014 has systematically analysed patent literature in the field [42].

This work will specifically target (i) the hydrogen evolution reaction (HER), (ii) the solar-to-hydrogen (STH) energy efficiency, and (iii) the apparent quantum yield (AQY). Firstly, the most relevant photocatalytic materials, as reported in both scientific literature and patent applications, are described in detail in Section 2. Section 3 addresses the most commonly employed sacrificial agents, with a focus on both mechanistic roles and economic considerations. Finally, Sections 4 and 5 provide an overview of the latest development in reactor configurations and associated challenges.

Through this integrated approach, we aim to provide a holistic overview of the current state of photocatalytic hydrogen production and offer actionable insights that can inform future research directions and accelerate the development of scalable and industrially viable photocatalytic systems.

2. Review of photocatalytic materials

This section provides a detailed review of recent developments in the design and synthesis of photocatalytic materials for hydrogen production. Table 1 and Table 2 summarise key findings from recent (2023 onward) literature and patent applications, respectively. This extensive survey of the field indicates that detailed, quantitative comparisons across studies remain challenging due to substantial variations in the experimental conditions, including light sources, sacrificial agents, catalyst loading and reactor configuration. It is worth noting that the purpose of this data collection is not to establish a direct performance ranking among distinct research efforts, but rather to provide a comprehensive and timely overview of recent academic literature. The routine reporting of efficiency metrics, such as AQY and STH efficiency,

Table 1
Summary of the recent academic literature on photocatalytic H_2 production from photoreforming of organics published between 2023 and 2025.

Academic Literature										
Material	Preparation method	Reactor Configuration	Sacrificial agent/ scavenger	Radiation	STH*	AQY*	HER*	Stability/ Reusability	Ref	Year
AuPd/ TiO_2	Anodization and vapor deposition method	Cylindrical reactor with a quartz glass window system	Triethanolamine	AM 1.5G Simulated Sunlight	Not reported	Not reported	2.92 mmol/ g_{cat}·h	Good stability within 4 cycles	[49]	2025
C_3N_4/TiO_2	Polymerization, sol-gel and photo-anchoring methods	Custom-made quartz reactor	Triethanolamine	250 W visible light	Not reported	Not reported	0.692 mmol/ g_{cat}·h	Not reported	[199]	2023
Pt-PCN	Not reported	Loop photoreactor	Methanol	365 nm LEDs	Not reported	0.75%	4.188 mmol/ g_{cat}·h	Stable for 70 h	[321]	2024
Ag-La-$CaTiO_3$	Sol-gel	Lab-made closed gas system	None	1200 W metal halide lamp	Not reported	Not reported	2.974 mmol/ g_{cat}·h	Stable for 30 h (10 cycles)	[322]	2024
AuNP@ CoTPyP	Physical mixing	Lab-made reactor	Methanol	300 W Xe lamp	Not reported	Not reported	3.21 mmol/ g_{cat}·h	Stable for 45 h (15 cycles)	[323]	2023
ZnS/CdS	Wet-chemical procedure and physically mixing	Pyrex glass reactor	Na_2S and Na_2SO_3	300 W Xe lamp	Not reported	60%	29 mmol/ g_{cat}·h	Good stability within 5 cycles	[324]	2023
Pt/TiO_2	Chemical reduction	Lateral irradiated stirred tank reactor in batch mode	Acetic acid, butyric acid, ethanol and buthanol	30 W LED (365 nm, 150 W/m^2)	Not reported	Not reported	0.445 mmol/ g_{cat}·h	Decreased hydrogen generation after the 1st cycle	[325]	2025
SiC-g-C_3N_4	Thermal synthesis via urea decomposition	Home-made Pyrex jacketed reactor	Polyethylene, terephthalate and bisphenol A	300 W solar lamp 10.7 mW/cm^2	Not reported	Not reported	0.018 mmol/ g_{cat}·h	Not reported	[326]	2025
Pt-CdS/TiO_2/ biochar	Low temperature solvothermal synthesis	Airtight pyrex container	Acetonitrile with Na_2CO_3 or NaOH	300 W xenon lamp	Not reported	Not reported	12.77 mmol/ g_{cat}·h	Good stability within 5 cycles	[327]	2024
Cu_2O-TiO_2	Ball milling	Compound Parabolic Collector photoreactor	Glycerol, ethanol and glucose	Solar radiation	1.71%	Not reported	188 mmol/ g_{cat}·h	Not reported	[328]	2025
CuNi/TiO_2	Photodeposition	Side-illuminated slurry reactor	Cellulose	0.49 W UV LED (365 nm)	Not reported	Not reported	0.489 mmol/ g_{cat}·h	Not reported	[329]	2025
Pt/TiO_2	Hydrothermal method and photodeposition of Pt	Gas-tight quartz reactor	Glucose or wastewater samples	AM 1.5G Xe lamp (1000 mW/cm^2)	Not reported	Not reported	4.5 mmol/ g_{cat}·h	Not reported	[330]	2025
Au/TiO_2	Photodeposition from waste derived Au	Annular glass batch reactor	Formic acid	125 W Hg lamp	Not reported	11.34% at 420 nm	3.61 mmol/ g_{cat}·h	Good stability within 4 cycles	[331]	2025
PtO_2/TiO_2	Ball milling	Annular glass batch reactor	Methanol	400 W Hg lamp	15.6%	38% in the UV-A range	54 mmol/ g_{cat}·h	Good stability within 4 cycles	[100]	2025
Carbon dots/TiO_2	Microwave-assisted synthesis and hydrothermal method	Cylindrical pyrex reactor	Ethanol, glycerol	300 W xenon lamp	Not reported	Not reported	0.51 mmol/ g_{cat}·h	Good stability within 3 cycles	[332]	2024
Pt-g-C_3N_4-TiO_2	Impregnation - calcination	Penn photoreactor	Triethanolamine, Glycerol, Glyceraldehyde and Dihydroxyacetone	LED (λ = 365 nm, 213 mW/cm^2 and λ = 450 nm, 325 mW/ cm^2)	Not reported	Not reported	13.2 mmol/ g_{cat}·h	Not reported	[333]	2024
CuO/TiO_2	Mechanical mixing - calcination	Compound Parabolic Collector photoreactor	Glycerol	Solar radiation, Q_{UV} 47 kJ/L	1.42%	Not reported	118.94 mmol/ g_{cat}·h	Not reported	[334]	2024
g-C_3N_4/CdS/NiS	Hydrothermal synthesis	Batch reactor	Polylactic acid	300 W xenon lamp	Not reported	Not reported	30.44 mmol/ g_{cat}·h	Decreased productivity during the first 5 h of irradiation	[335]	2024
$ReS_2/ZnIn_2S_4$	Solvothermal method	LabSolar-6A	Furfural alcohol	300 W xenon lamp	Not reported	1.8% at 420 nm	1.08 mmol/ g_{cat}·h	Good stability within 4 cycles	[336]	2023

(*continued on next page*)

Table 1 (*continued*)

Academic Literature									
Material	Preparation method	Reactor Configuration	Sacrificial agent/ scavenger	Radiation	STH*	AQY*	HER*	Stability/ Reusability	Ref	Year
$Co_3O_4/ZnIn_2S_4$	Wet chemistry approaches in conventional oven (Co_3O_4) and oil bath heating (composite)	LabSolar-6A	Triethanolamine	300 W xenon lamp (> 400 nm)	Not reported	8.51% at 438 nm	3.84 mmol/ g_{cat}·h	Good stability within 4 cycles	[97]	2023
Cu_7S_4/ $Zn_{0.2}Cd_{0.8}S$	Combination of solvothermal and co-precipitation methods	Quartz reactor with a top exposure	Na_2S (0.1 mol/L) and Na_2SO_3 (0.1 mol/L)	300 W xenon lamp (> 420 nm)	Not reported	6.7% at 440 nm	2.57 mmol/ g_{cat}·h	Good stability within 4 cycles	[95]	2023
Pt/PM6:ITCC-M: IDMIC-4F	Microemulsion with amphiphilic surfactant	LabSolar-6A	0.2 M Ascorbic acid	300 W xenon lamp (320 - 780 nm	Not reported	5.9% at 600 nm	307.0 mmol/ g_{cat}·h	Good stability within 4 cycles	[337]	2023
Au/TiO_2	Deposition-precipitation method in the presence of urea for Au deposition on TiO_2	Glass reactor with inlet and outlet for purging gas and collecting gaseous products	10% v/v glycerol as an electron donor	300 W Xenon lamp	Not reported	26.7% at 365 nm	14.695 mmol/ g_{cat}·h	Good stability for up to 8 h	[128]	2023
Cu/CeO_2	Hydrothermal (CeO_2) and precipitation-deposition of Cu	Quartz tube reactor	Methanol (50% *v*/ v)	Xenon lamp (Microsolar 300, Simulated Sunlight)	Not reported	Not reported	36 mL/ g_{cat}·min	Good stability for up to 12 h	[143]	2023
$Ag\text{-}Fe/TiO_2$	Sol-gel method	Pyrex glass reactor	Ethanol (50% v/v)	300 W Xenon lamp (visible light)	Not reported	Not reported	2.38 mmol/ g_{cat}·h	Not reported	[134]	2023
Au/Carbon dots/ CdS	Hydrothermal method for carbon dots and CdS	Quartz reactor	Na_2S (0.35 M) and Na_2SO_3 (0.25 M)	300 W xenon lamp (> 395 nm)	Not reported	Not reported	0.646 mmol/ g_{cat}·h	Good stability for up to 2 h	[129]	2023
$Au/SrTiO_3/TiO_2$	Combination of hydrothermal, etching and calcination methods for $SrTiO_3$ and TiO_2	Pyrex reactor	Methanol (10% v/ v)	300 W xenon lamp	Not reported	Not reported	0.328 mmol/ g_{cat}·h	Good stability within 4 cycles	[130]	2023
Au/ZnO/CuO	Sol-gel method	N_2-filled vessel	Glycerol (10% v/v)	300 W xenon lamp (> 400 nm)	Not reported	Not reported	4.65 mmol/ g_{cat}·h	Good stability within 5 cycles	[131]	2023
Cu/TiO_2 artificial olive leaf (Cu-AOL)	Ion exchange, calcination	8.5 mL cylindrical reactor	Glycerol (10% v/v)	150 W Xe lamp Newport solar simulator	Not reported	Not reported	3.56 mmol/ g_{cat}·h	Not investigated	[58]	2023
Pt@BIT-108(Fe)	Solvothermal method	20 mL reactor	1, 3-dimethyl-1, 3-dihydro-2-phenyl-2H-benzimidazole	Xe lamp (λ > 420 nm) 100 mW/cm^2	Not reported	Not reported	0.32 mmol/ g_{cat}·h	No decreased activity after 3 cycles (3 h each)	[338]	2023
Pt@TMF-Pt	In-situ partial hydrogenation	100 mL quartz window sealed with Pyrex reactor	Ascorbic acid (1 M)	300 W Xe lamp (λ > 420 nm)	Not reported	Not reported	33.18 mmol/ g_{cat}·h	No decreased activity after 3 cycles (5 h each)	[339]	2023
Co–TCPP(Pd)	Solvothermal method	100 mL optical reaction vessel	Ascorbic acid (1 M)	300 W Xe lamp (λ > 420 nm)	Not reported	3.79% (420 nm)	4.4 mmol/ g_{cat}·h	Slight decrease after 3 cycles	[340]	2023
$Pt@NH_2\text{-}MIL\text{-}125$	Solvothermal method	Reaction vessel with Pyrex top-irradiation type	TEOA (15% v/v)	300 W Xe lamp (λ > 420 nm)	Not reported	4.0% (420 nm)	2.64 mmol/ g_{cat}·h	No decreased activity after 3 cycles (3 h each)	[341]	2023
Au@PCN(Co)70	Solvothermal method	Quartz-type photoreactor	TEOA (10% v/v)	Solar simulator (150 mW/ cm2)	Not reported	1.7% (420 nm)	1.015 mmol/ g_{cat}·h	No decreased activity after 4 cycles	[221]	2023
$[Mo_3S_{13}]^{-2}$@ZnP-Pz-PEO-COF	Solvothermal method	Quartz flask	Lactic acid (15% v/ v)	300 W Xe lamp (λ > 420 nm)	Not reported	3.6% (600 nm)	11 mmol/ g_{cat}·h	No decreased activity after 6 cycles (2 h each)	[342]	2023
Co/Zn-Salen-COF	Precipitation and metalation	Pyrex top irradiated vessel	Ascorbic acid (5 mM)	300 W Xe lamp (λ > 420 nm)	Not reported	Not reported	1.378 mmol/ g_{cat}·h	Not investigated	[343]	2023
Pt@Ni-COF-SCAU-1	Solvothermal method	250 mL pyrex top-irradiated reaction cell	Ascorbic acid (0.1 M)	350 W Xe lamp (λ > 420 nm)	Not reported	43.2% (420 nm)	197.46 mmol/ g_{cat}·h	No decreased activity after 5 cycles (6 h each)	[344]	2023

(*continued on next page*)

Table 1 (*continued*)

Academic Literature									
Material	Preparation method	Reactor Configuration	Sacrificial agent/ scavenger	Radiation	STH*	AQY*	HER*	Stability/ Reusability	Ref	Year
Pt@COF-JLU35	Gradient heating method	Standard photocatalytic reactor	Ascorbic acid (0.1 M)	300 W Xe lamp (λ > 420 nm)	Not reported	3.21% (500 nm)	70.8 mmol/ g_{cat}·h	No decreased activity after 5 cycles (4 h each)	[345]	2023
TpBD COF@ZIS-10	Microwave-hydrothermal method	On-line trace gas analysis photoreaction device	Ascorbic acid (0.05 M)	300 W Xe lamp (λ > 420 nm)	Not reported	5.02% (420 nm)	2.3 mmol/ g_{cat}·h	No decreased activity after 8 cycles (3 h each)	[346]	2023
Cyano-functionalized polymers	Suzuki–Miyaura or Stille cross-coupling reactions	Pyrex top-irradiation reaction vessel	TEOA (25% v/v)	300 W Xe lamp (λ > 420 nm)	Not reported	8.4% (420 nm)	16.7 mmol/ g_{cat}·h	No decreased activity after 5 cycles (5 h each)	[347]	2023
5.5% Ti_3C_2/ graphitic carbon nitride (PGCN)	Self-assembly method	Quartz glass reactor with a side illuminated window	10% TEOA	300 W Xe lamp	Not reported	Not reported	4.095 mmol/ g_{cat}·h	After 3 cycles, there was no significant decline observed in the rate of hydrogen production of 5.5 wt% Ti_3C_2/ (PGCN)	[179]	2023
Ti_3C_2	Etching and delaminating method (LiF-HCl)	Closed vessel with a gas circulation system	0.35 M Na_2S 0.25 Na_2SO_3	300 W Xe lamp	1.3%	Not reported	0.763 mmol/ g_{cat}·h	Across five cycles, CdSe@10wt% Ti_3C_2 demonstrated consistent high photocatalytic activity	[348]	2023
$Mn_{0.25}Cd_{0.75}S$/ 100mg g-C_3N_4	Calcination and hydrothermal methods	Quartz reactor	0.35 M Na_2SO_3/ 0.25 M Na_2S	300 W Xe lamp	Not reported	Not reported	21.53 mmol/ g_{cat}·h	After 4 coonsecutive cycles, the hydrogen production rate of $Mn_{0.25}Cd_{0.75}S$/ 100mg g-C_3N_4 exhibited a decrease of 12%	[349]	2023
$CoMoO_4$/g-C_3N_4/ Sulfur Coal-based carbon QDS	Hydrothermal method	65 mL quartz reactor	10% TEOA	5 W LED lamp	1.78% (420 nm)	Not reported	4.92 mmol/ g_{cat}·h	After 4 consecutive hydrogen evolution cycles, $CoMoO_4$/g-C_3N_4/ 8%SQDS maintained its stability	[162]	2023
1% Pt 50% NH_4I 50% melamine *g-C_3N_4*	Hydrothermal and calcination methods	Batch reactor	10% triethanolamine, 0.1 M NaOH	425 LED lamp	Not reported	Not reported	2.12 mmol/ g_{cat}·h	After 4 consecutive runs, the hydrogen production rate declined by 62%	[161]	2023
15% V_2C/g-C_3N_4	Physical mixing method	150 mL slurry photocatalytic reactor	5% methanol/ triethanolamine (TEOA)	35 W Xe lamp	Not reported	Not reported	0.36 mmol/ g_{cat}·h	The photostability was poor in the water-methanol mixture (5 cycles) while it showed high stability in the water-TEOA mixture after 4 consecutive cycles.	[160]	2023
$Cd_{0.9}Zn_{0.1}S$/5% Ti_3C_2	Hydrothermal method	–	20% TEOA	300 W Xe lamp with an AM-1.5 filter	2.98% at 370 nm 0.81% at 456 nm	Not reported	4.5 mmol/ g_{cat}·h	After 4 cycles, a notable decline can be detected for $Cd_{0.9}Zn_{0.1}S$/ Ti_3C_2,	[178]	2023

*STH: Solar to hydrogen efficiency; AQY: Apparent quantum yield; HER: Hydrogen evolution reaction.

in addition to HER, could represent an important step toward improved standardization. However, as shown in Tables 1 and 2, these metrics are still not consistently reported in photocatalysis literature. This limitation underscores the continued need for greater standardization in the evaluation and reporting of photocatalytic performance.

2.1. Inorganic semiconductors

Intrinsic semiconducting materials exhibit conductive properties only when they are either sufficiently doped (to be n-type or p-type) or sufficient energy is supplied to excite electrons from the valence band (VB) to the conduction band (CB). As such, semiconductors possess a

Table 2
Summary of some photocatalysts used for hydrogen production and some novel photocatalysts patented between 2022 and 2025. STH was excluded from the table being not reported in the patents.

Patents										
Material	Preparation method	Reactor Config.	Sacrificial agent	Radiation	AQY*	HER*	Stability/ Reusability	Country	Ref	Year
$Ti_3C_2T_x$/CdS	Hydrothermal method	Not reported	Lactic acid/ cellulose	300 W Hg lamp	Not reported	7.562 mmol/ g_{cat}·h	Not reported	China CN118894490A	[186]	2024
$Ti_3C_2T_x$/CdS	Hydrothermal method	Not reported	Biomass	300 W Hg lamp	Not reported	20.427 mmol/ g_{cat}·h	Not reported	China CN118904373A	[187]	2024
Rh-Cr co-catalyst loaded Al-doped $SrTiO_3$ /TiO_2	Calcination and physical mixing methods	Reactor tank	None	300 W Xe lamp	Not reported	24 mmol/ g_{cat}·h	Not reported	China CN120054530A	[57]	2025
TiO_2/$ReS_{1.2}Se_{0.8}$	Calcination and photodeposition method	Not reported	Ethanol	300 W Xe lamp	Not reported	1.0175 mmol/ g_{cat}·h	Good stability for 4 cycles (2 h each)	China CN120243064A	[99]	2025
Cu-TiO_2	Pyrolysis treatment	Not reported	Methanol	300 W Xe lamp	Not reported	0.308 mmol/ g_{cat}·h	Not reported	China CN119386866A	[61]	2025
Bi_2WO_6-TiO_2	Sol-gel and hydrothermal method	Photocatalytic reaction device	None	300 W Xe lamp	Not reported	0.00248 mmol/ g_{cat}·h	Not reported	China CN116920823B	[98]	2023
$MoSe_2$/$MAPbBr_3$	Hydrothermal method	Not reported	HI	300 W Xe lamp	Not reported	1.7475 mmol/ g_{cat}·h	Good stability for 6 cycles (4 h each)	China CN116216633A	[350]	2023
Triphenilphosphine Ruthenium complex with graphitic carbon nitride	Room temperature suspension	Flat wall photoreactor	Methanol (5% v/v)	35 W Visible light (20 mW/cm^2)	5.18%	1.77 mmol/ g_{cat}·h	Not reported	US US12233403B1	[145]	2025
3D graphene/MXene	Hydrothermal method	Not reported	None	Xe lamp (200-1000 nm)	Not reported	1.30 mmol/ g_{cat}·h	71% after 5 cycles	China CN119303603A	[351]	2025
BN/CdS	Hydrothermal method	Reaction tank	TEOA (16% v/ v)	Xe lamp (simulated sunlight)	Not reported	0.26 mmol/ g_{cat}·h	Not reported	China CN119733542A	[352]	2025
5% LDH/$Cd_{0.5}Zn_{0.5}S$	Hydrothermal method	Sealed glass circulation system	Polyethylene terephthalate	300 W Xe lamp (λ > 420 nm)	Not reported	3.67 mmol/ g_{cat}·h	Not reported	China CN119771447A	[353]	2025
CdS@MoS_2	Hydrothermal method	Not reported	Sucrose (2 g in 100 mL NaOH aqueous solution)	Not reported	Not reported	0.39 mmol/ g_{cat}·h	Not reported	China CN119327487A	[354]	2025
Indium zinc sulfide-based composite catalyst	Hydrothermal method	Sealed reaction tank	TEOA (16% v/ v)	Xe lamp	Not reported	4.23 mmol/ g_{cat}·h	Not reported	China CN119733531A	[355]	2025
MoO_3/CuO	Hydrothermal method	Not reported	Ascorbic acid (55 mmol/L)	Xe lamp (λ > 420 nm)	Not reported	0.099 mmol/ g_{cat}·h	Not reported	China CN117463354A	[356]	2024
CdS-Ru	Hydrothermal method	Not reported	Lactic acid/ cellulose	Xe lamp (L40 filter)	Not reported	0.82 mmol/ g_{cat}·h	No decreased activity after 5 cycles (4 h each)	China CN118002153A	[357]	2024
NiS@MOF-808	Hydrothermal method	Reaction flask	TEOA/water (3:17 mol)	300 W Xe lamp (Intensity 21-23 A)	Not reported	8 mmol/ g_{cat}·h	Not reported	China CN117427690A	[358]	2024
N-doper ZnO/ Cu@CdZnS heterojunction	Hydrothermal method	Photoreactor	Na_2S/Na_2SO_3	300 W Xe lamp (180 mW/cm^2)	Not reported	8.78 mmol/ g_{cat}·h	No decreased activity after 4 cycles (4 h each)	China CN118807814A	[359]	2024
NH_2-MIL-125 ternary composite	Hydrothermal method	100 mL quartz reactor	TEA (2% v/v)	300 W Xe lamp (λ > 400 nm)	Not reported	0.070 mmol/ g_{cat}·h	Not reported	China CN116425996A	[360]	2023
MOF TiO_2-NiO material	Room temperature precipitation	Quartz reactor	Methanol 20% v/v	Not reported	Not reported	1.39 mmol/ g_{cat}·h	Not reported	China CN114950439A	[361]	2022
MIL-68 (In)	Vulcanization/ pyrolysis	Pyrex top irradiated vessel	Methanol/ Water (1:1-3 mol)	300 W Xe lamp	Not reported	215 mmol/ g_{cat}·h	Not reported	China CN117065767A	[362]	2023
Pt@TpPa-1-COF	Solid phase synthesis	150 mL jacketed beaker	Sodium ascorbate	300 W Xe lamp (λ > 420 nm) 265 W/ cm2	Not reported	0.719 mmol/ g_{cat}·h	Not reported	China CN114534783A	[363]	2022

(*continued on next page*)

Table 2 (*continued*)

Patents										
Material	Preparation method	Reactor Config.	Sacrificial agent	Radiation	AQY*	HER*	Stability/ Reusability	Country	Ref	Year
Pyrenyl COF	Schiff base condensation	Standard reactor	Ascorbic acid (0.1 M)	Xe lamp (λ > 420 nm)	Not reported	18.6 mmol/g_{cat}·h	Not reported	China CN116217849A	[236]	2023
Cu@BD-COF	Solvothermal method	Quartz reactor	Sodium ascorbate (10 g/L)	Xe lamp (λ > 420 nm)	Not reported	17.45 mmol/g_{cat}·h	Good stability after 4 h	China CN113856763A	[364]	2023
Pt@Triazinyl COF	Solvothermal method	Reaction device	Ascorbic acid	Xe lamp (λ > 420 nm)	Not reported	0.046 mmol/g_{cat}·h	Not reported	China CN116425935A	[365]	2023
Pt@BTT-BPY-COF	Solvothermal method	Quartz reactor	None	300 W Xe lamp (λ > 420 nm)	Not reported	0.03 mmol/g_{cat}·h	Slightly decreased activity after 8 cycles (1 h each)	China CN115646545A	[366]	2023
N-vacancy g-C_3N_4	Calcination	–	10% triethanolamine	3 W LED lamp	Not reported	3.26 mmol/g_{cat}·h	After 4 cycles, N-vacancy g-C_3N_4 showed high photostability	China CN112354553B	[367]	2023

*AQY: Apparent quantum yield; HER: Hydrogen evolution reaction.

non-zero band gap energy (E_g) distinguishing them from conductors ($E_g = 0$) and insulators ($E_g > 5$ eV). For photocatalytic applications, semiconductors with E_g in the range of approximately 1.9 eV to 3.9 eV are of practical interest, as this allows for the absorption of light in the UV to visible spectrum. This enables participation in redox reactions relevant to water splitting and photoreforming, and overcomes the overpotential and mass-transport losses associated with HER. The band gap energy is therefore a key physicochemical property influencing the suitability of an inorganic semiconductor for photocatalysis. Additional important factors include the morphology of the material and the associated specific surface area, as well as the number of active sites. The rate of recombination of photogenerated charge carriers, i.e. CB electrons (e^-) and VB holes (h^+) can also affect photocatalytic performance. Inorganic semiconductors have played a central role in photocatalytic hydrogen production since Fujushima and Honda investigated water-splitting over a TiO_2 catalyst in the early 1970s [43]. Indeed, TiO_2 remains a common material for photocatalytic hydrogen production, accounting for a large proportion of the undoped and doped semiconductors in the literature. The following sections provide an overview of recent advances in photocatalytic semiconductor materials, with a focus on their classification based on the presence or absence of dopant agents (Sections 2.1.1 and 2.1.2), as well as on the formation of heterostructures through the combination of different semiconductors (Section 2.1.3). The relevance of these material advances to large-scale implementation depends not only on their intrinsic optoelectronic properties but also on factors such as material availability, synthesis complexity, long-term stability, and compatibility with scalable reactor configurations, and these criteria are more explicitly addressed in patent-driven developments.

2.1.1. *Undoped inorganic semiconductors*

Over the past few decades, a wide range of inorganic semiconductors have been explored for photocatalytic hydrogen production, with metal oxides and metal sulfides featuring prominently due to their suitable band gap energies, chemical stability, and relative abundance [44]. Undoped inorganic semiconductors still represent a substantial proportion of materials reported in the literature on photocatalysis, accounting for nearly half of those discussed in this review. Among these, TiO_2 has dominated early-stage research, largely due to its chemical stability, low cost, favorable band-edge positions, and overall photocatalytic activity [45]. However, TiO_2 also presents well-known limitations that hinder its broader applicability including its wide bandgap (3.2 eV) and the rapid recombination of photogenerated electron–hole pair (e^-–h^+) [46].

Beyond TiO_2, Luo et al. achieved a significant HER of 328 mmol/g_{cat}·h using solar-driven methane steam reforming (MSR) with a plasmonic ZnCu alloy. The approach harnessed the photothermal conversion capacity of Cu nanoparticles to increase the ZnCu surface temperature to around 250 °C at a light intensity of 788 mW cm^{-2}, without the input of additional heat energy. Excitation of localized surface plasmon resonance of Cu under solar light irradiation led to the generation of both hot carriers and photothermal heating, which contributed to the rapid surface catalytic reaction and high HER [47]. Vempuluru et al. [48] produced a NiO/CuS nanocomposite which achieved a HER of 52.3 mmol/g_{cat}·h and a substantial quantum efficiency of 70% at λ = 768 nm.

Other notable results include Rajashekhar et al.'s HER result of 2.9 mmol/g_{cat}·h using plasmonic AuPd nanoparticles uniformly decorated on the surface of TiO_2 nanotube arrays [49] allowing radial separation of photogenerated charge carriers and Liu et al.'s HER result of 6.9 mmol/g_{cat}·h and AQY of 36.8% under simulated sunlight. Using a facile two-step solvothermal and hydrothermal method, Liu et al. synthesized ZnS with multiple internal phase junctions (MIPs) of alternating wurtzite and sphalerite – a so-called 'homojunction' [50]. This band gap arrangement promoted charge carrier separation, transport and surface localization for reduction of H^+ to H_2. Souza et al. achieved an AQY of 17% (λ = 254 nm) using Ta_2O_5 nanoparticles synthesized via the simple hydrolysis of imidazolium tantalate ionic liquids (ILs). The enhanced photocatalytic activity was attributed to the residual ionic liquid associated with the nanoparticles, which were proposed to create hydrophilic regions. These regions facilitated the adsorption and interaction of polar molecules, such as the sacrificial ethanol, with the active sites, thereby improving the overall hydrogen evolution performance [51].

Traditional 'bottom-up' approaches remain the most commonly employed for the synthesis of inorganic semiconductors used in photocatalysis. These include methods such as hydrothermal synthesis, sol-gel processing, calcination, as well as photodeposition, co-precipitation, and impregnation – the latter three being particularly prevalent for the deposition of co-catalysts. In recent years, however, several novel synthetic strategies emerged, aimed at enhancing material sustainability, functionality, and structural control, including a green solid-state combustion/bio-reduction method [52] and evaporation-induced self-assembly [53]. Others patented a hydrothermal method for preparing unique hollow, irregularly shaped rutile-phase TiO_2 microspheres, engineered to possess a high surface area and improved light-harvesting capabilities, thus boosting their photocatalytic performance [54]. The novel structure offered enhanced light-harvesting through light trapping and slow light effects, and increased surface reactivity leading to

improved efficiency in both hydrogen production and pollution degradation. This novel synthesis overcomes the limitations associated with conventional photocatalysts by offering a stable, effective solution for sustainable energy and environmental applications, especially in solar-driven hydrogen generation and pollutant degradation. Furthermore, niobium nitride (Nb_3N_5)-containing films have been patented [55] for various photocatalytic applications, including hydrogen generation. These materials are synthesized by converting an organic niobium precursor in the presence of N_2 gas, resulting in the formation of a nitride with controlled physicochemical properties, such as high electrical conductivity and stability, and strong visible-light absorption.

Notably, in the context of solar energy utilization, there is widespread use of visible light sources – such as Xe lamps or solar simulators – in the literature concerning inorganic undoped semiconductors for photocatalytic hydrogen production. This trend is particularly promising, given the notable hydrogen HER and AQY achieved under these conditions, underscoring the potential for real-world solar-driven applications. Despite these promising laboratory-scale performances, many undoped inorganic semiconductors reported in the literature remain limited by low durability under prolonged operation or by synthesis routes that are difficult to scale. Conversely, patents in this area increasingly emphasize structural robustness, simplified morphologies, and synthesis strategies compatible with large-scale manufacturing, underscoring a shift from proof-of-concept validation toward industrial feasibility.

2.1.2. Doped semiconductors

Doping of inorganic semiconductor photocatalysts involves the incorporation of other elements into the semiconductor crystal lattice, with the primary aim of introducing intermediate energy levels within the intrinsic band gap. This modification of the semiconductor is generally intended to enhance light absorption and suppress charge carrier recombination, thereby improving photocatalytic activity. While many studies report performance enhancements, some findings suggest that extrinsic defects introduced through doping may serve as recombination centers, ultimately leading to a reduction in photocatalytic activity. Thus, the impact of doping is highly dependent on the nature of the dopant, its concentration, and the host material's structure and properties.

2.1.2.1. Metal-doped semiconductors. In contrast to the dominance of Pt-loaded TiO_2 in the literature on undoped inorganic semiconductor photocatalysts, TiO_2-based systems do not prevail in the field of metal-doped inorganic semiconductors. Nonetheless, a significant HER of 23.5 mmol/g_{cat}·h with an AQY of 19% was achieved using Ag-doped TiO_2 [56]. In this case, Ag-doping effectively reduced the band gap of TiO_2 to 2.5 eV, enhancing visible light absorption. The improved photocatalytic properties of the material were attributed to TiO_2 oxygen vacancies and the presence of a Ti–Ag–O phase, which together facilitate more efficient charge transfer and charge carrier separation. In 2025, Xiaoxing et al. [57] prepared a novel Rh—Cr co-catalyst-loaded, Al-doped $SrTiO_3/TiO_2$ photocatalyst via calcination and physical mixing methods. The metal-doped photocatalyst offered improved carrier separation and strong stability, and demonstrated an outstanding HER of 24 mmol/g_{cat}·h.

Other notable TiO_2 based materials featured Cu doping. Martín-Gómez et al. used a biotemplating and ionic exchange method to synthesize a Cu-doped TiO_2 artificial olive leaf material, which achieved a HER of 3.56 mmol/g_{cat}·h during the photoreforming of glycerol under simulated solar illumination [58]. Rawool et al. produced Cu-doped TiO_2 ($Cu_{0.02}Ti_{0.98}O_{2-\delta}$) [59] obtaining an AQE of 7.5% and STH of 3.9% under sunlight, while Zhang et al. synthesized quantum Cu(II) nanodot-doped 2D ultrathin TiO_2 nanosheets [60], obtaining a HER of 1.46 mmol/g_{cat}·h. However, the absence of reported AQY and STH values in this latter study makes direct comparison with other systems more challenging. Guoyong et al. [61] published a patent detailing an in-situ remediation method to extract TiO_2 from waste selective catalytic reduction (SCR) catalyst carriers, directly synthesizing a high-performance Cu-TiO_2 photocatalyst with an impressive HER of 0.308 mmol/g_{cat}·h.

Other first-, second- and third-row transition metals featured in the literature as dopants, including Mo [62], In [63], W [64], Cd [65], Fe [66], Au [67] and Zn [68]. The In-doped ZnO of Chauhan et al., for example, was notable for achieving a HER of 2.47 mmol/g_{cat}·h under sunlight irradiation [63]. In addition to the transition metals mentioned, La emerged as a dopant in several cases [69,70] – twice with sodium tantalate – although the resulting HER was not particularly significant.

While these findings help mitigate some of the key limitations associated with traditional photocatalysts, the overall efficiencies of metal-doped semiconductors remain modest. Consequently, although they represent promising candidates for solar-driven hydrogen production within sustainable energy systems, significant advancements are still required before their full potential can be realized. Patent literature suggests a gradual transition away from highly optimized but complex doped systems toward compositions that balance performance gains with material cost, dopant abundance, and reproducibility. This divergence highlights the need to reassess doping strategies not only in terms of activity enhancement, but also with respect to economic competitiveness and long-term deployment.

Given the widespread use of noble metals and frequent use of heavy metal chalcogenides in the literature on inorganic semiconductor photocatalysts, it must be acknowledged that there is an inherent tension between the improved catalytic performance of these materials and their environmental sustainability.

While noble metal cocatalysts (e.g., Pt, Au, Pd) are often essential for achieving desirable efficiencies in hydrogen evolution, their environmental toxicity and economic scarcity necessitate rigorous mitigation and recovery strategies. Reducing the amount of metal loading, for example via the use of single atom catalysts, is one approach to reducing the environmental toxicity of these materials [71]. Preventing leaching of these metal cocatalysts can be achieved via increasing the intermolecular interactions between metal and photocatalyst or creating material architectures that isolate the metal from the aqueous environment, such as core-shell. The same is true of metal chalcogenides and their constituents (e.g. Cd, Pb, S, Se, Te) in large-scale applications, which pose an inherent environmental risk, particularly via leaching of these toxic elements into the environment. Techniques to prevent this are the focus of much current research and include surface functionalisation and other encapsulation techniques [72].

Minimising the environmental impact of metal cocatalysts also requires efficient recovery from spent photocatalysts. Hydrometallurgical recovery remains the standard approach, and can recover metals in high purity and yield, but requires the use of potentially toxic leaching agents [73]. More recent advances leverage the photocatalytic properties of the materials themselves to recover metal cocatalysts using specific photo-driven processes in an almost closed loop process [74]. Similarly, chalcogens are being recovered in closed loop processes via techniques including ambipolar electrolysis and deep eutetic solvent extraction [75,76]. A positive example of balancing the catalytic performance of chalcogenide-based materials with their environmental sustainability in large scale applications is the widespread and safe adoption, operation and disposal of thin-film CdS/CdTe solar cells.

2.1.2.2. Non-metal doped semiconductors. Compared to metal-doped, the literature on non-metal doped systems is considerably more limited, and the reported HER generally lower. Among non-metal dopants, only N-, C- and S- have been widely studied, with N-doping representing the majority of the research in this category. This trend reflects both the relative simplicity and maturity of metal-doped systems, as well as the ongoing challenges in optimizing non-metal dopants for efficient

photocatalytic performance.

Among the best performing photocatalysts, N-doped ZrO_2 was synthesized by Wang et al. achieving a HER of 2.12 mmol/g_{cat}·h [77]. As is generally the case for non-metal doping, N-doping provides intermediate energy levels within the band structure of the semiconductors, thereby modulating the band gap and enhancing visible light absorption.

Beyond this example, the majority of studies in this category have focused on non-metal doped TiO_2, with reported HER values below 1 mmol/g_{cat}·h. These results indicate that non-metal-doped photocatalysts, while offering insights into band gap engineering, are currently unlikely to outperform their metal-doped, dye-sensitized, or even undoped counterparts in practical hydrogen evolution applications.

2.1.2.3. Dye sensitized inorganic semiconductors. As an alternative to doping or loading of metals or non-metals onto inorganic semiconductors to improve their photocatalytic performance, dye sensitization is a method that was previously and successfully used in the development of dye sensitized solar cells [78]. Dye-sensitization can extend the light absorption of materials such as TiO_2 into the visible region, greatly improving their photoactivity [79].

A significant body of literature is now dedicated to dye-sensitized inorganic semiconductors, with some studies reporting performances that rival or even surpass those of undoped and metal-doped systems. For example, Koyyada et al. achieved a remarkable HER of 59.21 mmol/g_{cat}·h under sunlight by coupling a Ru-complex based dye sensitization of TiO_2 with a Pt co-catalyst [78]. The nanoparticle morphology usually employed for TiO_2 photocatalysts facilitated effective dye sensitization by providing a large surface area for dye anchoring.

For the reasons outlined above, and in common with undoped and non-metal doped inorganic semiconductors, TiO_2 features heavily in dye-sensitized literature. Huang et al. reported a Calix-3 sensitized Pt/TiO_2 system that achieved a commendable HER of 12.22 mmol/g_{cat}·h [80]. Other notable results were reported by Li et al. using an Eosin-Y sensitized Fe-B@Ni composite, which achieved an HER of 17.23 mmol/g_{cat}·h and an AQY of 51% ($\lambda = 420$ nm). Eosin-Y and related organic dyes are readily available with broad and strong absorptions in the visible region. As such, they are commonly employed in dye-sensitized photocatalysis, as reported by e.g. Xu et al. [81] and others [82,83]. Nevertheless, the practical deployment of dye-sensitized systems is often challenged by dye photostability, leaching, and regeneration requirements. These limitations are reflected in patent trends, which tend to prioritize immobilized sensitizers, robust organic dyes, or hybrid architectures designed to mitigate degradation and facilitate long-term operation.

Other commonly employed dyes include perylene dyes [84] and donor–π–acceptor type dyes [85]. These are characterized by π-electron rich donor groups and electron poor acceptor groups linked by a π-bridge which can facilitate the separation of photoinduced electrons and holes. Recently, Tahir patented an efficient photocatalyst composed of a triphenylphosphine ruthenium (RuP) complex supported on exfoliated graphitic carbon nitride. The system demonstrated enhanced visible-light absorption, efficient charge separation, and improved hydrogen evolution, achieving a hydrogen yield of up to 176 μmol with 3 wt% RuP loading [86]. Another dye was employed by Meng et al. [87] who patented a modified TiO_2 photocatalyst, developed by sensitizing anatase-phase TiO_2 with an organic dye via solvothermal treatment. The sensitization significantly extended the light absorption into the visible region ($\lambda \geq 400$ nm), enhancing photocatalytic activity under solar-like irradiation. Upon loading with Pt nanoparticles and using triethanolamine as a sacrificial agent, the photocatalyst achieved a HER of 2.15 mmol/g_{cat}·h, demonstrating excellent cycling stability under visible light.

2.1.3. Inorganic semiconductor heterojunctions

Semiconductor heterojunctions are engineered by combining two or more semiconductors with distinct bandgap energies or coupling semiconductors with metals. These structures extend the light absorption range of the photocatalyst while enhancing the efficiency of photogenerated electron-hole pair separation. Fig. 3 showcases different types of inorganic semiconductor heterojunctions including type-II, *Z*-scheme, S-scheme, Schottky, and p-n heterojunctions.

Type-II heterojunctions (Fig. 3 **(a)**) facilitate the spatial separation of electrons and holes between different semiconductor components, thereby suppressing recombination and increasing the availability of charge carriers for redox reactions on the photocatalyst surface.

A wide range of heterojunction photocatalysts involving type-II configurations have been reported in the literature. Similar to type-I systems, inorganic semiconductors – particularly metal chalcogenides and metal oxides – predominate in these studies. Most reported structures are binary heterojunctions; however, more complex ternary systems have also been explored to further enhance charge separation and photocatalytic performance [88–96]. In both type-I and type-II heterojunctions, one or more semiconductors often appear as solid solutions, specifically chalcogenides. The solid solution strategy is an effective route to tune the electronic band structure and the optical properties, enabling tailored photocatalytic performance for specific applications.

Under light irradiation, the p–n junction (Fig. 3 **(d)**) facilitates charge separation by driving photogenerated electrons to accumulate in the n-type semiconductor, while holes migrate to the p-type semiconductor. This directional movement of charge carriers significantly enhances electron–hole separation efficiency, improving photocatalytic performance.

Zhang et al. reported a p-n junction heterointerface system comprising *p*-type Co_3O_4 and *n*-type $ZnIn_2S_4$ semiconductors [97]. The heterojunction results in a photocatalytic HER 4.67 times higher than with pure $ZnIn_2S_4$ alone. Jianfeng et al.[98] prepared Bi_2WO_6-TiO_2 photocatalyst through sol-gel and hydrothermal methods, but its hydrogen production performance was significantly lower, reaching only 0.00248 mmol/g_{cat}·h. Yaorong et al. [99] developed a novel TiO_2/$ReS_{1.2}Se_{0.8}$ photocatalyst, which exhibited more active sites for hydrogen evolution, a lower charge carrier recombination rate, and a significantly higher hydrogen production efficiency compared to pure TiO_2, achieving a rate of 1.0175 mmol/g_{cat}·h.

Ma et al. recently developed a PtO_2/TiO_2 p-n heterojunction via ball milling, achieving an impressive HER of 54 mmol/g_{cat}·h at 20% PtO_2 under UV and visible light irradiation, with an outstanding STH efficiency of 15.6% and an AQY of 38% under UV irradiation. This work underscores the potential of simple mechanical synthesis methods for producing highly efficient photocatalysts for hydrogen production [100]. Several p-n heterojunctions along with their synthesis methods have been recently patented, including $Cu_2O/CaTiO_3$ [101], $Mn_{0.43}Cd_{0.57}S/ZnCo_2O_4$ [102], Cu_{2x} S/$Zn_{3.74}Ga_{1.02}S_{5.24}$ hollow nanosphere [103]. In all cases, the heterojunctions with different compositions exhibit significantly higher HER compared to the pure semiconductors.

In a *Z*-scheme heterojunction (Fig. 3 **(b)**), the two semiconductors exhibit a staggered band alignment reminiscent of a type-II structure; however, the charge carrier dynamics follow a distinct mechanism with a redox mediator facilitating the transfer of electrons between the semiconductors [104,105]. Specifically, photogenerated electrons in the CB of one of the semiconductors recombine directly with holes in the VB of the other semiconductor, retaining the highly reactive electrons and holes of both materials. This selective recombination preserves strong redox potential, overcoming the limitations of type-II systems while enabling efficient charge separation and broader light absorption. Typical redox mediators include Fe^{+3}/Fe^{+2}, IO_3^-/I^-, $Fe(CN)_6^{4-}/Fe(CN)_6^{3}$ [106].

Numerous studies have reported superior performance with high quantum yield of such heterojunctions in photocatalytic hydrogen evolution [107–111]. Shen R. et al. reported noble-metal-free cocatalyst

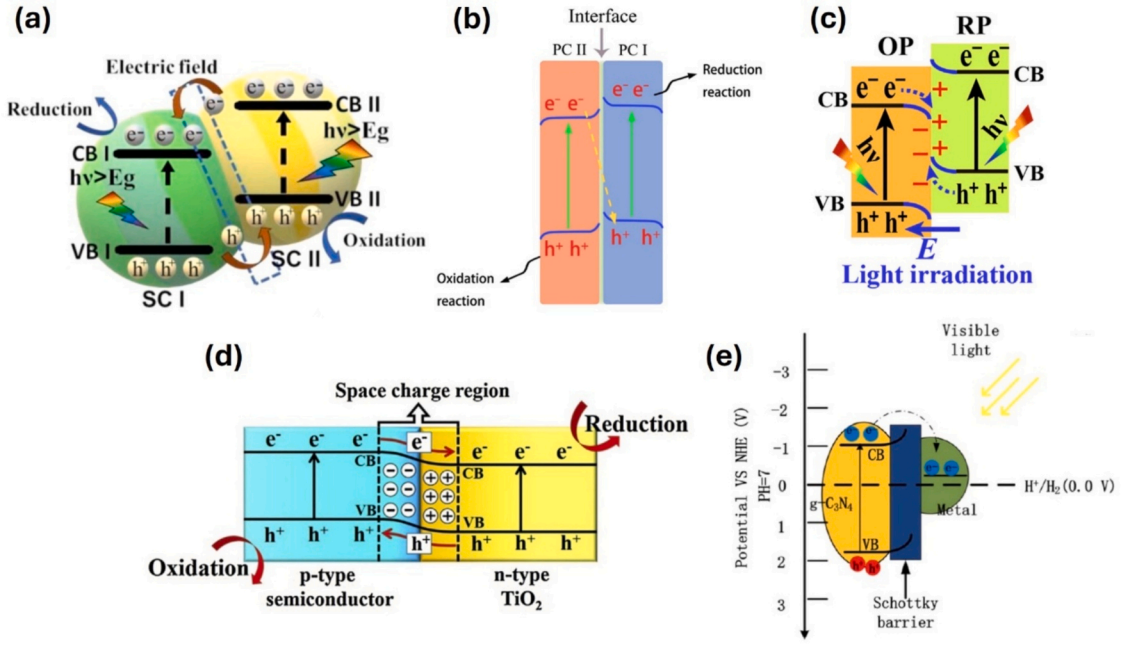

Fig. 3. Schematic diagrams of the photocatalytic mechanisms proposed for different semiconductor heterojunctions. (a) Type-II heterojunction [148]. (b) Z-scheme heterojunction [149]. (c) S-scheme heterojunction. Reprinted with permission from [150]. Copyright 2020 Elsevier. (d) p-n heterojunction [151]. Copyright 2017 Elsevier. (e) Schottky heterojunction. Reprinted with permission from [152]. Copyright 2018 American Chemical Society.

β-NiS, which exhibits metallic characteristics with a high density of states at the Fermi level. When integrated with CdS and Fe_2O_3 semiconductors in a *Z*-scheme heterostructure [112], the resulting ternary system demonstrated excellent performance in the hydrogen evolution reaction achieving a high quantum efficiency.

Another charge carrier transfer mechanism for heterojunctions, referred to as S-scheme (Fig. 3 **(c)**), has recently received significant attention [113]. The S-scheme mechanism consists of a combination of carrier dynamics of type-II and Z-scheme. In this configuration, the two semiconductors are designated as the reduction photocatalyst (RP) and the oxidation photocatalyst (OP) (Fig. 3 **(f)**) and form a staggered band arrangement similar to type-II. The first mechanistic step involves electron migration from CB of RP to CB of OP, with holes simultaneously transferring from VB of OP to VB of RP, as per type-II heterojunction charge carrier behvaiour. As time progresses, the generated interfacial electric field prohibits this carrier transfer and forces VB holes of RP to recombine with the CB electrons of OP. Thus, the energetic electrons and energetic holes remain in the CB of RP and VB of OP respectively to perform the desired redox reactions [113,114].

The recent development of S-scheme heterojunction photocatalysts represents a significant advancement in the field of photocatalytic hydrogen production. Additionally, the patent landscape features a wealth of S-scheme-based heterojunction designs for efficient hydrogen production. For instance, $Zn_{0.5}Cd_{0.5}S/WO_3$ has been proposed to follow a typical S-scheme mechanism with a hydrogen production rate of 9.15 mmol/g_{cat}·h using lactic acid as the sacrificial agent [115]. A continuous multi-step electron transfer can also be induced to form a dual S-scheme on a ternary semiconductor system. This is the case of an $In_2O_3/SnIn_4S_8$/CdS heterojunction for hydrogen production under visible light, recently patented with its environmentally friendly synthesis method [116].

A plethora of Schottky heterojunctions (Fig. 3 **(e)**) typically consisting of the combination of semiconductors with metals have been reported in the literature as potential photocatalytic hydrogen evolution catalysts [117]. Examples of such systems comprising single noble metals include Pt-based [118–125], Au-based [126–131] and Ag-based heterojunctions [132,133]. Several non-noble metal containing heterojunctions also showed remarkable performance, such as Cu-[134] Bi-[135] and Ni-based heterojunctions [136–138]. Some studies have shown that bimetallic co-catalyst systems can outperform monometallic ones, due to synergistic effects. In coupled plasmonic systems, enhanced efficiency arises from overlapping or complementary localized surface plasmon resonance (LSPR) peaks, while in plasmonic–non-plasmonic combinations, the synergy between plasmonic excitation and catalytic activity contributes to improved performance [139]. Bimetallic exciton-plasmon coupled systems such as, Pt—Rh [140], Pt—Au [141], Ag—Ru [142], Ag—Fe [143], and Au—Ag [144] based photocatalysts have demonstrated enhanced photocatalytic hydrogen production compared to their corresponding single-metal counterparts. This improvement is attributed to synergistic interactions between the metal components, leading to more efficient charge separation and light utilization. Indeed, the photocatalyst patented by Tahir (see Section 2.1.2.3) showed significant performance improvements when further integrated into a RuP–Ti_3C_2@TiO_2/ECN heterostructure. The synergistic interaction among the components resulted in a remarkably high hydrogen production of 5.3 mmol/g_{cat} after 4 h, corresponding to an AQY of 5.18% [145]. One of the highest HER achieved using non-TiO_2 metal-doped inorganic semiconductor heterojunctions was reported by Su et al., who synthesized a Mo-doped/Ni-supported $ZnIn_2S_4$-wrapped $NiMoO_4$ S-scheme heterojunction. The success of the material was attributed to synergistic effects of the heterojunction, Mo-doping and Ni-support which promoted broad light absorption and improved charge carrier separation [62], obtaining 5.14 mmol/g_{cat}·h in the presence of triethanolamine and AQY of 30% at 400 nm. Many of the above-mentioned metal-semiconductor systems consist of two semiconductors, which showed either type-II or direct *Z*-scheme mechanism. In all-solid-state Z-scheme a solid-state electron mediator is introduced between the two semiconductors of the Z-scheme system [146]. Electron migration occurs from the CB of the first semiconductor to the VB of the second semiconductor, where they recombine with photogenerated holes. This electron-shuttling mechanism, facilitated by a mediator, is more rapid and efficient due to the suppression of electron backflow. Common electron mediators used in such systems are Au, Pt, Ag, and Bi. Recently, Chen W. et al. demonstrated that even semiconductor quantum dots can serve as electron mediators in all-solid-state *Z*-scheme ternary system

[147]. In another study, Bi nanoparticles were reported to perform a dual role in an S-scheme heterostructure. Beyond their plasmonic effect in enhancing carrier concentration, Bi also functioned as a recombination center between CdS and TiO_2 [129]. Upon recombination of photogenerated holes in the VB of CdS with electrons in the CB of TiO_2, the remaining high-energy charge carriers in both semiconductors efficiently participated in redox reactions. This mechanism closely resembles that of an all-solid-state Z-scheme.

2.1.4. Carbides and nitrides

This section highlights additional photocatalyst structures that are not discussed in the preceding paragraphs. These include but are not limited to bare and modified g-C_3N_4 [153–165], $Ti_3C_2T_x$ [166–187], and graphene-based materials [188,189]. Despite variations in the experimental reaction conditions, the analysis focuses on evaluating photocatalytic activity based on the rate of H_2 evolution.

Although several of these photocatalysts have exhibited limited performance in photocatalytic hydrogen production, various factors can significantly influence their performance. For instance, the incorporation of noble metal nanoparticles onto the semiconductor surface has been shown to significantly enhance the efficacy of photocatalytic reforming reactions, as previously discussed, [153,172,190–195] as well as the morphologies of the photocatalysts [169,172,173,175,191,196–198]. These structural modifications can lead to an increased surface area, hence facilitating the presence of active adsorption sites, inhibiting the recombination of electron-hole pairs, enhancing the electrical conductivity, and improving photocatalytic activity [172,173,175,176,180,192,197,198]. Li and coworkers synthesized g-C_3N_4@Ti_3C_2 quantum dots (QD) to enhance the photocatalytic activity of g-C_3N_4 for hydrogen production [172]. Their findings showed a significant increase of 26-fold compared to the initial pristine g-C_3N_4 nanosheets. This value is three times greater than the Pt/g-C_3N_4 composite (1.9 mmol/g_{cat}·h) and ten times higher than the Ti_3C_2 Mxene sheet/g-C_3N_4 (0.52 mmol/g_{cat}·h). The enhancement of the photocatalytic activity can be primarily attributed to the increased surface area, which results in a higher density of active sites. In addition, it is worth noting that metallic g-C_3N_4@Ti_3C_2 QDs can serve as electron acceptors and exhibit exceptional electrical conductivity, hence leading to enhanced separation of photoexcited carriers [172]. However, a recent study by Jones et al. [153] investigated the photocatalytic potential of g-C_3N_4 through the incorporation of Pt atoms. The hydrogen evolution activity of Pt/g-C_3N_4 composites was found to be limited due to the occurrence of self-poising phenomena on the C_3N_4 surface. Martínez-García et al. [199] reported on a rationally designed C_3N_4/TiO_2 heterojunction, composed of anatase and brookite TiO_2 phases, for enhanced photocatalytic hydrogen production under visible light. The composites were fabricated by combining C_3N_4, prepared via polymerization, with TiO_2, synthesized using a sol-gel method, and joined through a photoanchoring technique to form the heterojunction. Among the tested compositions, the catalyst with 5% C_3N_4 content demonstrated the highest performance, achieving a HER of approximately 0.69 mmol/g_{cat}·h. This superior efficiency was attributed to the formation of a staggered-type heterojunction that facilitates a direct *Z*-scheme charge transfer mechanism. Others [200] prepared a sodium-boron co-doped, nano-layered graphite-like carbon nitride (g-C_3N_4) photocatalyst through thermal polymerization of specific carbon, nitrogen, sodium, and boron precursors. By co-doping g-C_3N_4 with sodium and boron, light absorption and charge separation efficiency are improved, while nano-layered morphology increases the surface area and active sites, further boosting hydrogen evolution under visible light. Compared to undoped or singly doped g-C_3N_4, the material demonstrates superior photocatalytic efficiency, reduced bandgap, and enhanced charge carrier dynamics. In this context, other authors [201] patented a novel photocatalyst based on Zr and Mg - doped tantalum nitride (TaN) designed to enhance hydrogen production through water splitting. Doping modifies the electronic structure of TaN, enhancing its ability to absorb light and facilitate charge separation, which are critical for effective water splitting. Impregnation methods were employed, obtaining uniform doping and desirable structural properties for optimal catalytic activity. Under the best conditions, a limited AQY of 0.55% was obtained at $\lambda = 400$ nm.

Su et al. [173] improved the HER of TiO_2 by combining it with both a monolayer and a multilayer co-catalyst ($Ti_3C_2T_x$). The monolayer $Ti_3C_2T_x$/TiO_2 composite exhibited more than 9.1 times higher hydrogen production compared to pure TiO_2 and 2.5 times higher than the multilayer composite. This remarkable boost in activity was attributed to the excellent electrical conductivity of the monolayer $Ti_3C_2T_x$ and the facilitated separation of photoinduced electrons and holes in the MXene/TiO_2 interface. Regrettably, over 16 h (consisting of 4 cycles) of reaction, the rate of photocatalytic HER declined from 2.6 mmol/g_{cat}·h to 2.3 mmol/ g_{cat}·h. This decrease in activity was attributed to the potential detachment of certain TiO_2 particles from the $Ti_3C_2T_x$ flakes, leading to compromised contact and subsequently reduced performance of the $Ti_3C_2T_x$/TiO_2 composites. Similarly, Zhuang et al. [171] investigated the photocatalytic performance of Ti_3C_2/TiO_2 composites with varying Ti_3C_2 content. The maximum HER achieved is 6.9 mmol/g_{cat}·h, representing a 3.8-fold increase compared to the TiO_2 nanosheet. However, a decline in photocatalytic efficiency was observed as the concentration of Ti_3C_2 increased from 3 wt% to 5 wt%. This reduction in performance was attributed to the presence of an excessive amount of Ti_3C_2, which may hinder light penetration and reduce effective illumination of the TiO_2 surface. The produced composites exhibited significant stability following five cycles, suggesting that no detachment of TiO_2 occurred. A novel 1 T-WS_2@TiO_2@Ti_3C_2 composite photocatalyst was developed for highly efficient hydrogen (H_2) evolution from water, achieving a remarkable production rate of 3.4098 mmol/g_{cat}·h [202]. This performance, nearly 50 times higher than that of pure TiO_2 nanosheets, is attributed to the synergistic use of highly conductive Ti_3C_2 MXene and metallic 1 T-WS_2 as dual co-catalysts. This unique structure facilitates the rapid transfer of photoexcited electrons from TiO_2, significantly suppressing charge recombination, increasing carrier lifetime, and achieving efficient spatial charge separation. The introduction of 1 T-WS_2 nanoparticles at an optimal loading of 15 wt% also increases the material's specific surface area and the density of active sites, further boosting its catalytic activity and demonstrating excellent stability over 24 h. Li et al.[180] prepared Mo_xS@TiO_2@Ti_3C_2 photocatalyst for enhanced photocatalytic hydrogen production from water splitting. This material features TiO_2 nanosheets grown directly on a highly conductive Ti_3C_2 MXene substrate, with MoS_2 rich in molybdenum vacancies (Mo_xS) uniformly distributed across the surface. The synthesis was achieved through a two-step hydrothermal process, creating a unique structure where Ti_3C_2 and MoS_2 act as dual co-catalysts. The optimized composite, prepared with a hydrothermal treatment at 160 °C, achieved an exceptional HER of 10.5058 mmol/g_{cat}·h, a result 193 times higher than pure TiO_2 nanosheets and 6 times higher than the equivalent composite without molybdenum vacancies. This significant improvement is attributed to the molybdenum vacancies increasing the number of active sites and suppressing charge carrier recombination, combined with the extraordinary conductivity of Ti_3C_2 MXene and MoS_2, which greatly enhances electron transfer and separation efficiency.

Tie et al. [203] provided a comprehensive elucidation of the reaction mechanism governing the production of H_2 at the ZnS/Ti_3C_2 interface, which was also proposed by several studies, see Fig. 4 **(b)**. Irradiation of ZnS promotes electron excitation to the conduction band, leaving reactive holes in the valence band. The enhancement is attributed to the excellent electrical conductivity of the ultrathin Ti_3C_2 nanosheets, which act as an active co-catalyst to promote the transfer of photoinduced electrons from ZnS, suppress the recombination of electron-hole pairs, and prolong charge carrier lifetime. Also, the CB electrons of the ZnS shuttle to the surface of Ti_3C_2, owing to the tight interface generated between ZnS and Mxene. The highly conductive Ti_3C_2 nanosheets act as an efficient co-catalyst, utilizing these electrons to reduce

protons (H^+) from the solution to generate hydrogen gas. This effective charge separation resulted in a significantly enhanced HER of 0.50 mmol/g_{cat}·h. This performance was nearly four times higher than that of pure ZnS (0.12 mmol/g_{cat}·h) and also surpassed a comparable ZnS/RGO composite.

Ran et al. [181] explained this synergetic effect due to the efficient charge separation and numerous —O terminations characterizing Ti_3C_2 nanoparticles. Furthermore, Xiao et al. [176] have reported the synergistic effects observed between the n-type semiconductor CdS and the highly conductive 2D Ti_3C_2 MXene nanosheets. The 1D/2D Schottky heterojunction enhanced charge separation and reduced the Schottky barrier. As anticipated, the composite exhibits 7 times higher hydrogen production compared to that of the pure CdS nanorods. This observed synergistic effect was explained by Lin et al. [183] for the Ti_3C_2/O-doped g-C_3N_4 2D—2D composite through both density functional theory (DFT) and band theory. That study demonstrated that, upon irradiation, the electrons transfer from the CB of g-C_3N_4 to Ti_3C_2 via the Schottky-junction interface and the built-in electric field. According to Fig. 4 **(a)**, this leads to the band alignment between these two components, preventing the electron transition back to g-C_3N_4. As a result, the photocatalyst is characterized by enhanced charge separation, and improved HER, leveraging the electrons accumulated on the Ti_3C_2 surface.

In addition, the specific hole scavenger participating in the oxidation step can play a significant role in facilitating charge separation and migration reported by the literature. Jones et al. [153] reported a substantial 14-fold enhancement in the rate of hydrogen generation when TEOA was utilized as a hole scavenger for Pd/C_3N_4, in contrast to the utilization of methanol. The efficiency of TEOA as a hole scavenger was shown to be only twice that of methanol when Pd/TiO_2 was employed, however. Similarly, lactic acid as a sacrificial agent showed higher activity for hydrogen production compared to triethanolamine and methanol [203].

2.2. Metal-organic and organic semiconductors

2.2.1. Metal-organic frameworks

Metal-organic frameworks (MOFs) are a class of crystalline porous materials consisting of inorganic nodes, which can be single metal atoms or metal clusters, interconnected with organic ligands. Their unique structure consists of open networks that contain voids, which result in high specific surface areas (1000-10,000 m^2g^{-1}) and pore volumes (up to 4.4 m^3g^{-1}) [204]. MOFs have unique properties which make them excellent candidates as photocatalysts compared with traditional inorganic semiconductors: (i) The modular nature of MOFs allows them to be tailored to enhance specific photocatalytic properties: for instance, different combinations of metal nodes and organic ligands can be selected to improve light absorption and reactant adsorption; (ii) the porous structure of MOFs facilitates the exposure of the active sites and reduces the charge transfer path, thereby improving the separation of electrons and holes; (iii) the highly ordered structure of MOFs provides an ideal platform for studying the structure-activity relationships in the photocatalytic process.

To fully leverage the potential of MOFs as photocatalysts, it is crucial that the synthesis methods of MOFs are not only facile, but also economic and readily scalable. Solvothermal and hydrothermal methods are well-established approaches for the synthesis of MOF-based photocatalysts as reported in Table 1 summarizing the use of MOFs for the hydrogen evolution reaction. The use of cost-effective ligands, such as benzoic acid derivatives [205–207] further enhances the economic feasibility of using MOF-based photocatalysts for hydrogen production.

Fig. 5 shows the different mechanisms that induce photocatalytic activity in a MOF-based photocatalyst [208]. In a pristine MOF (Fig. 5 **(a)**), the organic ligand typically absorbs the photons from incident light. The excited electrons are then transferred to the inorganic cluster (Me_xO_y). In this case, critical properties determining the photocatalytic response of the MOF are the energy required to excite an electron of the ligand from its ground state to an excited state (ΔE_{abs}), and the energy required to transfer the excited ligand's electron to the inorganic cluster's unoccupied orbital (ΔE_{LMCT}) [209]. This ligand-to-metal electron transfer ensures the separation of the photogenerated charges and prevent their rapid recombination. However, for many commonly used MOFs this pathway is thermodynamically unfavourable due to a positive ΔE_{LMCT}. In such cases, recombination of photogenerated charge carriers often dominates, leading to low quantum efficiencies despite strong light absorption by the organic linker. Consequently, significant efforts have been directed toward the design of photocatalytic MOF in which the unoccupied metal-centred orbitals lie at lower energy than the lowest unoccupied ligand orbital. This can be achieved through metal-node substitution, linker functionalization, defect engineering, or modulation of metal-ligand coordination environments, all of which enable systematic tuning of the MOF band structure [210]. These strategies aim to achieve a close-to-zero or even negative ΔE_{LMCT}, therby enabling a thermodynamically favorable charge transfer pathway [211]. Importantly, recent mechanistic studies further indicate that such band-structure optimization can also mitigate charge-induced degradation pathways by reducing charge accumulation on the organic linker, thereby contributing to improved photocatalyst stability under prolonged light irradiation [212].

A different approach to employ MOFs for photocatalysis is to use them as carriers to encapsulate other photocatalytically active materials. In this case, the MOF scaffold can simply contain a photocatalyst (Fig. 5 **(b)**) or take part in the charge transfer mechanism (Fig. 5 **(c)**).

For instance, Shi et al. reported a HER of 7.1 mmol/g_{cat}·h using a pristine Cu-I-bpy (bpy = 4,4'-bipyridine) without the use of co-catalysts and TEA as a sacrificial agent [213]. Ru-TBP and Ru-TBP-Zn MOFs were demonstrated to produce hydrogen with a rate of 0.13 and 0.24 mmol/g_{cat}·h under visible light irradiation [214] (Fig. 6 **(a)**).

A pristine Co-MOF (Fig. 6 **(d)**) was synthesized through a one-pot solvothermal method and reported to produce hydrogen with a rate of 1.1 mmol/g_{cat}·h under visible light irradiation, although in the presence of $Ru(bpy)_3Cl_2$ as a photosensitizer [215].

Some MOFs incorporate ligands which enable hydrogen production when exposed to visible light irradiation. For instance, porphyrin-based

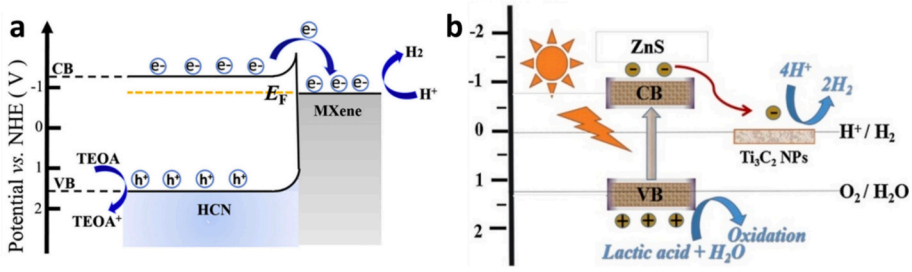

Fig. 4. (a) The mechanism of photocatalytic H_2-evolution of MX1/HCN Schottky-junction [183]. Copyright 2019 Elsevier. (b) The mechanism of the electron transfer and the enhanced photocatalytic H_2 evolution performance in the ZnS/Ti_3C_2 system [203]. Copyright 2019 Elsevier.

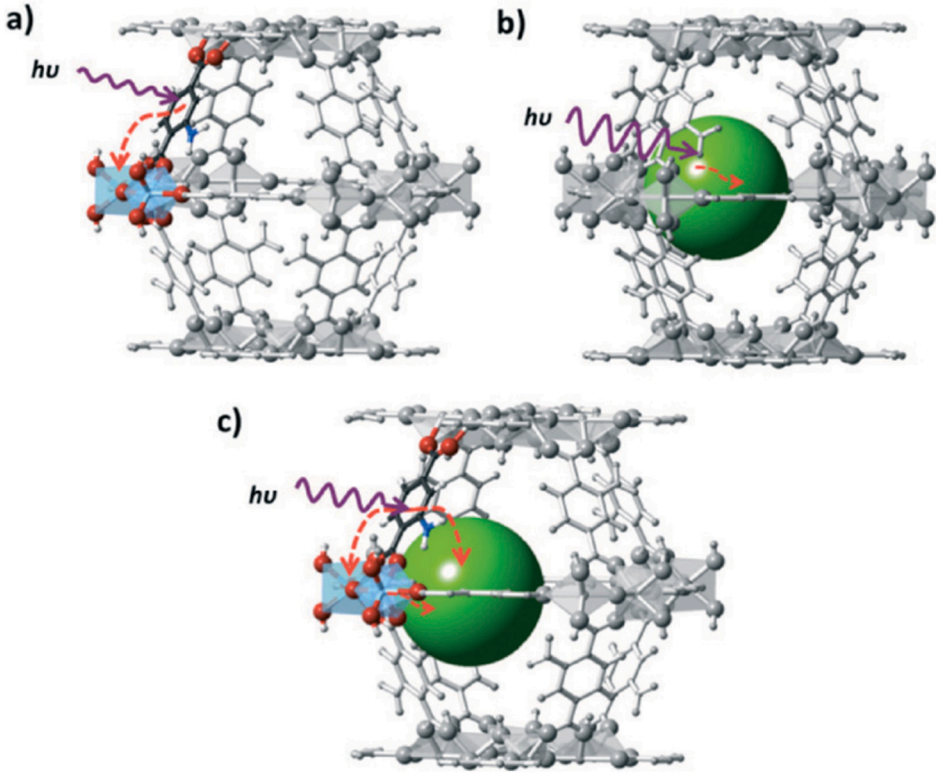

Fig. 5. Schematic mechanism to induce photocatalytic activity in a MOF-based photocatalyst. (a) Pristine MOF: The organic ligand acts a light-sensitizing antenna, and the charge is transferred from the ligand to the inorganic cluster. (b) The MOF encapsulates a photocatalyst that absorbs light. (c) Charge transfer occurs between the MOF and the encapsulated photocatalyst [208].

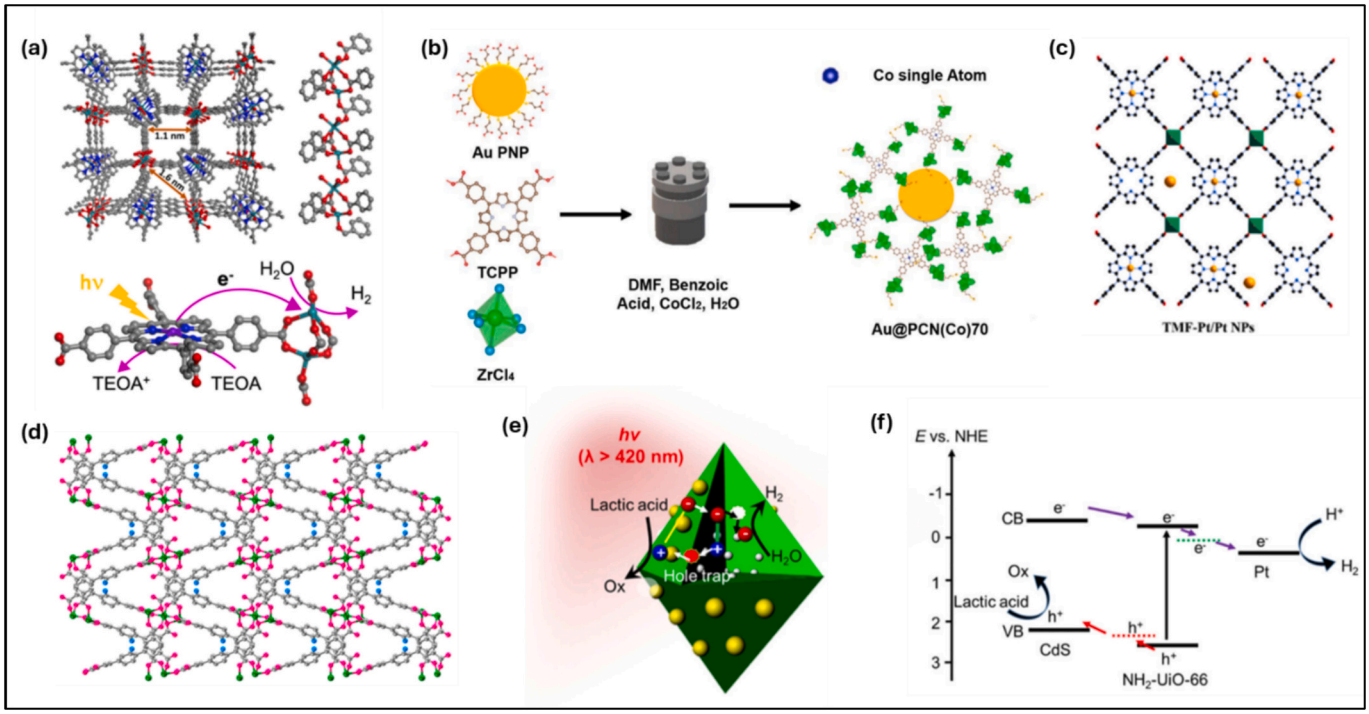

Fig. 6. (a) Ru-TBP crystal structure down the (100) direction with coordination environment of the Ru2 paddlewheel and proposed hydrogen production mechanism. Reprinted with permission from [213]. Copyright 2018 American Chemical Society. (b) Schematic illustration of the one-pot solvothermal synthesis of Au@PCN(Co)70. Reprinted with permission from [221]. Copyright 2023 Elsevier. (c) Illustration of a 2D MOFs photocatalyst synthesized through in-situ partially reducing the Ti-based MOFs with Pt embedded in the porphyrin center (TMF—Pt). Adapted with permission from [225]. Copyright 2023 Elsevier. (d) Crystal structure of Co-MOF with color code: Co, green; O, pink; N, blue; C, gray. Reprinted with permission from [215]. Copyright 2018 American Chemical Society. (e) Mechanism of photoinduced carrier dynamics for Pt@NH_2-UiO-66/CdS, with a hole-trap transfer pathway for enhanced HER photocatalytic activity and (f) Band diagram of photocatalytic processes in Pt@NH_2-UiO-66/CdS. Reprinted with permission from [224]. Copyright 2022 Springer Nature.

ligands demonstrate an excellent photocatalytic response under visible light irradiation due to their UV–vis absorption spectrum displaying the characteristic Soret and Q bands [216]. For instance, different MOFs incorporating tetrakis(4-carboxyphenyl) porphyrin as a ligand were demonstrated to be particularly efficient in the hydrogen production under visible light irradiations [217–219]. Additionally, the introduction of a metal centre in the porphyrin ligand enhances the efficiency of separation of electrons and holes. Metalloporphyrin ligands included in Co- [220], Zr-based [221] MOFs were successfully synthesized by a one-pot solvothermal method (Fig. 6 **(b)**) and used for photocatalytic hydrogen production under visible light irradiation. Modification at the metal node level have also been the focus of patented technologies. For example, Kyriakos et al. presents Ti-based MOFs characterized by single or multiple ligand types [222]. The use of Ni_2P as a co-catalyst boosts the HER to 0.89 mmol/g_{cat}·h under visible light irradiation.

Despite the recent efforts in developing co-catalyst-free systems, the literature of photocatalytic hydrogen production is still dominated by co-catalyst-decorated MOFs. The co-catalysts are typically noble metal nanoparticles that (i) trap the electrons resulting in an enhancement of the separation of the photoinduced charges, and (ii) offer reducing active centers for the protons. These nanoparticles can be either pre-synthesized or generated in situ during the synthesis of the MOF.

Ti-based MOFs with Pt embedded in the porphyrin center and loading Pt nanoparticles (Fig. 6 **(c)**) have recently demonstrated a remarkably high photocatalytic HER (33.2 mmol/g_{cat}·h) under visible light irradiation [220]. The preparation method and the applications of this highly efficient MOF have been patented in 2022 [223]. A newly patented catalyst features a hollow structure derived from MIL-68 (In). This innovative heterojunction catalyst, in the form of a MOF composite material, demonstrates exceptional capabilities in the synergistic photothermal reforming of methanol. The optimal HER is achieved at 210 °C, reaching a peak of 67.4 mmol/g_{cat}·h. The remarkable potential of MOFs for photocatalytic hydrogen production is largely due to the efficient charge separation. For instance, a ternary composite Pt@NH_2-UiO-66/CdS achieved an AQY of 40.3% at $\lambda > 400$ nm irradiation, attributed to charge separation following an efficient photogenerated hole-transfer band-trap pathway [224] (Fig. 6 **(e)-(f)**).

2.2.2. *Covalent organic frameworks*

Covalent organic frameworks (COFs) display outstanding catalytic properties such as exceptional porosity and large specific surface area. In contrast to MOFs, COFs showcase higher thermal and chemical stability, attributed to the absence of the fragile coordination bonds between metal nodes and organic linkers. Their purely covalent backbones confer enhanced resistance to hydrolysis and photoinduced degradation, making COFs particularly attractive for photocatalytic applications under aqueous and prolonged light-irradiation conditions [226]. COFs' physical and chemical characteristics can be altered by changing the building block allowing for molecular control of their band gap configuration. Being non-metal containing systems, COFs typically exhibit reduced overall costs compared to metal containing structures and significantly align with the principles of green chemistry and sustainability. However, it is worth noting that despite some pristine COFs have been tested for the photocatalytic hydrogen production, their activity is often limited by inefficient exciton dissociation and rapid electron-hole recombination, and the incorporation of metal co-catalysts is therefore frequently required for improved performances. Photogenerated charge separation in COFs is typically governed by exciton generation within π-conjugated domains, followed by exciton migration and dissociation at donor-acceptor interfaces or cocatalyst junctions [226,227]. As a result, integrating electron donor-acceptor molecules is a typical strategy to design COFs with improved electron-hole separation and charge transport efficiencies. For instance, Wang et al. constructed a vinylene-linked π-conjugate using benzotrithiophene as the donor moiety and the electron-deficient benzobisthiazole and cyanovinylene linkages as the acceptor units. The strong donor-acceptor coupling within the BTH-3 framework enabled efficient exciton separation and electron migration toward Pt cocatalyst sites resulting in a HER of 15.1 mmol/g_{cat}·h and AQY of 0.79% ($\lambda = 420$ nm) in the presence of TEOA [228]. Similarly, Yu et al. synthesized a PETZ-COF combining tetraphenylethylene as an electron donor moiety and thiazolo[5,4-d] thiazole as an electron acceptor moiety. With the assistance of Pt as a co-catalyst the system exhibited a HER of 7.23 mmol/g_{cat}·h and AQY of 2.7% ($\lambda = 420$ nm) using ascorbic acid as a sacrificial agent [229]. Zhao et al. further demonstrated that structural regulation at the molecular level can directly influence exciton dissociation efficiency by tuning the spatial separation between acceptor units. By adjusting the space length between triazine and 2, 2'-bipyridine moieties, the resulting NKCOF-113-M facilitated enhanced exciton dissociation and charge transport. Assisted by Pt as a co-catalyst, the system exhibited a HER of 13.1 mmol/g_{cat}·h with an outstanding AQY of 56.2% at $\lambda = 475$ nm [230].

The immobilization of functional groups on the backbones of the COF's building unit is another common strategy to facilitate the separation and transfer of photogenerated electrons and holes. For instance, electron-absorbing functional groups such as strongly electronegative halogen atoms can regulate the localized electron cloud density and suppress the electron-hole recombination rate. Chen et al. synthesized a Py-ClTP-BT-COF via polycondensation of chlorinated benzothiadiazole (BT) units. Using Pt as a co-catalyst, this photocatalytic system revealed an HER of 8.87 mmol/g_{cat}·h and an AQY of 8.5% ($\lambda = 420$ nm) in the presence of ascorbic acid as a sacrificial agent. The fluorination of BT units, resulting in the Py-FTP-BT-COF showed a decreased photocatalytic activity (2.87 mmol/ g_{cat}·h) [231]. The cyano group is an alternative electron-absorbing functional group. Cyano-substituted alkene-linked COFs yielded a HER of 2.33 mmol/g_{cat}·h under visible light irradiations, significantly higher than the corresponding imine- and imide-linked counterparts (< 0.04 mmol/ g_{cat}·h) [232]. An extraordinary activity (HER of 112 mmol/g_{cat}·h) with AQY up to 82.6% was recently reported for nanosheets obtained by ball milling of cyano-COFs using Pt as a co-catalyst. This was ascribed to the substantially prolonged charge carrier lifetime due to the incorporation of the β-ketene-cyano group as a donor-acceptor pair into the COF nanosheet.

Ma et al. reported the synthesis of a sp^2-carbon-linked triazine based COF (COF-JLU100) characterized by exceptional crystallinity and large BET surface area (1223 m^2/g). The cyano-vinylene segments of the framework extended the visible-light response range resulting in more photogenerated carriers and high HER (107.38 mmol/g_{cat}·h) [233]. Powder X-ray diffraction patterns demonstrated that the adoption of a gradient heating synthesis method enhanced the degree of structural order of the framework compared with traditional processes, favoring the transport of the photogenerated electrons.

The development of heterojunction hybrids-based COFs proves to be an efficient strategy for mitigating the electron-hole recombination issue arising from the poor electrical conductivity of COFs. He et al. engineered a COF with periodically ordered π skeletons and immobilized $[Mo_3S_{13}]^{-2}$ reaction centres. This framework facilitated efficient electron transfer from the antennae to the catalytic centres. Characterized by ligating walls and hydrophilic channels, these photocatalytic systems achieved a HER of 11 mmol/g_{cat}·h and a AQY pf 3.6% (600 nm) without the use of a noble metal co-catalyst [234]. Shen et al. synthesized a Ni-intercalated fluorenone-based COF (Ni-COF-SCAU-1), which exhibited excellent HER (197.46 mmol/g_{cat}·h) and AQY (43.2 at 420 nm). The strategic insertion of Ni at the interface was observed to polarize the electric field in COF-SCAU-1, thereby enhancing exciton dissociation info free charge carriers and accelerating their transfer from the bulk to the surface [235].

While a significant portion of these materials incorporates noble metals as co-catalysts, examples of COFs used as photocatalysts without the need for a co-catalyst have also been documented [236]. The patents predominantly emphasize COF preparation methods, with a particular emphasis on solvothermal synthesis. Li and Wang recently documented

the performance of a 2,4,6-tris(4-aminophenyl)-1,3,5-triazine (TAPT) COF, demonstrating an exceptional HER of 33.91 mmol/g_{cat}·h when utilizing TEOA as a sacrificial agent [237]. Synthesis methods of particular interest are those that obviate the necessity for ultrahigh vacuum conditions, possess mild operating parameters, entail brief synthesis durations, and exhibit low energy consumption, rendering them suitable for large-scale production. In this context, a patented solid-phase method has been developed to synthesize a single-atom Pt-embedded COF [238]. This COF has also been synthesized using a microwave-assisted solvothermal approach, demonstrating its application in hydrogen production from seawater with a notable production rate of 41.3 mmol/g_{cat}·h, utilizing ascorbic acid as a sacrificial agent [239].

2.2.3. Conjugated polymers

Linear conjugated polymers, consisting of one-dimensional skeleton photoactive π-systems, stand as an appealing platform for the facilitation of photocatalytic hydrogen production. Distinguished by their unique electronic structures, these systems efficiently absorb light across a broad spectrum, encompassing visible and near-infrared regions. Key advantages of conjugated polymers lie in their tunable electronic and optical properties, facile synthesis under mild operating conditions, and robust chemical stability which mitigates concerns related to photobleaching.

Moreover, the inherent π-conjugation along the polymer backbone enables them with unique photogenerated charge carrier separation and transport properties. Upon photoexcitation, tightly bound excitons are generated along the conjugated chains; their dissociation typically requires internal donor-acceptor motifs, backbone polarization, or interfaces with cocatalysts that provide energetic driving forces for charge separation. This feature is critical to catalyze photoredox reactions, underscoring the key role that conjugated polymers play in the intricate interplay of processes leading to hydrogen production [240]. Band-structure regulation through backbone copolymerization, heteroatom incorporation, and side-chain engineering has been shown to reduce exciton binding energies, extend carrier lifetimes, and improve directional charge transport toward catalytic sites. Over the last few decades, a diverse array of reactions has been utilized in the synthesis of linear conjugated polymers, including Sonogashira–Hagihara coupling, Suzuki–Miyaura cross-coupling, Yamamoto coupling, Heck coupling, Friedel–Crafts alkylation, Schiff base reaction, among others. The selection of the appropriate synthetic method and the adjustment of the reaction operating parameters allow the incorporation of various building blocks in the polymer skeleton providing greater flexibility in the synthesis [241]. Importantly, recent mechanistic studies have also highlighted degradation pathways in conjugated polymer photocatalysts under aqueous and prolonged illumination – such as backbone oxidation or recombination-induced deactivation – emphasizing the need to couple electronic optimization with stability-oriented molecular design [242].

A common strategy to form highly delocalized conjugated systems is introducing planar conjugated building blocks into the skeletons of linear conjugated polymers. For example, Yang et al. synthesized a series of linear conjugated polybenzothiadiazoles by alternating the substitution position of the electron-withdrawing benzothiadizole unit on the phenyl unit as a co-monomer [243]. A similar donor-acceptor functionality was identified in a PyDTDO-3 conjugated polymer which exhibited a notable HER of 50.2 mmol/g_{cat}·h when combined with carbon nitride in an S-scheme heterojunction [244].

Sprik et al. synthesized a series of para-substituted low molecular weight oligo(phenylene)s and poly(*p*-phenylene)s that incorporated planarized units such as fluorenes, carbazoles, and dibenzo[*b*,*d*]thiophene [245]. Among these structures, the incorporation of the dibenzo[*b*,*d*]thiophene sulfone unit in the planarized *co*-polymer exhibited a HER of 1.49 mmol/g_{cat}·h with an AQY of 7.2% without the addition of any metal co-catalyst.

Sulfone units also showed excellent hydrogen production rates when incorporated into a homopolymer of dibenzo[*b*,*d*]thiophene [246]. The introduction of hydrophilic groups into the side chain has been shown to enhance the interaction between water molecules and the photocatalyst surface through the formation of hydrogen bonding. For instance, the conjugated polymer PF6A-DBTO2, functionalized with adenine, demonstrated a HER of 21.93 mmol/g_{cat}·h in the absence of a metal co-catalyst under visible light conditions[247].

Heterojunctions based on conjugated polymers are frequently encountered in patent literature. A recent patent describes the synthesis method and photocatalytic application of an innovative heterojunction comprising a halogenated aromatic linear conjugated polymer and g-C_3N_4. This novel heterojunction demonstrated a notable HER of 49.21 mmol/g_{cat}·h, accompanied by an AQY of 46.7 at $\lambda = 475$ nm. The polymer was synthesized through Suzuki or Stille coupling reactions [248]. Kosco et al. patented a novel photocatalyst exhibiting an exceptional hydrogen evolution reaction, achieving a rate of 64.43 mmol/g_{cat}·h. This system featured a heterojunction between a donor polymer (PTB7-Th) and a non-fullerene acceptor (EH-IDTBR) within Pt-decorated organic nanoparticles [249].

As extensively reviewed in Section 2.2, organic photocatalysts primarily derive their performance from structural attributes rather than from intrinsic electronic properties. Their exceptionally high surface areas, tunable porosity, and modular chemical design enable precise control over light absorption and reactant accessibility. However, their photocatalytic performance is often constrained by poor intrinsic electrical conductivity and strong exciton binding, which hinder efficient charge separation and long-range charge transport. As a result, many high-performing organic systems rely on noble-metal co-catalysts or donor-acceptor molecular engineering to approach or exceed the activity of state-of-the-art inorganic photocatalyst. When such strategies are successfully implemented, exceptionally high HERs can be achieved, in some cases rivaling or surpassing inorganic benchmarks.

2.3. Photocatalytic materials in large-scale applications

This section has reviewed a large number and wide range of materials for photocatalytic hydrogen production, however the transition of these materials from laboratory-scale proof-of-concept to industrial viability requires a significantly broader evaluation. In the laboratory setting, HER and AQY remain the primary metrics for evaluating material performance. Large-scale deployment however relies on more comprehensive performance metrics, for example material and process stability, precursor cost and availability, synthesis scalability, and life-cycle sustainability [250]. A summary analysis of the materials discussed above is therefore presented here.

TiO_2 represents the current benchmark for stability and cost-effectiveness among inorganic semiconductors for large-scale applications. The viability of TiO_2 is supported by established production methods and supply chains, and it offers excellent resistance to photocorrosion. However, the general reliance on UV irradiation – which represents less than 5% of the solar spectrum at the Earth's surface of TiO_2 limits solar-to-hydrogen (STH) efficiency, rendering it economically less feasible for standalone solar hydrogen production applications in its unmodified form [251]. The large-scale viability of TiO_2 does not however extend to other inorganic semiconductors, such as metal sulfides and oxides, for which established large-scale production methods do not always exist, and which suffer more readily from photocorrosion.

Doping (metal and non-metal) and dye sensitization can shift absorption of inorganic semiconductors into the visible range, mitigating the reliance on less abundant UV light. While doping strategies may be scalable, they can often introduce recombination centers that limit quantum efficiency. Dye-sensitized systems, despite superior visible-light harvesting, suffer from critical instability due to dye desorption and photobleaching under long-term irradiation, making them largely unsuitable for robust, large-scale photoreactors [250,251]. Inorganic semiconductor heterojunctions offer significant potential for efficiency

in large-scale applications by spatially separating charge carriers, minimising recombination. However, the complexity of synthesizing multi-component interfaces at scale introduces significant reproducibility challenges and high capital expenditures (CAPEX), necessitating precise engineering that may offset efficiency gains[252]. MOFs and COFs provide unparalleled surface area and structural tunability. However, as previously discussed, MOFs can struggle with instability, and the cost of organic linkers remains prohibitive for large-scale production. COFs improve upon the stability of MOFs via robust covalent linkages and offer a metal-free alternative, however their synthesis typically requires expensive monomers and long crystallization times, limiting their cost-effectiveness. Graphitic carbon nitride benefits from the use of earth-abundant, low-cost precursors (e.g., urea, melamine) and simple thermal syntheses, and offers excellent chemical stability in aqueous environments. The efficiency of g-C_3N_4 in bulk form can however suffer due to low surface area and high charge recombination [253]. Finally, conjugated polymers offer molecular tunability of electronic and optical properties, allowing use of the full solar light bandwidth and improved efficiency. Metal-free versions reduce environmental toxicity, but metal doping is often required to achieve suitable efficiencies [253].

3. Sacrificial agents: choice and mechanism

The simultaneous treatment of wastewater and hydrogen production presents a dual-purpose solution, enabling both sustainable energy generation and environmentally responsible wastewater management [254]. Fig. 7 illustrates the growing interest and expanding research efforts in utilizing wastewater for hydrogen generation, highlighting the continued need for development and innovation in this field. Tak et al. [255] reviewed a variety of systems designed to evaluate the potential of wastewater for generating hydrogen-rich gas. These technologies employ distinct mechanisms, varied configurations, and procedures. The technologies were broadly classified into three distinct categories: light-dependent, light-independent, and other approaches. Given the scope of this review, we will focus specifically on the advantages of light-dependent technologies that employ photocatalysts.

Several studies have provided innovative approaches to the simultaneous wastewater purification and hydrogen production [184,254,256–258]. In 2022, Wang et al. [257] reported the use of Bi-assisted modified CdS/TiO_2 nanotube arrays with ternary S-scheme heterojunction for hydrogen production from photoreforming. The photocatalyst exhibited significant performance, achieving an 85.41% rhodamine B and 100% methylene blue degradation efficiency. The rate of hydrogen production achieved a value of 3.15 mmol/g_{cat}·h and remained constant for four consecutive cycles. Wei et al. [259] conducted a study on the degradation of antibiotic-containing wastewaters using 8% $MoS_2@Zn_xCd_{1-x}S$ material. After a duration of 5 h, a total of 630 μmol of hydrogen was generated through a 30% reduction of amoxicillin. Nevertheless, the photocatalyst exhibited inadequate stability, attributed to surface poisoning. Carbon QD/$KNbO_3$ composites also represent environmentally friendly photocatalytic systems for wastewater treatment, with simultaneous hydrogen production. The experimental findings demonstrated that the crystal violet dye degradation rate and HER were 70% and 0.47 mmol/g_{cat}·h in 4 h, respectively [260]. Moreover, Zhang et al. [258] reported the exceptional performance of the hierarchical assembly of $ZnIn_2S_4$ on reduced graphene oxide (RGO) and MoS_2 QDs. This composite material was employed for the purpose of wastewater treatment and hydrogen production. The RGO facilitates electron transfer, and the highly dispersed MoS_2 increases the number of exposed catalytic sites. Further experimentation was conducted to evaluate the photocatalytic purification of rhodamine B (RhB), eosin Y (EY), fulvic acid (FA), methylene blue (MB), and p-nitrophenol (PNP). The degradation efficiencies and TOC removal rates were 91% and 75% for PNP, 92.2% and 72% for FA, 98.5% and 80% for MB, 98.6% and 84% for EY, and 98.8% and 88% for RhB, respectively. In a related study, Iervolino et al. [261] demonstrated hydrogen production from glucose degradation in wastewater using an optimized 67 wt% Ru-doped $LaFeO_3$ photocatalyst. Complete glucose degradation and hydrogen production of 5.46 mmol/L was obtained after 4 h of irradiation.

Nasr et al. [262] performed a feasibility analysis on an up-flow anaerobic staged reactor (UASR) to assess its potential for generating hydrogen from starch wastewater. The study reveals that in acidic conditions, the UASR reactor successfully generated hydrogen with a

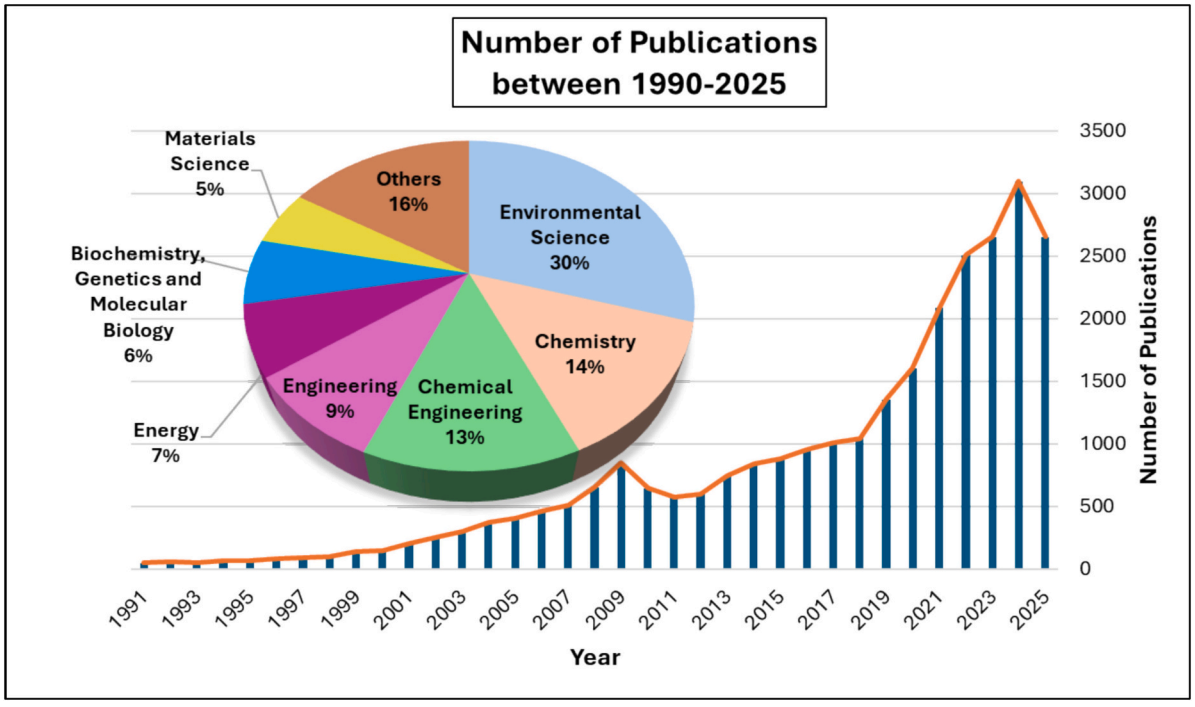

Fig. 7. Statistics of hydrogen and wastewater publications during the 1990-2025 period.
(Scopus database for the search "Hydrogen and wastewater" in all subject areas.)

yield of 793 L of H_2/kg per COD removed, which accounts for 57% of the theoretical value.

Moreover, a solar pilot plant scale demonstrated the effective treatment of wastewater using a Au/TiO_2 photocatalyst for the dual purpose of simultaneous hydrogen production and organic pollutant removal [263]. The system achieved a hydrogen yield of 6.5 mmol/L after 5 h of irradiation, with an accumulated radiation energy of 100 kJ/L. That study showed that the concentration of dissolved organic carbon (DOC) positively influenced hydrogen generation, whereas the ionic strength associated with dissolved inorganic salts (e.g., NaCl and Na_2SO_4) had a detrimental effect. The optimal rate of photocatalytic hydrogen production was achieved when formic acid was used as the sacrificial agent.

4. Review of reactor configurations

While most reported photocatalytic reactor designs have been developed at laboratory scale, their relevance to industrial implementation strongly depends on engineering-related aspects that go beyond the conceptual description of the configuration. Issues such as photon utilization efficiency, mass and heat transfer limitations, hydrodynamic behaviour, gas–liquid separation, operational safety, and scalability constraints become increasingly critical as reactor size increases. Therefore, the evaluation of photocatalytic reactors should not only focus on their geometrical arrangement but also on their suitability for continuous operation, ease of maintenance, energy consumption, and integration with auxiliary units required for hydrogen separation and storage.

From an application-oriented perspective, photocatalytic systems offer significant benefits in relation to the environmentally friendly production of H_2 as a result of their straightforward operation, minimal electricity usage, and low maintenance requirements. From a techno-economic perspective, some authors assessed the commercial viability of different solar-driven hydrogen generation technologies by considering their efficiency in converting solar energy into hydrogen, economic feasibility, durability, and sustainability [264]; from this point of view, photocatalytic hydrogen production has the potential to produce H_2 at the lowest cost, both through organic photoreforming and photocatalytic water splitting. Nevertheless, the current efficiency of these processes remains inadequate, therefore necessitating further investigations in controlled laboratory environments. The selection of an appropriate photocatalytic reactor has significant importance in the exploration of photocatalytic processes. Accordingly, photon management, mass and heat transport, hydrodynamics, gas separation, and maintenance requirements vary significantly among different reactor layouts. The representative photocatalytic reactor configurations are reviewed by highlighting their underlying design principles alongside the key engineering challenges and opportunities associated with scale-up and large-scale operation.

From an engineering perspective, photocatalytic reactors at laboratory scale are primarily designed to enable rapid catalyst screening and fundamental studies, rather than to reproduce realistic operating conditions. Although these systems are essential for understanding reaction mechanisms and intrinsic photocatalyst activity, they often neglect phenomena such as light attenuation in large volumes, non-ideal mixing, pressure drop, and heat accumulation. Consequently, performance metrics obtained in small-scale batch reactors cannot be directly extrapolated to large-scale systems without dedicated reactor engineering considerations. Nevertheless, these systems represent a necessary starting point for reactor development and are therefore briefly reviewed below. At the laboratory scale, the majority of photoreactors adopted are flask-type glass batch systems, and for fundamental photocatalyst screening, simple top-down illumination photoreactors are predominantly employed. Wang et al. [265] irradiates the reaction vessel. The simple structure and the enhanced airtightness control reduce the reliance on glass instruments and minimize scattering (Fig. 8). The outer side of the reaction container is covered with a metallic silver layer to reflect light and prevent transmission, improving the light utilization rate. The larger reaction container volume allows a better light utilization, while the circular light spot passes more effectively through the reactor's entrance. As such, their relevance to direct industrial translation remains inherently limited.

Before scaling up to industrial applications, it is indeed important to assess the photocatalytic activity of different photocatalysts. Rapid screening methods that allow high-throughput assessment of photocatalytic performance can significantly enhance research efficiency and accelerate the discovery of new, effective photocatalysts. In this context, some researchers have developed and patented a multi-channel performance evaluation device, using a Pd/WO_3 film able to change the color as a response to different hydrogen concentrations, to quickly screen the activity of a certain photocatalyst in water decomposition. The device simultaneously screens multiple compounds for photocatalytic hydrogen production, and at the same time enables miniaturization of the reactor, which greatly reduces the amount of the compound required for testing [266]. Currently, laboratory-scale photocatalytic reactors often exhibit low light usage efficiency, potentially causing light pollution due to transmission through the observation windows. To address these limitations, some researchers have recently proposed an internally illuminated photocatalytic hydrogen generation reactor [267]. The setup consists of a reactor shell with an open structure at its top end, including an appropriate opening (Fig. 9). The feeding port facilitates the introduction of water and catalysts. The lamp hole enables the insertion or extraction of the lamp post. Additionally, the light post is affixed to the lateral surface of the secondary enclosure and may be deactivated by raising the secondary closure, providing a user-friendly means of operation. In this configuration, the reactor shell contains the water and the catalyst, which are housed within the seat trough. In the presence of the lamp post's illumination, the process of water splitting occurs, resulting in the separation of hydrogen and oxygen. The lamp post is securely positioned at the centre of the reactor shell, ensuring uniform and effective illumination of the surrounding reactants and is equipped with an external protective covering. The side wall of the reactor shell features an internal transparent window, which is shielded by an opaque outer to prevent unwanted light leakage. Additionally, a lateral wall is equipped with an external visual window; both the internal and external windows are aligned on the same horizontal plane. The arrangement of the inner and outer double-layer visual windows, along with the light-blocking outer cover, serves to effectively prevent any leakage of the light source. By utilizing the external visual window, it is possible to monitor the reaction conditions within the reactor shell, while significantly reducing light pollution.

Irrespective of the configuration, photocatalytic reactor performance is governed by the coupled effects of photon transfer, mass transfer, hydrodynamics, and heat management. Reactor geometry directly influences light penetration depth, catalyst utilization efficiency, and gas

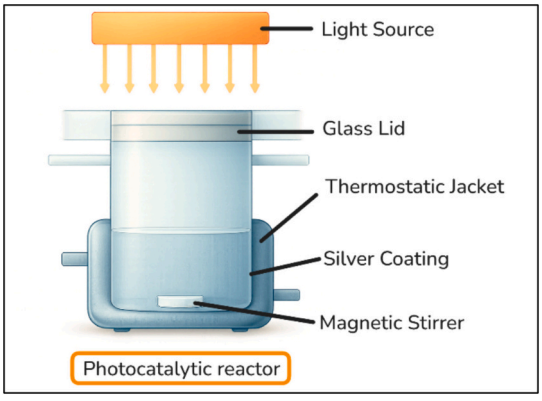

Fig. 8. Schematic representation of a top-down photocatalytic reactor. (Redrawn based on Wang et al. [265].)

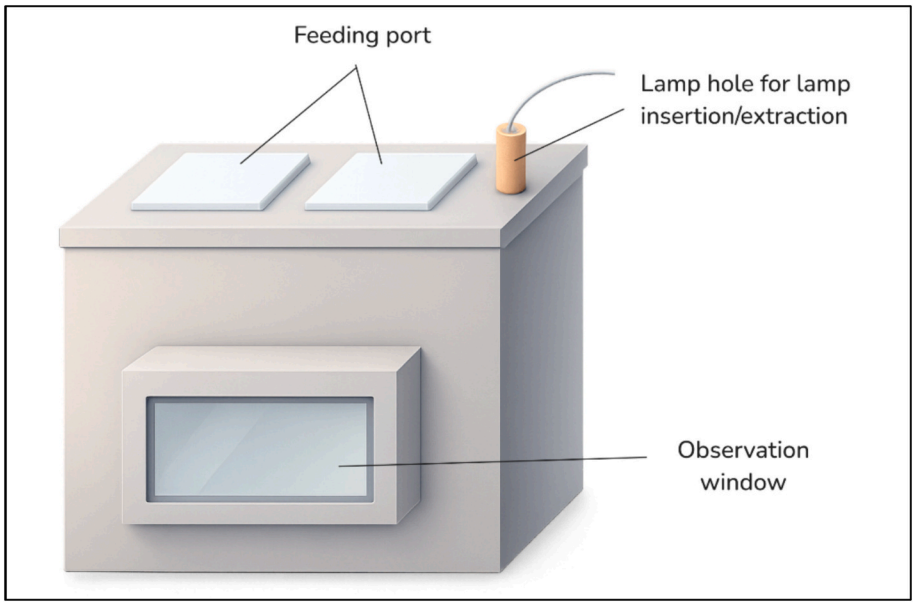

Fig. 9. Schematic representation of an internal illumination photocatalytic hydrogen generation reactor. (Redrawn based on Yang et al. [267].)

disengagement behaviour. The critical design and scale-up of a photocatalytic reactor are essential for the successful implementation of photocatalytic technologies, as these improve process efficiency and reduce the associated costs by maximizing solar energy conversion. Inadequate design often leads to photon oversaturation, catalyst agglomeration, inefficient gas removal, and excessive parasitic energy consumption. For large-scale implementation, reactor engineering must therefore balance: (i) photon management, including light distribution, reflection losses, and solar intermittency; (ii) mass transfer, particularly the transport of reactants to and products away from the photocatalyst surface; (iii) Hydrodynamics, affecting mixing energy, pressure drop, and residence time distribution; (iv) thermal effects, as partial conversion of light to heat can both enhance reaction kinetics and impose material constraints. Advanced reactor models integrating reaction kinetics with radiation transport and fluid dynamics are increasingly recognized as indispensable tools for rational reactor design and scale-up.

For future commercialization of these technologies, large-scale applications, engineering, and design strategies are thus still needed. In particular, there is a specific requirement for the development of a novel photocatalytic reactor system that exhibits high efficiency, cost-effectiveness, and durability. To support future design and implementation, it is essential to evaluate the advantages and limitations of various systems, while advancing system design and prototype development. This will enable the collection of real-time data necessary for accurate and reliable techno-economic feasibility assessments. Building on these fundamental reactor-level considerations, large-scale photocatalytic plant design requires thorough evaluation of additional system-level aspects before engineering calculations can be performed. For an optimal reactor design, it is important to consider numerous factors [268], including (i) tools such as mirrors and reflectors based on dimensions, materials, and cleaning method, (ii) photocatalyst, and (iii) radiation source-based reactor geometry. The industry faces significant challenges in designing and constructing efficient photocatalytic reactors due to complexities such as fluid pumping energy, pressure drop, temperature, tubing materials, and water matrix species. The development of efficient photocatalytic reactors and models [269], which integrate reaction kinetics, hydrodynamics, and both mass and radiation transport phenomena, enables a priori performance prediction and optimisation [270].

When moving toward pilot- and industrial-scale applications, the design of photocatalytic reactors must explicitly address the challenges associated with solar energy utilization, including the low energy density of sunlight, its intermittency, and the need for efficient light collection and distribution over large reaction areas. Reactor configurations such as tubular systems, flat-panel reactors, and concentrator-based designs have therefore been proposed to enhance photon flux while maintaining acceptable mass transfer and hydrodynamic conditions. However, these advantages are often accompanied by increased system complexity, higher capital costs, and stricter requirements in terms of optical alignment and material durability. While academic studies on photocatalytic hydrogen production predominantly focus on catalyst performance and laboratory-scale validation, patent literature places greater emphasis on technological maturity, system integration, and pathways toward commercialization. Specifically, patented solutions often address engineering constraints such as continuous operation, scalability, durability, and gas separation, which are only marginally explored in lab research. The following examples illustrate how these patented reactors attempt to bridge the gap between fundamental research and practical implementation.

In this context, the feasibility of developing and assembling photocatalytic systems on a pilot scale was illustrated more than ten years ago [271,272], by employing tubular reactors and parabolic concentrators for wastewater treatment. More recently, several authors have proposed the use of photocatalyst panels for photocatalytic water-splitting reactors designed for H_2 production [273]. Fattorusso and Puga [274], for instance, invented a photocatalytic panel reactor able to use direct light contact (real or artificial) to degrade wastewater and produce hydrogen. The system consists of a flat-panel reactor (See Fig. 10 **(a)**), featuring a shallow container and a top transparent window able to capture incident light. The photocatalyst is immobilized on a thick bed (1÷100 μm). The simple design and the possibility of using the solar source without the need for light concentration are the most interesting advantages of this setup. With a prototype of 200x300x30 mm^3, the authors reported a hydrogen production of about 0.33 L in the presence of 1.5 L of a solution sourced from a local juice production plant when Pt/TiO_2 was used as photocatalyst with natural sunlight for 3 h (between 12:00 and 15:00, average irradiance of 0.87 kW/m^2). Compared to laboratory-scale photoreactors, this patented configuration explicitly targets operational simplicity, catalyst immobilization, and system robustness,

reflecting a shift from performance-driven laboratory optimization toward engineering solutions suitable for pilot-scale deployment. Other authors [275] including (i) a circulating liquid storage tank (with methanol solution), (ii) a circulating pump, and a (iii) photocatalytic reactor unit (composed of strip-shaped reaction plates and light-transmitting plates along the inclined direction, forming the liquid channel) connected through pipelines (See Fig. 10 **(b)**). A steam drum was installed above the second liquid storage tank for separating and storing hydrogen. The system demonstrated an improved hydrogen production efficiency via methanol photoreforming: by using CoP/TiO_2 composite or WO_3 photocatalyst, 90% of methanol conversion was reached, attributed to the continuous recycling of the liquid stream. Hydrogen production efficiency reached approximately 5% with CoP/TiO_2 and 5.7% with WO_3. In contrast, when the reaction liquid was not recycled, the efficiency dropped to around 2%; notably, one of the key advantages of this system is the reduced overall electricity consumption achieved through the effective use of solar energy. These patented reactor systems highlight a clear technological evolution from batch laboratory reactors toward integrated, continuously operated solar-driven systems. From a commercialization perspective, such designs prioritize liquid recirculation and reduce auxiliary energy consumption, rather than solely maximizing intrinsic photocatalytic activity.

Several studies demonstrated the feasibility of scaling up a photocatalytic hydrogen generation system [276,277]. Additionally, solar photocatalytic tubular reactors on a pilot scale have been designed for H_2 generation from water while utilizing additional organic or inorganic compounds (as hole scavengers). Compound parabolic concentrator reactor (CPC) is one of the most common configurations for photocatalytic H_2 production, as reported by different authors [19,276].

The choice between slurry-based and immobilized photocatalytic reactors represents one of the most critical engineering decisions for large-scale hydrogen production. While slurry reactors typically offer superior mass transfer and higher apparent reaction rates, they introduce additional challenges related to catalyst recovery, continuous mixing, and operational costs. Conversely, immobilized systems simplify downstream processing and improve operational stability but may suffer from reduced photon and reactant accessibility. A comprehensive engineering assessment is therefore required to identify the most suitable configuration for industrial implementation, taking into account efficiency, reliability, and economic feasibility. Patent literature suggests that these two reactor families correspond to distinct commercialization pathways, with slurry-based systems favoring higher reaction efficiency and immobilized configurations offering advantages in terms of operational stability, catalyst recovery, and regulatory compliance. The market competitiveness of each approach therefore depends on the specific application scenario and system integration requirements. Although demonstration prototypes have been developed for photocatalytic H_2 production, the absence of a commercial-scale plant at present can be attributed to the insufficient investigation into industrial-scale systems, and the dearth of dependable data to establish the economic viability of this technology. For example, a significant portion of the literature on photocatalysis focuses on photocatalyst design and engineering. In contrast to slurry/suspension systems, substantial effort has been recently devoted to the construction of large-scale photocatalyst panel-based reactors, where the postreaction treatment requirement is straightforward. Nevertheless, the past achievements of a slurry-based photocatalytic prototype plant, which included its effective construction and increased efficiencies, suggest that photocatalytic H_2 generation is feasible with the proper configuration of a slurry system. Despite the requirement for postreaction catalyst separation, slurry reactors provide a multitude of advantages, including a simple design, a substantial photocatalyst surface area relative to the reactor area, improved light penetration, and enhanced mass transfer. Conducting a methodical evaluation of immobilized and slurry photoreactors in the context of large-scale photocatalytic hydrogen gas production is crucial to ascertain the economic and practical feasibility of each configuration. To address challenges related to the separation of the photocatalytic material, some inventors [278] proposed a photocatalytic reactor design

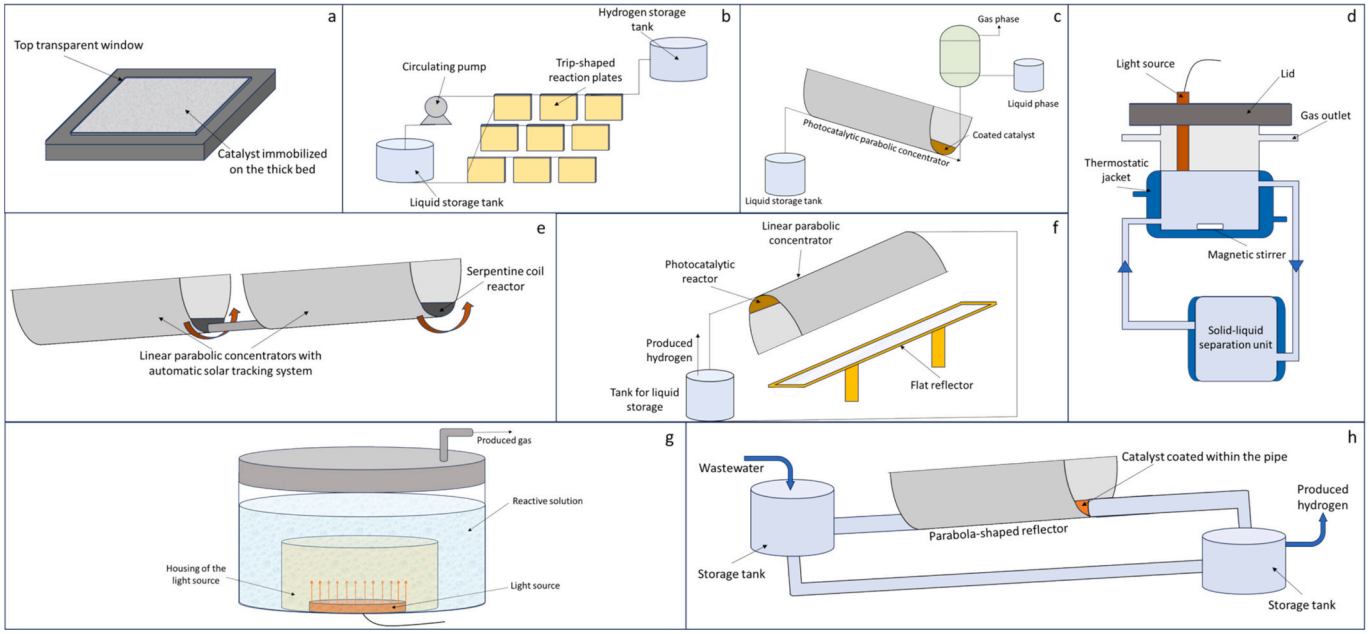

Fig. 10. Schematic representation of different patented configurations for photocatalytic reactors. (a) flat-panel reactor with a shallow container and a top transparent window to capture incident light [274]; (b) Strip-shaped reaction plates with circulating liquid storage tank [298]; (c) Compound parabolic concentrator with fixed-film catalyst and gas-liquid separator [283]; (d) Two-bed photocatalytic decomposition water hydrogen production system composed of a photocatalytic reaction bed and a hole sacrificial regeneration bed [284]. (e) Photocatalytic reactor with high-precision automatic tracking of the sun, with an axial solar focuser and a serpentine coil reactor, placed at the centre of the linear parabolic concentrator [279]; (f) Secondary reflection concentrating system with a linear parabolic concentrator and a flat reflector; (g) Photocatalytic reactor with housing of the light source directly placed in the reaction system [296]; (h) Continuous pipe-based photocatalytic reactor with photocatalyst coated within the pipe [297].

that employs a magnetic mineral as the photocatalyst. This configuration offers a simple and practical solution, allowing seamless integration into a wastewater discharge system by pumping the aqueous mixture directly into the reactor.

The development of large-scale, easy-to-manage, and high-throughput photoreactors is crucial for effective outdoor operation. Various solar reactors have been developed for photocatalytic applications, such as the parabolic trough concentrator (PTC), compound parabolic concentrator (CPC), inclined flat plat reactor (IFPR), thin film fixed bed reactor (TFFBR), and double skin sheet reactor (DSSR). Given the diffuse nature and relatively low intensity of solar radiation, the integration of efficient solar light concentrators is critical for achieving high photocatalytic performance. Numerous efforts have been made to demonstrate photocatalysis feasibility at the pilot scale, highlighting its potential for industrial implementation. However, most of the pilot demonstrations were designed for photocatalytic detoxification or biological purposes, while only a few examples are reported for photocatalytic hydrogen production. Solar photocatalytic degradation and hydrogen production share similarities, such as anautogenous redox reactions, well mixing and high disturbance, and low overall efficiencies. Differences between engineering solar photocatalytic water detoxification and hydrogen-generating reactors include the need for post-processing procedures, separation of photocatalysts, and the requirement of nontoxic photocatalytic materials when treating industrial or biologically contaminated water. Scaling up photocatalytic reactors for hydrogen production presents a promising pathway for sustainable energy storage and to contribute to the transition toward a cleaner and more resilient future energy infrastructure. However, practical applications indicate that most photocatalytic reactors are still constructed and operated at a relatively small scale. To advance the technology, a range of large-scale and cost-effective reactors have been developed for pilot demonstration of direct solar photocatalytic hydrogen production technology. In both academic and patent literature, tubular reactors containing suspended photocatalysts are frequently proposed for this purpose [276,279–281]. Generally, indeed, most studies report hydrogen production normalized to the mass of catalyst used. However, increasing the catalyst loading often leads to reduced efficiency, primarily due to limited light penetration and catalyst agglomeration [282]. Optimizing the amount of photocatalytic material to be used remains a crucial factor in improving the overall process efficiency. In slurry photoreactors, however, the need for continuous mixing introduces additional energy requirements, leading to higher operating costs and challenges in catalyst recovery and reuse. In this context, in 2020, some authors [283] invented a fixed-film solar photocatalytic hydrogen production device, based on a compound parabolic concentrator, which is able to improve the efficiency of the process and reduce the operating costs (Fig. 10 **(c)**). A sinking method was used to improve solar energy utilization and adjust the distribution of concentrated light on the photocatalytic reactor, enhancing the performance. The device includes a liquid storage tank, a photocatalytic reactor with a concentrating component, and a gas-liquid separator. The condensing component includes a compound parabolic concentrator and a plane reflector. The gas-liquid separator separates and removes moisture from the gas outlet. The device also includes an angle adjustment mechanism, a stainless steel or acrylic glass reactor box body, and a silicon rubber gasket. This innovation enhances the photocatalytic hydrogen production process by integrating a condensing unit designed with a compound parabolic concentrator and employing a sinking method to optimize light capture. The parameter measurement component includes a radiometer and a temperature probe. The sinking design improves the utilization rate of solar energy and adjusts the distribution of concentrated light on the photocatalytic reactor, reducing unevenness and improving the overall performance. The reactor cover plate is made of acrylic glass, providing high light transmittance and good chemical, mechanical, and weather resistance. Currently, one of the most commonly employed reactor configurations is a single-bed photocatalytic device, in which the catalyst, hole sacrificial agent, and water are all present within the same reaction bed. However, maintaining a stable hydrogen production in such systems requires the continuous replenishment of sacrificial agents, which limits their practical applicability. The construction of a highly efficient and stable photocatalytic reaction system is crucial for the practical use of solar photocatalytic hydrogen production. Some authors [284] proposed a novel two-bed photocatalytic decomposition water hydrogen production system (Fig. 10 **(d)**). The system consists of a photocatalytic reaction bed and a hole sacrificial regeneration bed, with the water outlet connected to both components. The system features a quartz reactor with a light source and a tank body with a separator for filtering a barrier-reducing active solid chemical agent. Key advantages of this setup include the use of a stable inorganic anion as a hole-sacrificing agent, which undergoes oxidation by photogenerated holes and subsequent regeneration. Additionally, the dual-bed photocatalytic configuration contributes to maintaining a constant concentration of the sacrificial agent, while minimising light-blocking effects.

The utilization of solar energy in the broader field of photocatalysis is predominantly directed toward the degradation of organic matter. Conversely, there are only few studies regarding the direct conversion of water decomposition into hydrogen under solar or visible light radiation [285,286]. Advanced solar concentrating technology and high-efficiency photocatalytic reactors are essential for efficient solar energy utilization [287]. One of the earliest related inventions, proposed in 2007, consisted of a photocatalytic reactor with a stainless-steel support with a local latitude angle, a compound parabolic concentrator fixed by bearings, and a tubular reactor connected in series through PVC pipes [288]. The compound parabolic concentrator is a reflective surface made of a curved surface and an aluminium film coated with alumina. The invention offers advantages such as low cost, adaptability to weather conditions, and the ability to monitor reaction conditions in real-time. The number of composite parabolic concentrators and tube reactors can be arbitrarily increased or decreased according to design requirements, making it applicable to various fields and facilitating further scale-up. More recently, a new photocatalytic reactor with high-precision automatic tracking of the sun was invented [279] (Fig. 10 **(e)**) to maximize solar energy use and improve the efficiency in terms of hydrogen production. The photocatalytic reactor was mainly composed of an axial solar focuser and a serpentine coil reactor, placed at the centre of the linear parabolic concentrator. Among the key advantages of this invention are the effective mixing between the introduced catalyst and the reaction medium, as well as the integration of an automatic solar tracking system. However, despite the presence of solar tracking, the incident angle of the solar radiation remains a critical parameter influencing the efficiency of photocatalytic hydrogen generation. When the angle deviates from perpendicular, there is a significant decrease in the usage rate of sunlight, reducing the overall photocatalytic efficiency. To overcome this limitation, some authors [289] proposed a secondary reflection concentrating system (Fig. 10 **(f)**) and explored its potential application in a photocatalytic hydrogen production reactor. The secondary reflection concentrating system consists of several components, including a linear parabolic concentrator and a flat reflector. The linear parabolic concentrator is positioned with its concave surface facing the flat reflector. The mount is stationary, and the upper end of the mounting seat contains both a polar axis and a main rotating shaft. Lastly, the flat reflector is mounted onto the polar axis. In addition to the aforementioned approach, it has been proposed to incorporate a photosensitive element within the concave inner region of the flat reflector. The circulation system consists of a tube for the photocatalytic water splitting hydrogen generation process, a tank for liquid storage, and two pipes for circulation. The tube for the reaction of photocatalytic water splitting and hydrogen production is positioned at the concave focal point of the linear parabolic concentrator. As an additional favorable approach, the photocatalytic water splitting, and hydrogen production reaction tube is constructed using a glass fibre mesh that is

coated with a photocatalyst. Furthermore, the photosensitive component is situated on the photocatalytic water splitting and hydrogen production reaction tube. This modification enhances the efficiency of solar energy utilization and enables the adjustment of light concentration on the distribution of the photocatalytic water splitting hydrogen production reactor. Consequently, this adjustment facilitates the enhancement of photocatalytic hydrogen production performance. Compared to the average HER of 0.4 mmol/g_{cat}·h achieved with a single linear parabolic concentrator; the present invention achieved an improved average HER of 0.9 mmol/g_{cat}·h. This demonstrates that the utilization of secondary reflection in this process significantly enhances the efficiency of photocatalytic water splitting for hydrogen generation. The hydrogen yield resulting from the utilization of a flat mirror concentrator is, on average, 2.2 times greater than that obtained with a single linear parabolic concentrator. This design enhances the utilization of solar energy and is adaptable to the operating requirements across various latitudinal locations. Additionally, the system is noted for its ease of installation and commissioning in practical engineering applications.

In addition to reactor performance, large-scale photocatalytic hydrogen production imposes stringent safety and process integration requirements. The simultaneous generation of hydrogen and oxygen, together with the need for gas separation and thermal management, introduces additional design constraints that are often negligible at laboratory scale. Addressing these aspects at the reactor design stage is essential to ensure safe operation, reduce auxiliary energy consumption, and improve the overall efficiency of the photocatalytic system.

The comparison between academic and patent literature reveals a persistent gap between laboratory-scale innovation and commercial deployment. While academic research continues to emphasize photocatalyst activity and reaction efficiency, patented technologies increasingly focus on system integration, operational reliability, and compliance with industrial constraints. Safety concerns associated with hydrogen production and storage represent a major obstacle to practical large-scale implementation [290–292]. Indeed, the production process involves the coexistence of hydrogen and oxygen and requires the development of a reliable method to effectively separate them. Current approaches involve the utilization of argon gas combined with a two-stage membrane gas separation technique [293]. However, one of the membranes, designed for separating argon and oxygen, generally requires elevated operating temperatures, thus increasing the external heating equipment and costs and expanding the land utilization area. To address this issue, some inventors proposed the use of a heat-absorbing component in combination with the photocatalytic reactor unit [294]: the heat-absorbing component captures sunlight at higher wavelengths that are not used in the photocatalytic hydrogen production process, thereby generating heat. The generated heat is then transferred to the separation unit, eliminating the need for supplementary electric heating devices or heat concentrators.

Reducing the costs of the photocatalytic processes is crucial for the effective applicability of these systems to industrial scale. Although photocatalytic processes are typically studied at 25 °C, temperature clearly plays a great role on the reaction rate. The conversion of the light radiation into thermal energy can decrease the costs of the auxiliary electric energy supply [295]. In these regards, some authors [296] have proposed the heating of the reactant solution by using the exhaust heat from a light source, by placing the housing of the light source directly in water, bringing the water into direct contact with the surface of the light source device that generates heat (See Fig. 10 **(g)**). This feature eliminates the heating costs thereby improving the overall energy efficiency. Based on the above-mentioned issues, several authors have proposed some reactor configurations which can be suitable to address one or more issues that currently hinder the industrial applicability of the photocatalytic processes. Most of the photocatalytic reactors, for example, are not suitable for use at elevated temperatures and pressures (i.e., temperatures higher than 100 °C and/or pressures above 150 kPa). Consequently, some authors [297] invented a robust continuous pipe-based photocatalytic reactor in which the photocatalyst is coated within the pipe, able to operate up to 125 °C and 200 kPa (See Fig. 10 **(h)**). The pipes, with different thickness (0.5 ÷ 50 nm) based on the required operative pressure, can be elongated and used in modules (100 or more photocatalytic reactors), under real or simulated solar conditions. In the case of solar-based processes, a parabola-shaped reflector, such as a parabolic mirror, and a heliostat were used to improve the light efficiency. In the case of artificial light, a prism was used to use a different radiation wavelength based on the photocatalyst used, thus using the unfocused portions for other purposes.

5. Challenges, cost assessment, and opportunities

The primary hurdles associated with photocatalytic reforming arise from the complex matrix of authentic (real) wastewater, which typically contains complex organic compounds, inorganic ions, and suspended solids. These components can adsorb strongly onto the photocatalyst surface, blocking the active sites, hindering light penetration and absorption, and permanently poisoning the catalyst, thereby reducing the catalytic activity over time [299–302]. These components can compete with the target pollutants or the reduction reaction itself [303]. For example, dissolved organic matter acts as a radical scavenger, consuming highly reactive species (OH) intended for pollutant degradation [304]. In addition, inorganic ions such as chloride, sulfate, carbonate and bicarbonate can exhibit inhibitory effects by scavenging reactive oxygen species or occupying active sites [305–307]. Suspended solids and turbidity in wastewater significantly scatter and absorb incident light, reducing the amount of radiation reaching the catalyst surface and severely compromising the photo-catalytic reaction rate [308]. Unlike simulated wastewater with controlled conditions, the ever-changing composition, concentration, and pH of actual effluent make consistent performance challenging. In addition, photocorrosion is also a challenge especially for the sulfide-based photocatalyst such as CdS, although metallic co-catalyst can help inhibit this [257]. Researchers have developed several strategies to mitigate these negative effects and optimize dual-functionality systems. One of the strategies is employing multi-component systems to improve charge carrier separation and utilization, extending the catalyst lifetime and operational stability. Two-dimensional Ti_3C_2 Mxene nanosheets and MoS_2 QDs blended with $ZnIn_2S_4$ on reduced graphene oxide enhanced RhB degradtion (around 98%) and allowed for measurable hydrogen production of 45 μmol. MXene materials specifically offer good electrical conductivity and a large specific surface area, promoting efficient charge separation and transport to active sites [258]. Incorporating defects, such as molybdenum vacancies in MoS_2, increases active sites and suppresses carrier recombination, leading to enhanced hydrogen production rates, highly beneficial when competing reactions are present [180]. Also, using noble metal protection such as depositing Bi nanoparticles acts as an electron recombination center and successfully inhibits the photocorrosion of sulfide-based materials such as CdS in the CdS/Bi/TiO_2 heterojunction, thus enhancing stability for simultaneous wastewater treatment and hydrogen production [257]. Another alternative is processing optimization, such as integrating the photocatalytic step with upstream treatments reduces the load of inhibitory substances. Advanced Oxidation Processes utilizing UV and H_2O_2 have been successfully implemented as pre-treatment for municipal wastewater to remove turbidity and Total Organic Carbon (TOC) before membrane filtration, improving overall water quality and subsequent process efficiency. In addition, adjusting the solution pH can optimize the reaction environment to favor either hydrogen production or pollutant degradation, as the reaction kinetics of many organic pollutants are highly pH dependent. For instance, moderate pH conditions can mitigate hydroxyl radical scavenging, promoting pollutant degradation [304]. Advanced engineering solutions also involve high-efficiency flow reactors like the NETmix which enhances mass transfer to overcome diffusion and

surface fouling limitations, thereby maintaining a consistent, effective reaction environment [309].

A comprehensive cost assessment of using wastewater for hydrogen production is necessary to understand the economic feasibility of this technology and to identify the key cost drivers. This assessment should consider various factors such as capital and operational expenses, energy consumption, the type of wastewater, the technology used for hydrogen production, the scale of production, the location of the plant, revenue streams from hydrogen sales, and byproduct utilization. By systematically analysing these costs and benefits, stakeholders can make informed decisions regarding the implementation of wastewater-based hydrogen production technologies. Hönig et al. [310] investigated the feasibility and potential benefits of integrating hydrogen production with wastewater treatment processes. Through an analysis of techno-economic factors, the study evaluates the levelized cost of hydrogen (LCOH) and assesses the economic viability of this integrated approach. The findings suggest that utilizing byproduct oxygen can significantly lower the LCOH of hydrogen production and increase energy efficiency, thereby improving the economic feasibility and sustainability of hydrogen fuel generation. In addition, Jing et al. [311] recently published a study detailing the conceptual design and techno-economic assessment of a novel hydrogen energy production method that is combined with a water treatment and recovery process. The study assesses the potential advantages of utilizing wastewater treatment in the framework of a synergistic hydrogen production strategy. Two separate scenarios were evaluated for supplying the required thermal energy to the electrolyser. In the first scenario, thermal energy is supplied by a fossil fuels-powered preheater, while the second scenario sources the required thermal energy from a solar farm equipped with parabolic trough collectors (PTCs), designed based on the geographical data of Dubai (UAE). By incorporating renewable energy sources into fossil fuel-powered facilities, it is possible to reduce the release of greenhouse gases and enhance the overall sustainability of wastewater treatment and hydrogen generation operations. The findings indicated that the Levelized cost of hydrogen (LCH) increased by roughly 38.7% in the second scenario compared to the first scenario. The increased value of LCH in the second scenario can be attributable to the significant capital expenditure linked to solar collectors. Furthermore, the overall conversion efficiency for the proposed hydrogen production technique was calculated to be 53.3%. The suggested technology demonstrates a notable level of competitiveness and dependability in terms of diminishing water use. While the utilization of a PTC-based solar farm instead of a heater result in a higher cost for producing hydrogen fuel in the suggested approach, the environmental advantages of utilizing solar energy in contrast to fossil energy can be considerably more substantial.

Nasr et al. [262] provided a comprehensive cost and economic analysis of a fully operational starch wastewater treatment facility with a capacity of 400 m^3/d. According to the estimate, the starch wastewater treatment plant would recoup its initial investment in 5.75 years, with an internal rate of return of 12%. The biogas profit from hydrogen generation reached a peak of 5.3 ± 0.57 US$/GJ in comparison to the global gas price range of 7-8 US$/GJ. In 2022, Barghash et al.[312] conducted two case studies on the Al Ansab sewage treatment plant located in the governate of Muscat, Oman. The study assesses the viability of utilizing treated effluent as a water supply to produce green hydrogen through proton exchange membrane (PEM) electrolysis, as depicted in Fig. 11. The electrolysis system consists of an electrolyzer stack, a power supply system, a hydrogen and oxygen separator, and a storage facility. The findings indicate that the revenue generated by Al Ansab STP in a traditional scenario amount to 7.02 million OMR per year. However, adopting sustainable alternatives to generate hydrogen through the Proton Exchange Membrane (PEM) electrolyzer system would yield higher revenues. Specifically, a capacity of 1500 kg H_2 per day would result in an annual revenue of 8.30 million OMR, while a capacity of 50,000 kg H_2 per day would generate an annual revenue of 49.73 million OMR.

The electrolytic synthesis of hydrogen generates oxygen as a by-product, which can enhance the efficiency and effectiveness of the wastewater treatment process during the aeration phase. Gameron et al. [313] conducted a case study using Northern Ireland Water's wastewater treatment network. That study examines the viability of integrating a wastewater treatment plant with a hydrogen facility at the same location and assesses the economic and technological feasibility of this combination. The findings indicate that although the introduction of concentrated oxygen injection can enhance the effectiveness and capacity of the water treatment procedure, the combined worth of tangible and intangible advantages is projected to be less than 1% of the market value of the necessary oxygen. The study proposes that by-product oxygen could serve as a concentrated oxygen source. This oxygen may be utilized to reduce the cost of hydrogen production or to recover energy, potentially offsetting approximately 0.5%–2% of the energy required for hydrogen generation. Overall, the study suggests that co-locating wastewater treatment plants and hydrogen facilities is a viable option for improving energy efficiency and reducing emissions.

As highlighted in this section, the use of wastewater for hydrogen production offers a sustainable and multifaceted approach to address the intertwined challenges of energy production, environmental protection, and resource management. However, several challenges remain, particularly in optimizing catalyst performance in complex wastewater matrices, and ensuring cost-effectiveness under real-world operating conditions. Further interdisciplinary research into the technological, economic, and policy aspects of wastewater-based hydrogen production is required to highlight its importance in aiding the transition to a cleaner and more sustainable energy future.

Photoelectrochemical (PEC) water-splitting remains considerably more expensive than conventional hydrogen routes, with reported levelized costs of hydrogen (LCOH) ranging from roughly ~ \$8 $kg^{-1}H_2$ for prototype PEC systems, compared with about \$6.22 $kg^{-1}H_2$ for an off-grid photovoltaic-electrolysis (PV-E) plant (10.9% solar-to-hydrogen efficiency) and \$5.5 $kg^{-1}H_2$ for grid-electricity electrolysis. By contrast, steam-methane reforming (SMR) delivers hydrogen at roughly \$1.5 $kg^{-1}H_2$, and wind-turbine-coupled electrolysis can achieve a cumulative energy demand as low as 9.1 MJ $kg^{-1}H_2$, far below the 34–680 MJ $kg^{-1}H_2$ required by most PEC designs. The higher PEC cost is driven primarily by the PEC module itself, which accounts for nearly half of the total (\$4.61 $kg^{-1}H_2$) and is dominated by expensive membranes (\$1.50 $kg^{-1}H_2$) and photo-active materials (1.35 $kg^{-1}H_2$). The PEC system is still above the PV-E projection of \$3.8 $kg^{-1}H_2$. Coupling PEC hydrogen production with value-added chemical synthesis (e.g., methyl succinic acid) can improve the net energy balance and move the LCOH toward market-competitive levels, but such integration remains essential for any realistic economic case. Overall, current evidence indicates that PEC hydrogen is an order of magnitude more costly than steam-methane reforming (SMR) and remains less competitive than mature PV-E systems, with substantial technical and cost breakthroughs required for it to become a viable alternative [314–316].

A comprehensive techno-economic assessment was conducted for large-scale solar hydrogen production via Shaner et al. [315] for photoelectrochemical (PEC) and photovoltaic–electrolytic (PV-E) systems, each designed for an output of 10,000 kg H_2 per day (3.65 kt yr^{-1}). Assuming identical overall plant efficiencies of 9.8%, the base-case capital investment required for the unconcentrated PEC system and the off-grid PV-E system was estimated at \$205 million and \$260 million, respectively, corresponding to levelized hydrogen costs (LCH) of \$11.4 kg^{-1} for PEC and \$12.1 kg^{-1} for PV-E at the plant gate. Incorporation of 10× solar concentration reduced the PEC base-case capital cost to approximately \$160 million, and at an assumed efficiency of 20% yielded an LCOH of \$9.2 kg^{-1}. In contrast, the grid-supplemented PV-E system exhibited a substantially lower capital cost of \$66 million; when combined with solar-to-hydrogen and grid electrolysis efficiencies of 9.8% and 61%, respectively, the resulting LCOH decreased to \$6.1 kg^{-1}.

Prasad et al. [317] provided a cradle-to-gate life cycle assessment

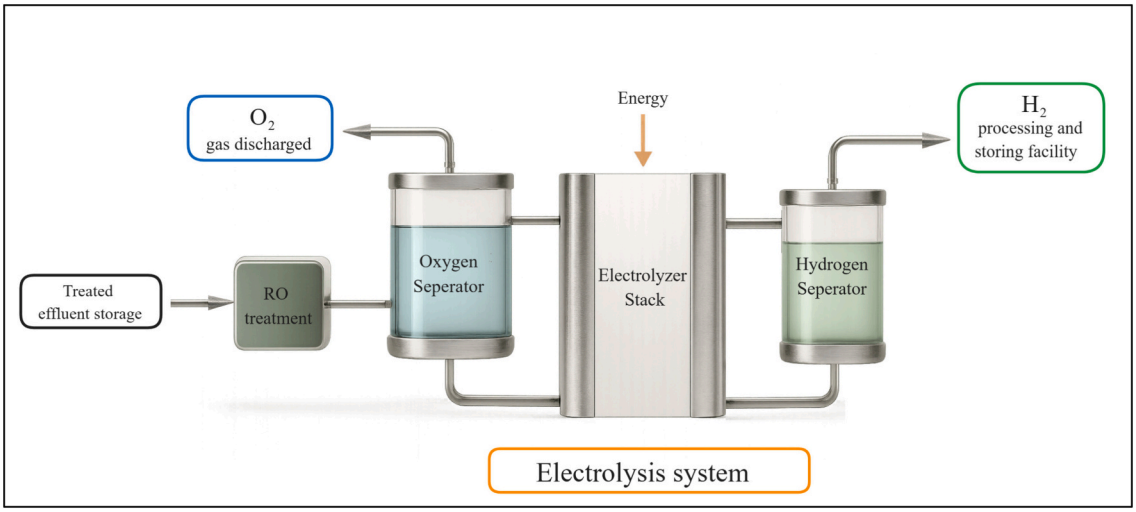

Fig. 11. Flow process of the electrolysis system.
(Adapted from Barghash et al. [312].)

(LCA) for six hydrogen production routes. The paper identified the photoelectrochemical anion-exchange-membrane (PEC AEM) reactor as having the lowest global warming potential (≈ 1.17 kg CO_2-eq $kg^{-1}H_2$) among the alternatives; it also records the smallest land-use (0.112 m^2 a crop-eq $kg^{-1}H_2$), fossil-resource scarcity (0.36 kg oil-eq $kg^{-1}H_2$), mineral-resource scarcity (0.0124 kg Cu-eq $kg^{-1}H_2$), freshwater eutrophication (0.26 kg P-eq $kg^{-1}H_2$), and particulate-matter formation (0.14 kg $PM_{2.5}$-eq $kg^{-1}H_2$), with the residual impacts largely driven by the acrylic-glass window and the PVC reactor frame. PEC AEM is also responsible for a relatively high human carcinogenic toxicity potential (1.48 kg 1,4-DCB-eq $kg^{-1}H_2$) compared with other routes; in contrast, steam-methane reforming exhibits the highest Global warming potential (GWP) (≈ 13.8 kg CO_2-eq $kg^{-1}H_2$), land-use (0.189 m^2 a crop-eq $kg^{-1}H_2$), and fossil-resource scarcity (7.83 kg oil-eq $kg^{-1}H_2$), underscoring its environmental disadvantage, while the environmental performance of solar-driven pathways (PEC AEM, PEC PEM, solar-PV PEMWE) is sensitive to the regional electricity mix, with the PEC AEM reactor's GWP ranging from 1.27 kg CO_2-eq $kg^{-1}H_2$ in the EU to 1.17 kg CO_2-eq $kg^{-1}H_2$ in India; however, the paper does not present a quantitative techno-economic assessment or levelized cost of hydrogen for any of the technologies, limiting direct cost comparisons in a review.

On the technology-readiness axis, PV-coupled PEM and alkaline electrolysis are commercially deployed and benefit from rapidly falling Capital Expenditures (CAPEX) and LCOH projections driven by learning in both PV and electrolyzer manufacturing, whereas PEC and particulate photocatalytic systems, including PCR, remain largely at laboratory or early pilot scale, despite encouraging large-area demonstrations of solar H_2 production and illustrative designs (e.g., *Z*-scheme raceway reactors) that indicate potential long-term competitiveness if high STH efficiencies, long lifetimes and low absorber/catalyst costs can be achieved [318–320].

Within this multi-dimensional framework, photocatalytic reforming is best viewed as a complementary pathway: its current absolute efficiencies and projected hydrogen costs are not yet competitive with PV–PEM or optimized biomass gasification at scale, but its ability to couple solar H_2 generation with valorization or remediation of low-value organic streams may yield favorable effective costs and environmental footprints in niche applications where waste treatment is a dominant constraint. As Shaner et al. mentioned, neither incremental nor combined technical improvements are sufficient to make solar-derived hydrogen cost-competitive with hydrogen produced from fossil fuels [315].

6. Conclusions and outlook

The advancements in photocatalytic reforming technologies for solar-driven hydrogen production have been comprehensively analysed, integrating insights from both the scientific literature and the patent landscape. The transition to a sustainable hydrogen economy is contingent upon the development of efficient, economically viable, and scalable photocatalytic systems. From a materials perspective, innovations in inorganic semiconductors such as bandgap engineering, heterojunction design, as well as the incorporation of plasmonic and co-catalyst functionalities have significantly improved HER. Notably, S- and Z-scheme heterojunctions have demonstrated superior charge separation dynamics, paving the way for enhanced STH efficiencies. Among the analysed materials, MOFs, COFs and conjugated polymers resulted promising for photocatalyst design due to their tunable structures, high surface areas, and compatibility with visible light absorption.

The use of sacrificial agents derived from wastewater has emerged as a promising strategy that enables the simultaneous generation of renewable H_2 and the degradation of organic pollutants. This approach aligns with the principles of the circular economy and enhances the overall sustainability of photocatalytic systems. However, the practical implementation of such processes is still limited by critical challenges, such as catalyst deactivation and photocorrosion under realistic wastewater conditions.

At the reactor level, substantial progress has been achieved in designing novel photoreactor architectures that enhance photon utilization, mass transfer, and light penetration. While high-throughput screening platforms and internally illuminated systems have improved laboratory efficiencies, the transition to pilot and industrial scales is hindered by a lack of standardized performance metrics and techno-economic models. Analysis of the patent landscape reveals parallel innovation trend, specifically in co-catalyst engineering, hybrid heterojunction architectures, and novel reactor configurations. However, despite promising proof-of-concept systems, commercial-scale deployment remains limited by high material and system cost, durability issues, and uncertainties associated with long-term operation under real solar irradiation.

Future research efforts must increasingly prioritize the translation of laboratory-scale breakthroughs into industrially relevant photocatalytic reforming systems. From a material standpoint, emphasis should be placed on the development of earth-abundant, low-cost photocatalysts with intrinsic chemical and photochemical stability, capable of maintaining performance over extended operational periods. Replacing noble

metals with non-noble metal co-catalysts (e.g., Ni, Co, Mo, Cu) while achieving hydrogen evolution rates comparable to Pt-based references represents a critical objective. Rational catalyst design should integrate durability considerations alongside activity metrics, moving beyond short-term hydrogen evolution rates toward long-term stability and recyclability benchmarks. Concrete targets include the design of photocatalysts capable of operating continuously for >1000 h in simulated or real industrial wastewater, while retaining at least 80-90% of their initial hydrogen production rate.

From a system integration perspective, the transition from slurry-based reactors to immobilized or structured catalyst configurations will be critical to improving catalyst handling, reducing downstream separation costs, and enabling continuous operation. The design of scalable photoreactors must account for realistic solar irradiation conditions, photon and mass transport limitations, thermal management, and reactor modularity, particularly for decentralized hydrogen production scenarios. Efficient utilization of the broad solar spectrum is the key to achieving higher STH efficiencies. In this context, photothermal-photocatalytic hybrid reactors that couple broadband light absorption with thermal reforming pathways represent a promising route. Coupling hydrogen production with biomass valorization processes, such as the photocatalytic reforming of lignocellulosic material, glycerol from biodiesel production, or fermentation effluents, offers additional opportunities to enhance overall process economics and sustainability. Equally important is the establishment of standardized testing protocols, including outdoor solar testing, harmonized efficiency metrics, and reproducible benchmarking conditions, to enable meaningful comparison across studies. Comprehensive techno-economic analysis and life-cycle assessments should be systematically integrated into future research to identify cost drivers, environmental trade-offs, and realistic performance targets required for market competitiveness.

Finally, closer alignment between academic research, industrial stakeholders, and policy frameworks will be essential to accelerate technology readiness. Patent-informed research strategies, pilot-scale demonstrations, and cross-sector collaborations can play a critical role in bridging the gap between proof-of-concept systems and commercial deployment. In this context, photocatalytic reforming has the potential to evolve from an emerging research topic into a key enabling technology for sustainable hydrogen production, provided that coordinated advances in materials science, reactor engineering, and system-level integration are achieved.

CRediT authorship contribution statement

Marica Muscetta: Writing – original draft, Investigation, Formal analysis, Conceptualization. **Hebah S. Jarusheh:** Writing – original draft, Investigation, Formal analysis. **Gareth Williams:** Writing – original draft, Investigation, Formal analysis. **Kazi M. Alam:** Writing – review & editing, Investigation. **Karthik Shankar:** Writing – review & editing, Supervision. **Giovanni Palmisano:** Writing – review & editing, Supervision, Conceptualization. **Sergio Vernuccio:** Writing – review & editing, Writing – original draft, Supervision, Funding acquisition, Conceptualization.

Declaration of competing interest

The authors declare that they have no known competing financial interests or personal relationships that could have appeared to influence the work reported in this paper.

Acknowledgment

This paper is based upon work supported primarily by the Worldwide Universities Network (WUN) Research Development Fund and by the Royal Society International Exchange grant (IES\R3\203083). SV additionally acknowledges support from the Royal Academy of Engineering Industrial Fellowship (IF-2425-19-AI102) and from EPSRC/NERC-funded Great British Chemicals programme (UKRI2199).

Data availability

Data will be made available on request.

References

[1] T. Ahmad, D. Zhang, A critical review of comparative global historical energy consumption and future demand: the story told so far, Energy Rep. 6 (2020) 1973–1991, https://doi.org/10.1016/J.EGYR.2020.07.020.
[2] Review of World Energy 2023 | 72 nd edition, 2023.
[3] J. Wang, W. Azam, Natural resource scarcity, fossil fuel energy consumption, and total greenhouse gas emissions in top emitting countries, Geosci. Front. 15 (2024) 101757, https://doi.org/10.1016/J.GSF.2023.101757.
[4] M. Amin, H.H. Shah, A.G. Fareed, W.U. Khan, E. Chung, A. Zia, Z.U. Rahman Farooqi, C. Lee, Hydrogen production through renewable and non-renewable energy processes and their impact on climate change, Int. J. Hydrog. Energy 47 (2022) 33112–33134, https://doi.org/10.1016/J.IJHYDENE.2022.07.172.
[5] I. Energy Agency, Net Zero by 2050 - A Roadmap for the Global Energy Sector. www.iea.org/t&c/, 2021 (accessed April 23, 2024).
[6] Y.K. Dwivedi, L. Hughes, A.K. Kar, A.M. Baabdullah, P. Grover, R. Abbas, D. Andreini, I. Abumoghli, Y. Barlette, D. Bunker, L. Chandra Kruse, I. Constantiou, R.M. Davison, R. De, R. Dubey, H. Fenby-Taylor, B. Gupta, W. He, M. Kodama, M. Mäntymäki, B. Metri, K. Michael, J. Olaisen, N. Panteli, S. Pekkola, R. Nishant, R. Raman, N.P. Rana, F. Rowe, S. Sarker, B. Scholtz, M. Sein, J.D. Shah, T.S.H. Teo, M.K. Tiwari, M.T. Vendelø, M. Wade, Climate change and COP26: are digital technologies and information management part of the problem or the solution? An editorial reflection and call to action, Int. J. Inf. Manag. 63 (2022), https://doi.org/10.1016/j.ijinfomgt.2021.102456.
[7] Q. Hassan, S. Algburi, A.Z. Sameen, H.M. Salman, M. Jaszczur, Green Hydrogen: A Pathway to a Sustainable Energy Future, 2023, https://doi.org/10.1016/j.ijhydene.2023.08.321.
[8] U. Bossel, B. Eliasson, Energy Hydrogen Economy. www.efcf.com/reports, 2003.
[9] L. Zhang, C. Jia, F. Bai, W. Wang, S. An, K. Zhao, Z. Li, J. Li, H. Sun, A comprehensive review of the promising clean energy carrier: hydrogen production, transportation, storage, and utilization (HPTSU) technologies, Fuel 355 (2024) 129455, https://doi.org/10.1016/j.fuel.2023.129455.
[10] M. Katebah, M. 'moun Al-Rawashdeh, P. Linke, Analysis of Hydrogen Production Costs in Steam-Methane Reforming Considering Integration With Electrolysis and CO 2 Capture, 2022, https://doi.org/10.1016/j.clet.2022.100552.
[11] M.R.G. Pangestu, Z. Malaibari, A. Muhammad, F.N. Al-Rowaili, U. Zahid, Comprehensive review on methane pyrolysis for sustainable hydrogen production, Energy Fuel 38 (2024) 13514–13538, https://doi.org/10.1021/acs.energyfuels.4c01551.
[12] A.L. Moghaddam, S. Hejazi, M. Fattahi, M.G. Kibria, M.J. Thomson, R. AlEisa, M. A. Khan, Methane pyrolysis for hydrogen production: navigating the path to a net zero future, Energy Environ. Sci. 18 (2025) 2747–2790, https://doi.org/10.1039/D4EE06191H.
[13] A.F. Alkaim, T.A. Kandiel, R. Dillert, D.W. Bahnemann, Photocatalytic hydrogen production from biomass-derived compounds: a case study of citric acid, Environ. Technol. (U. K.) 37 (2016) 2687–2693, https://doi.org/10.1080/09593330.2016.1158871.
[14] M. Imizcoz, A.V. Puga, Assessment of photocatalytic hydrogen production from biomass or wastewaters depending on the metal co-catalyst and its deposition method on TiO2, Catalysts 9 (2019), https://doi.org/10.3390/catal9070584.
[15] A. Pareek, R. Dom, J. Gupta, J. Chandran, V. Adepu, P.H. Borse, Insights into renewable hydrogen energy: recent advances and prospects, Mater. Sci. Energy Technol. 3 (2020) 319–327, https://doi.org/10.1016/J.MSET.2019.12.002.
[16] S.E. Hosseini, Hydrogen From Solar Energy, a Clean Energy Carrier From a Sustainable Source of Energy, 2019, pp. 1–22, https://doi.org/10.1002/er.4930.
[17] A. Kovač, D. Marciuš, L. Budin, Solar hydrogen production via alkaline water electrolysis, Int. J. Hydrog. Energy 44 (2019) 9841–9848, https://doi.org/10.1016/j.ijhydene.2018.11.007.
[18] G. Liu, Y. Sheng, J.W. Ager, M. Kraft, R. Xu, Research advances towards large-scale solar hydrogen production from water, EnergyChem 1 (2019) 100014, https://doi.org/10.1016/j.enchem.2019.100014.
[19] Q. Wei, Y. Yang, J. Hou, H. Liu, F. Cao, L. Zhao, Direct solar photocatalytic hydrogen generation with CPC photoreactors: system development, Sol. Energy 153 (2017) 215–223, https://doi.org/10.1016/j.solener.2017.05.064.
[20] M. Gao, T. Zhang, G.W. Ho, Advances of photothermal chemistry in photocatalysis, thermocatalysis, and synergetic photothermocatalysis for solar-to-fuel generation, Nano Res. (2022), https://doi.org/10.1007/s12274-022-4795-3.
[21] C. Shi, F. Kang, Y. Zhu, M. Teng, J. Shi, H. Qi, Z. Huang, C. Si, F. Jiang, J. Hu, Photoreforming lignocellulosic biomass for hydrogen production: optimized design of photocatalyst and photocatalytic system, Chem. Eng. J. 452 (2023), https://doi.org/10.1016/j.cej.2022.138980.
[22] S.W. Sharshir, A. Joseph, M.M. Elsayad, A.A. Tareemi, A.W. Kandeal, M. R. Elkadeem, A review of recent advances in alkaline electrolyzer for green hydrogen production: performance improvement and applications, Int. J. Hydrog. Energy 49 (2024) 458–488, https://doi.org/10.1016/J.IJHYDENE.2023.08.107.

[23] M. Felgenhauer, T. Hamacher, State-of-the-art of Commercial Electrolyzers and On-site Hydrogen Generation for Logistic Vehicles in South Carolina, 2015, https://doi.org/10.1016/j.ijhydene.2014.12.043.
[24] S. Shiva Kumar, H. Lim, An overview of water electrolysis technologies for green hydrogen production, Energy Rep. 8 (2022) 13793–13813, https://doi.org/10.1016/J.EGYR.2022.10.127.
[25] M. Kirch, J.-M. Lehn, J.-P. Sauvage, Hydrogen Generation by Visible Light Irradiation of Aqueous Solutions of Metal Complexes. An Approach to the Photochemical Conversion and Storage of Solar Energy, 1979.
[26] C.Y. Toe, C. Tsounis, J. Zhang, H. Masood, D. Gunawan, J. Scott, R. Amal, Advancing photoreforming of organics: highlights on photocatalyst and system designs for selective oxidation reactions, Energy Environ. Sci. 14 (2021) 1140–1175, https://doi.org/10.1039/D0EE03116J.
[27] L. Chang, S.T. Yong, S.P. Chai, L.K. Putri, L.L. Tan, A.R. Mohamed, A review of methanol photoreforming: elucidating the mechanisms, photocatalysts and recent advancement strategies, Mater. Today Chem. 27 (2023) 101334, https://doi.org/10.1016/J.MTCHEM.2022.101334.
[28] T. Li, N. Tsubaki, Z. Jin, S-scheme heterojunction in photocatalytic hydrogen production, J. Mater. Sci. Technol. 169 (2024) 82–104, https://doi.org/10.1016/J.JMST.2023.04.049.
[29] N. Skillen, H. Daly, L. Lan, M. Aljohani, C.W.J. Murnaghan, X. Fan, C. Hardacre, G.N. Sheldrake, P.K.J. Robertson, Photocatalytic reforming of biomass: what role will the technology play in future energy systems, Top. Curr. Chem. 380 (5) (2022) 1–40, https://doi.org/10.1007/S41061-022-00391-9.
[30] D. Zhou, D. Li, S. Yuan, Z. Chen, Recent advances in biomass-based photocatalytic H2 production and efficient photocatalysts: a review, Energy Fuel 36 (2022) 10721–10731, https://doi.org/10.1021/ACS.ENERGYFUELS.2C01904.
[31] K.A. Davis, S. Yoo, E.W. Shuler, B.D. Sherman, S. Lee, G. Leem, Photocatalytic hydrogen evolution from biomass conversion, Nano Convergence 8 (1) (2021) 1–19, https://doi.org/10.1186/S40580-021-00256-9.
[32] J. Ma, K. Liu, X. Yang, D. Jin, Y. Li, G. Jiao, J. Zhou, R. Sun, Recent advances and challenges in photoreforming of biomass-derived feedstocks into hydrogen, biofuels, or chemicals by using functional carbon nitride photocatalysts, ChemSusChem 14 (2021) 4903–4922, https://doi.org/10.1002/CSSC.202101173.
[33] D. Banerjee, N. Kushwaha, N.P. Shetti, T.M. Aminabhavi, E. Ahmad, Green hydrogen production via photo-reforming of bio-renewable resources, Renew. Sust. Energ. Rev. 167 (2022) 112827, https://doi.org/10.1016/J.RSER.2022.112827.
[34] C. Shi, F. Kang, Y. Zhu, M. Teng, J. Shi, H. Qi, Z. Huang, C. Si, F. Jiang, J. Hu, Photoreforming lignocellulosic biomass for hydrogen production: optimized design of photocatalyst and photocatalytic system, Chem. Eng. J. 452 (2023) 138980, https://doi.org/10.1016/J.CEJ.2022.138980.
[35] M. Ashraf, N. Ullah, I. Khan, W. Tremel, S. Ahmad, M.N. Tahir, Photoreforming of waste polymers for sustainable hydrogen fuel and chemicals feedstock: waste to energy, Chem. Rev. 123 (2023) 4443–4509, https://doi.org/10.1021/ACS.CHEMREV.2C00602.
[36] H. Zhao, J. Liu, N. Zhong, S. Larter, Y. Li, M.G. Kibria, B.L. Su, Z. Chen, J. Hu, Biomass photoreforming for hydrogen and value-added chemicals co-production on hierarchically porous photocatalysts, Adv. Energy Mater. 13 (2023) 2300257, https://doi.org/10.1002/AENM.202300257.
[37] K. Ćwieka, K. Czelej, J.C. Colmenares, K. Jabłczyńska, Ł. Werner, L. Gradoń, Supported plasmonic nanocatalysts for hydrogen production by wet and dry photoreforming of biomass and biogas derived compounds: recent progress and future perspectives, ChemCatChem 13 (2021) 4458–4496, https://doi.org/10.1002/CCTC.202101006.
[38] E.I. García-López, L. Palmisano, G. Marcì, Overview on photoreforming of biomass aqueous solutions to generate H2 in the presence of g-C3N4-based materials, ChemEngineering 7 (2023) 11, https://doi.org/10.3390/CHEMENGINEERING7010011.
[39] A. Augustin, C. Chuaicham, M. Shanmugam, B. Vellaichamy, S. Rajendran, T.K. A. Hoang, K. Sasaki, K. Sekar, Recent development of organic–inorganic hybrid photocatalysts for biomass conversion into hydrogen production, Nanoscale Adv. 4 (2022) 2561–2582, https://doi.org/10.1039/D2NA00119E.
[40] H.Y. Chung, R.J. Wong, H. Wu, D. Gunawan, R. Amal, Y.H. Ng, Scalable and integrated photocatalytic reactor systems for solar-to-fuel production: photoredox and photoreforming processes, Adv. Energy Mater. 15 (2025), https://doi.org/10.1002/aenm.202404956.
[41] P. Mani, S. Shenoy, P.J.J. Sagayaraj, N. Agamendran, S. Son, N. Bernaurdshaw, H. Kim, K. Sekar, Scaling up of photocatalytic systems for large-scale hydrogen generation, Appl. Phys. Rev. 12 (2025), https://doi.org/10.1063/5.0223598.
[42] S. Protti, A. Albini, N. Serpone, Photocatalytic generation of solar fuels from the reduction of H2O and CO2: a look at the patent literature, Phys. Chem. Chem. Phys. 16 (2014) 19790–19827, https://doi.org/10.1039/C4CP02828G.
[43] A. Fujishima, K. Honda, Electrochemical photolysis of water at a semiconductor electrode, Nature 238 (1972) 37–38, https://doi.org/10.1038/238037a0.
[44] F. Zhong, H. Zhuang, Q. Gu, J. Long, Structural evolution of alkaline earth metal stannates MSnO3 (M = Ca, Sr, and Ba) photocatalysts for hydrogen production, RSC Adv. 6 (2016) 42474–42481, https://doi.org/10.1039/C6RA05614H.
[45] E.M.N.T. Edirisooriya, P.S. Senanayake, H.B. Wang, M.R. Talipov, P. Xu, H. Wang, Photo-reforming and degradation of waste plastics under UV and visible light for H2 production using nanocomposite photocatalysts, J. Environ. Chem. Eng. 11 (2023) 109580, https://doi.org/10.1016/j.jece.2023.109580.
[46] B. Rico-Oller, A. Boudjemaa, H. Bahruji, M. Kebir, S. Prashar, K. Bachari, M. Fajardo, S. Gómez-Ruiz, Photodegradation of organic pollutants in water and green hydrogen production via methanol photoreforming of doped titanium oxide nanoparticles, Sci. Total Environ. 563–564 (2016) 921–932, https://doi.org/10.1016/j.scitotenv.2015.10.101.
[47] S. Luo, H. Lin, Q. Wang, X. Ren, D. Hernández-Pinilla, T. Nagao, Y. Xie, G. Yang, S. Li, H. Song, M. Oshikiri, J. Ye, Triggering water and methanol activation for solar-driven H_2 production: interplay of dual active sites over Plasmonic ZnCu alloy, J. Am. Chem. Soc. 143 (2021) 12145–12153, https://doi.org/10.1021/jacs.1c04315.
[48] N.R. Vempuluru, C. Kanakkampalayam Krishnan, R. Parnapalli, J. Velusamy, S. Marappan, S. Pitchaimuthu, M. Murikinati, S. Muthukonda Venkatakrishnan, Solar hydrogen generation from organic substance using earth abundant CuS–NiO heterojunction semiconductor photocatalyst, Ceram. Int. 47 (2021) 10206–10215, https://doi.org/10.1016/j.ceramint.2020.12.062.
[49] H. Rajashekhar, D. Vrushabendrakumar, M.M. Rana, K.M. Alam, R.K.V. Raman, C.X. Li, N. Chaulagain, K. Shankar, Bimetallic AuPd alloy nanoparticles on TiO2 nanotube arrays: a highly efficient photocatalyst for hydrogen generation, Nanotechnology 36 (2025), https://doi.org/10.1088/1361-6528/adb15f.
[50] W. Liu, E. Ha, L. Wang, L. Hu, L.Y.S. Lee, K.-Y. Wong, Creating multiple parallel internal phase junctions on ZnS nanoparticles as highly active catalytic sites, Adv. Mater. Interfaces 5 (2018) 1800611, https://doi.org/10.1002/admi.201800611.
[51] V.S. Souza, J.D. Scholten, D.E. Weibel, D. Eberhardt, D.L. Baptista, S.R. Teixeira, J. Dupont, Hybrid tantalum oxide nanoparticles from the hydrolysis of imidazolium tantalate ionic liquids: efficient catalysts for hydrogen generation from ethanol/water solutions, J. Mater. Chem. A Mater. 4 (2016) 7469–7475, https://doi.org/10.1039/C6TA02114J.
[52] A.H. Jawhari, N. Hasan, I.A. Radini, K. Narasimharao, M.A. Malik, Noble metals deposited LaMnO3 nanocomposites for photocatalytic H2 production, Nanomaterials 12 (2022) 2985. https://www.mdpi.com/2079-4991/12/17/2985.
[53] Y. AlSalka, A. Hakki, J. Schneider, D.W. Bahnemann, Co-catalyst-free photocatalytic hydrogen evolution on TiO2: synthesis of optimized photocatalyst through statistical material science, Appl. Catal. B 238 (2018) 422–433, https://doi.org/10.1016/j.apcatb.2018.07.045.
[54] W. Tingting, Z. Genrui, X. Jixiang, L. Xiaojing, L. Na, W. Lei, Preparation Method of Hollow Irregular Rutile TiO2 Microspheres With High Photocatalytic Activity, CN116618035A, 2023.
[55] I. Australia, AU2012347103B2 - Niobium Nitride and Method for Producing Same, Niobium Nitride-containing Film and Method for Producing Same, Semiconductor, Semiconductor Device, Photocatalyst, Hydrogen Generation Device, and Energy System, 2013.
[56] D. Gogoi, A. Namdeo, A.K. Golder, N.R. Peela, Ag-doped TiO2 photocatalysts with effective charge transfer for highly efficient hydrogen production through water splitting, Int. J. Hydrog. Energy 45 (2020) 2729–2744, https://doi.org/10.1016/J.IJHYDENE.2019.11.127.
[57] F. Xiaoxing, L. Xinyu, S. Lianjuan, Y. Jie, Co-Catalyst-Loaded Al-Doped SrTiO3/TiO2 Heterojunction Photocatalyst As Well as Preparation Method and Application Thereof, CN120054530A, 2025.
[58] J. Martín-Gómez, S. Reca-Expósito, F.J. López-Tenllado, J. Hidalgo-Carrillo, A. Marinas, F.J. Urbano, Synthesis of Fe-TiO2 and Cu-TiO2 based materials by olive leaves biotemplating—application to hydrogen production from glycerol photoreforming, Nanomaterials 13 (2023) 664, https://doi.org/10.3390/NANO13040664/S1.
[59] S.A. Rawool, M.R. Pai, A.M. Banerjee, R.D. Bapat, C. Nayak, A.K. Tripathi, Lab scale optimization of various factors for photocatalytic hydrogen generation over low cost Cu0.02Ti0.98O2-δ photocatalyst under UV/visible irradiation and sunlight, Int. J. Hydrog. Energy 43 (2018) 1271–1284, https://doi.org/10.1016/J.IJHYDENE.2017.11.090.
[60] M. Zhang, R. Sun, Y. Li, Q. Shi, L. Xie, J. Chen, X. Xu, H. Shi, W. Zhao, High H2 evolution from quantum Cu(II) nanodot-doped two-dimensional ultrathin TiO2 nanosheets with dominant exposed {001} facets for reforming glycerol with multiple electron transport pathways, J. Phys. Chem. C 120 (2016) 10746–10756, https://doi.org/10.1021/ACS.JPCC.6B01030.
[61] H. Guoyong, W. Chunxia, W. Zhuo, M. Ling, Preparing a Catalyst for Photodecomposition of Water to Produce Hydrogen Using Waste Titanium Dioxide Carrier, CN119386866A, 2025.
[62] H. Su, C. Rao, L. Zhou, Y. Pang, H. Lou, D. Yang, X. Qiu, Mo-Doped/Ni-supported $ZnIn_2S_4$-wrapped, Green Chem. 24 (2022) 2027–2035, https://doi.org/10.1039/D1GC04397H.
[63] R. Chauhan, M. Shinde, Y. Sethi, Y. Waghadkar, S.R. Rondiya, N.Y. Dzade, S. Gosavi, M. Muddassir, Indium-doped ZnOas efficient photosensitive material for sunlight driven hydrogen generation and DSSC applications: integrated experimental and computational approach, J. Solid State Electrochem. 25 (2021) 2279–2292, https://doi.org/10.1007/S10008-021-04999-7/TABLES/2.
[64] R. Fiorenza, M. Bellardita, S. Scirè, L. Palmisano, Effect of the addition of different doping agents on visible light activity of porous TiO2 photocatalysts, Mol. Catal. 455 (2018) 108–120, https://doi.org/10.1016/J.MCAT.2018.06.002.
[65] T.N.S. Trindade, L.A. Silva, Cd-doped SnO2/CdS heterostructures for efficient application in photocatalytic reforming of glycerol to produce hydrogen under visible light irradiation, J. Alloys Compd. 735 (2018) 400–408, https://doi.org/10.1016/J.JALLCOM.2017.11.134.
[66] W.K. Jo, Y.J. Jin, 2D graphene-assisted low-cost metal (Ag, Cu, Fe, or Ni)-doped TiO2 nanowire architectures for enhanced hydrogen generation, J. Alloys Compd. 765 (2018) 106–112, https://doi.org/10.1016/J.JALLCOM.2018.06.181.
[67] E.M.N.T. Edirisooriya, P.S. Senanayake, H.B. Wang, M.R. Talipov, P. Xu, H. Wang, Photo-reforming and degradation of waste plastics under UV and visible light for H2 production using nanocomposite photocatalysts, J. Environ. Chem. Eng. 11 (2023) 109580, https://doi.org/10.1016/J.JECE.2023.109580.

[68] S. Tian, H. Ren, W. Sun, Y. Song, H. Ge, A. Yang, W. Zheng, Y. Zhao, CdIn 2 S 4 microspheres embedded with mesoporous Zn-doped g-C 3 N 4 ultrathin nanosheets for efficient photocatalytic hydrogen evolution †, New J. Chem. 48 (2024) 3695, https://doi.org/10.1039/d3nj05590f.
[69] J. Xu, F. Huo, Y. Zhao, Y. Liu, Q. Yang, Y. Cheng, S. Min, Z. Jin, Z. Xiang, In-situ La doped Co3O4 as highly efficient photocatalyst for solar hydrogen generation, Int. J. Hydrog. Energy 43 (2018) 8674–8682, https://doi.org/10.1016/J.IJHYDENE.2018.03.126.
[70] M. Rafique, N.R. Khalid, M. Irshad, F. Shafiq, M. Usman, Y. Fouad, M. Imran, M. A. Assiri, W.M. Ashraf, Visible light-active pure and lanthanum-doped copper oxide nanostructures for photocatalytic degradation of methylene blue dye and hydrogen production, Energy Sci. Eng. 11 (2023) 2601–2613, https://doi.org/10.1002/ESE3.1476.
[71] L. Sun, L. Han, J. Huang, X. Luo, X. Li, Single-atom catalysts for photocatalytic hydrogen evolution: a review, Int. J. Hydrog. Energy 47 (2022) 17583–17599, https://doi.org/10.1016/j.ijhydene.2022.03.259.
[72] J. Il Kwak, S.-H. Nam, L. Kim, Y.-J. An, Potential environmental risk of solar cells: current knowledge and future challenges, J. Hazard. Mater. 392 (2020) 122297, https://doi.org/10.1016/j.jhazmat.2020.122297.
[73] H. Dong, J. Zhao, J. Chen, Y. Wu, B. Li, Recovery of platinum group metals from spent catalysts: a review, Int. J. Miner. Process. 145 (2015) 108–113, https://doi.org/10.1016/j.minpro.2015.06.009.
[74] J. Cao, Y. Chen, H. Shang, X. Chen, Q. Qiao, H. Li, Z. Bian, Aqueous photocatalytic recycling of gold and palladium from waste electronics and catalysts, ACS ES&T Eng. 2 (2022) 1445–1453, https://doi.org/10.1021/acsestengg.1c00505.
[75] D.J. Bradwell, S. Osswald, W. Wei, S.A. Barriga, G. Ceder, D.R. Sadoway, Recycling ZnTe, CdTe, and other compound semiconductors by ambipolar electrolysis, J. Am. Chem. Soc. 133 (2011) 19971–19975, https://doi.org/10.1021/ja208577j.
[76] C.G. Poll, G.W. Nelson, D.M. Pickup, A.V. Chadwick, D.J. Riley, D.J. Payne, Electrochemical recycling of lead from hybrid organic–inorganic perovskites using deep eutectic solvents, Green Chem. 18 (2016) 2946–2955, https://doi.org/10.1039/C5GC02734A.
[77] Y. Wang, Y. Zhang, H. Lu, Y. Chen, Z. Liu, S. Su, Y. Xue, J. Yao, H. Zeng, Novel N-doped ZrO 2 with enhanced visible-light photocatalytic activity for hydrogen production and degradation of organic dyes, RSC Adv. 8 (2018) 6752–6758, https://doi.org/10.1039/C7RA12938F.
[78] G. Koyyada, N.S. Pilli, J.H. Jung, K.K. Mandari, B. Shanigaram, M. Chandrasekharam, Shining light on panchromatic ruthenium sensitizers towards dye-sensitized photocatalytic hydrogen evolution, Int. J. Hydrog. Energy 43 (2018) 6963–6976, https://doi.org/10.1016/J.IJHYDENE.2018.02.117.
[79] Y.F. Chen, J.F. Huang, M.H. Shen, J.M. Liu, L.B. Huang, Y.H. Zhong, S. Qin, J. Guo, C.Y. Su, A porous hybrid material based on calixarene dye and TiO2 demonstrating high and stable photocatalytic performance, J. Mater. Chem. A Mater. 7 (2019) 19852–19861, https://doi.org/10.1039/C9TA06038C.
[80] L.Y. Huang, J.F. Huang, Y. Lei, S. Qin, J.M. Liu, Porous hybrid materials based on mesotetrakis(hydroxyphenyl) porphyrins and TiO2 for efficient visible-light-driven hydrogen production, Catalysts 10 (2020) 656, https://doi.org/10.3390/CATAL10060656.
[81] M. Xu, X. Song Jia, D. Zhao, C. Shan Zhao, H. Ke, C. Chen, Modification of Ni2P with LaPO4 for efficiently photocatalytic and electrocatalytic production of green-H2, Catal. Today 402 (2022) 310–318, https://doi.org/10.1016/J.CATTOD.2022.05.023.
[82] P. Wang, F. Jin, X. Pan, C. Yang, Y. Shen, Z. Jin, Graphdiyne nanosheets integrated with Ni6MnO8 via in situ calcination: a robust S-scheme heterojunction for enhanced eosin Y-sensitized photocatalytic hydrogen production, Sol. RRL 8 (2024) 2400345, https://doi.org/10.1002/SOLR.202400345.
[83] J. Shin, J. Lee, X. Xiao, T. Yu, Enhancing catalytic activity of TiO2 nanoparticles through acid treatment in eosin-Y sensitized photohydrogen evolution reaction system, Heliyon 10 (2024) e30765, https://doi.org/10.1016/j.heliyon.2024.e30765.
[84] J. Warnan, J. Willkomm, Y. Farré, Y. Pellegrin, M. Boujtita, F. Odobel, E. Reisner, Solar electricity and fuel production with perylene monoimide dye-sensitised TiO 2 in water, Chem. Sci. 10 (2019) 2758–2766, https://doi.org/10.1039/C8SC05693E.
[85] P. Dong, A. Zhang, J. Pan, K. Gao, Z. Wang, X. Xi, An all-organic S-scheme heterojunction containing donor–acceptor type conjugated polymer and C3N4 nanosheets assembled via π–π interaction for photocatalytic H2 generation, Appl. Surf. Sci. 615 (2023) 156414, https://doi.org/10.1016/J.APSUSC.2023.156414.
[86] M. Tahir, US12233403B1 Triphenylphosphine Ruthenium Photocatalyst for Hydrogen Production. https://worldwide.espacenet.com/patent/search/family/094690793/publication/US12233403B1?q=Dye%20sensitized%20photocatalyst%20hydrogen%20generation, 2025.
[87] Z. Meng, W. Dan, Y. Kang, L.I. Jianwei, L. Ying, Z. Yadong, L. Wei, Y. Chenlong, L. U. Lin, H. Xin, Z. Jianliang, Y.U. Jie, T. Ming, Modified Titanium Dioxide As Well as Preparation Method and Application, 2023.
[88] L. Ye, Z. Ma, Y. Deng, Y. Ye, W. Li, M. Kou, H. Xie, X. Zhikun, Y. Zhou, D. Xia, P. K. Wong, Robust and efficient photocatalytic hydrogen generation of ReS2/CdS and mechanistic study by on-line mass spectrometry and in situ infrared spectroscopy, AppCB 257 (2019) 117897, https://doi.org/10.1016/J.APCATB.2019.117897.
[89] V. Preethi, S. Kanmani, Performance of four various shapes of photocatalytic reactors with respect to hydrogen and sulphur recovery from sulphide containing wastestreams, J. Clean. Prod. 133 (2016) 1218–1226, https://doi.org/10.1016/J.JCLEPRO.2016.06.016.
[90] J. Hou, Y. Yang, J. Zhou, Y. Wang, T. Xu, Q. Wang, Flexible CdS and PbS nanoparticles sensitized TiO2 nanotube arrays lead to significantly enhanced photocatalytic performance, Ceram. Int. 46 (2020) 28785–28791, https://doi.org/10.1016/J.CERAMINT.2020.08.041.
[91] R. Chen, X. Bai, Y. Luo, L. Qian, M. Ma, X. She, Rational designing of dual-functional photocatalysts for simultaneous hydrogen generation and organic pollutants degradation over Cd0.5Mn0.5S/CoP, Int. J. Hydrog. Energy 47 (2022) 32921–32927, https://doi.org/10.1016/J.IJHYDENE.2022.07.174.
[92] S. Zhu, Y. Cui, X. Wang, Y. Liu, W. Chen, Y. Zhang, Q. Wang, TiO2 NTAs decorated with thin CuBi2O4 nanosheets for efficient photocatalytic dye degradation and hydrogen generation, Ceram. Int. 48 (2022) 6627–6637, https://doi.org/10.1016/J.CERAMINT.2021.11.212.
[93] Y. Liu, C.F. Li, X.Y. Li, W.B. Yu, W. Da Dong, H. Zhao, Z.Y. Hu, Z. Deng, C. Wang, S.J. Wu, H. Chen, J. Liu, Z. Wang, L.H. Chen, Y. Li, B.L. Su, Molybdenum disulfide quantum dots directing zinc indium sulfide heterostructures for enhanced visible light hydrogen production, J. Colloid Interface Sci. 551 (2019) 111–118, https://doi.org/10.1016/J.JCIS.2019.05.001.
[94] Q. Xie, M. Wang, Y. Xu, X. Li, X. Zhou, L. Hong, L. Jiang, W.-F. Lin, S Vacancy Modulated Zn x Cd 1Àx S/CoP Quantum Dots for Efficient H 2 Evolution from Water Splitting under Visible Light, 2021, https://doi.org/10.1016/j.jechem.2021.03.019.
[95] X. Liu, Y. Zhang, H. Wang, J. Yan, L. Yan, K. Li, H. Guo, W. Gong, J. Lin, Highly efficient visible-light-driven photocatalytic hydrogen production on Cu7S4/Zn0.2Cd0·8S p-n binary heterojunctions, Int. J. Hydrog. Energy 48 (2023) 2171–2185, https://doi.org/10.1016/J.IJHYDENE.2022.10.114.
[96] M. Dan, S. Wei, D.E. Doronkin, Y. Li, Z. Zhao, S. Yu, J.-D. Grunwaldt, Y. Lin, Y. Zhou, Novel MnS/(InxCu1-x)2S3 composite for robust solar hydrogen sulphide splitting via the synergy of solid solution and heterojunction, Appl. Catal. B 243 (2019) 790–800, https://doi.org/10.1016/j.apcatb.2018.11.016.
[97] Y. Zhang, D. Chen, N. Li, Q. Xu, H. Li, J. Lu, Fabricating 1D/2D Co3O4/ZnIn2S4 core–shell heterostructures with boosted charge transfer for photocatalytic hydrogen production, Appl. Surf. Sci. 610 (2023) 155272, https://doi.org/10.1016/J.APSUSC.2022.155272.
[98] J. Jianfeng, W. Minmin, Y. Xiaolei, D. Xinyu, Preparation Method of Nano Bi2WO6-TiO2 Visible Light Water Splitting Catalyst, CN116920823A, 2023.
[99] S. Yaorong, G. Yiyao, Z. Wei, M. Aiyun, H. Bin, H. Peigang, S-doped ReSe2 Photocatalytic Hydrogen Promoter as Well as Preparation Method and Application Thereof, CN120243064A, 2025.
[100] R. Ma, G. Williams, M. Muscetta, S. Vernuccio, Enhanced photocatalytic hydrogen evolution via ball-milled PtO2/TiO2 heterojunction photocatalyst: an alternative approach for efficient energy production, Chem. Eng. J. 507 (2025) 160228, https://doi.org/10.1016/J.CEJ.2025.160228.
[101] Y. Shengyan, Y. Junfeng, D. Yanhui, C. Hao, S. Ping, S. Hang, Q. Weiping, P-n Heterojunction Composite Photocatalyst cu 2 O/MTiO 3 Preparation Method and Application, CN114984965A, 2023.
[102] F. Sheng, Z. Yun, D. Xiaojun, F. Lufang, MCS/ZCO Composite Photocatalyst for Photocatalytic Hydrogen Production and Preparation Method, CN114749189A, 2023.
[103] D. Wen, G. Huanhuan, L. Zhihong, Cu2-xS@Zn3.74Ga1.02S5.24 Hollow Nanosphere p-n Type Heterojunction Photocatalytic Material and its Photocatalytic Hydrogen Production Application, CN117482962A, 2025.
[104] G. Liao, C. Li, X. Li, B. Fang, Emerging polymeric carbon nitride Z-scheme systems for photocatalysis, Cell Rep. Phys. Sci. 2 (2021), https://doi.org/10.1016/J.XCRP.2021.100355.
[105] M. Edwin Malefane, P. John Mafa, T. Thokozani Innocent Nkambule, M. Elizabeth Managa, A. Tawanda Kuvarega, Modulation of Z-scheme photocatalysts for pharmaceuticals remediation and pathogen inactivation: design devotion, concept examination, and developments, Chem. Eng. J. 452 (2023), https://doi.org/10.1016/j.cej.2022.138894.
[106] Y. Kang, H. Qi, G. Wan, C. Zhen, X. Xu, L.C. Yin, L. Wang, G. Liu, H.M. Cheng, Ferroelectric polarization enabled spatially selective adsorption of redox mediators to promote Z-scheme photocatalytic overall water splitting, Joule 6 (2022) 1876–1886, https://doi.org/10.1016/J.JOULE.2022.06.017.
[107] P. Wang, S. Fan, X. Li, J. Wang, Z. Liu, C. Bai, M.O. Tadé, S. Liu, Piezotronic effect and hierarchical Z-scheme heterostructure stimulated photocatalytic H2 evolution integrated with C-N coupling of benzylamine, Nano Energy 89 (2021) 106349, https://doi.org/10.1016/J.NANOEN.2021.106349.
[108] C.Q. Li, X. Du, S. Jiang, Y. Liu, Z.L. Niu, Z.Y. Liu, S.S. Yi, X.Z. Yue, Constructing direct Z-scheme heterostructure by enwrapping ZnIn2S4 on CdS hollow cube for efficient photocatalytic H2 generation, Adv. Sci. 9 (2022) 2201773, https://doi.org/10.1002/ADVS.202201773.
[109] H. Cui, B. Li, Y. Zhang, X. Zheng, X. Li, Z. Li, S. Xu, Constructing Z-scheme based CoWO4/CdS photocatalysts with enhanced dye degradation and H2 generation performance, Int. J. Hydrog. Energy 43 (2018) 18242–18252, https://doi.org/10.1016/J.IJHYDENE.2018.08.050.
[110] C. Guo, L. Chu, Q. Zhang, Z. Li, G. Yang, F. Peng, The zinc vacancy induced CdS/ZnS Z-scheme structure as a highly stable photocatalyst for hydrogen production, J. Alloys Compd. 888 (2021) 161620, https://doi.org/10.1016/J.JALLCOM.2021.161620.
[111] X. Wang, X. Wang, J. Huang, S. Li, A. Meng, Z. Li, Interfacial chemical bond and internal electric field modulated Z-scheme Sv-ZnIn2S4/MoSe2 photocatalyst for efficient hydrogen evolution, Nat. Commun. 12 (1) (2021) 1–11, https://doi.org/10.1038/s41467-021-24511-z.

[112] R. Shen, L. Zhang, X. Chen, M. Jaroniec, N. Li, X. Li, Integrating 2D/2D CdS/α-Fe2O3 ultrathin bilayer Z-scheme heterojunction with metallic β-NiS nanosheet-based ohmic-junction for efficient photocatalytic H2 evolution, Appl. Catal. B 266 (2020) 118619, https://doi.org/10.1016/J.APCATB.2020.118619.
[113] Q. Xu, L. Zhang, B. Cheng, J. Fan, J. Yu, S-scheme heterojunction photocatalyst, Chem 6 (2020) 1543–1559, https://doi.org/10.1016/J.CHEMPR.2020.06.010.
[114] M. Lin, H. Chen, Z. Zhang, X. Wang, Engineering interface structures for heterojunction photocatalysts, Phys. Chem. Chem. Phys. 25 (2023) 4388–4407, https://doi.org/10.1039/D2CP05281D.
[115] W. Shu, G. Jian, L. Yuping, Z. Hui, L. Xin, Y. Denghui, D. Peng, Zn (zinc) 0.5 Cd 0.5 S/WO 3 Heterojunction Multifunctional Photocatalyst and Preparation Method Thereof, CN117414849A, 2024.
[116] H. Qiuying, C. Chuanxiang, Y. Haiqian, Y. Lei, D. Ying, Preparation Method and Application of Ternary In2O3@SnIn4S8/CdS Heterojunction Photocatalyst, CN116493024A, 2024.
[117] S. Hamdan, M.J. Wigglesworth, M. Muscetta, R. Ma, M.I. Helal, N. Martsinovich, G. Palmisano, S. Vernuccio, Unravelling the photoactivity of metal-loaded TiO2 for hydrogen production: insights from a combined experimental and computational analysis, Int. J. Hydrog. Energy 118 (2025) 394–406, https://doi.org/10.1016/J.IJHYDENE.2025.03.184.
[118] Y. Zhou, X. Ye, D. Lin, Enhance photocatalytic hydrogen evolution by using alkaline pretreated corn stover as a sacrificial agent, Int. J. Energy Res. 44 (2020) 4616–4628, https://doi.org/10.1002/ER.5242.
[119] H. Nagakawa, M. Nagata, Photoreforming of organic waste into hydrogen using a thermally radiative CdO x/CdS/SiC photocatalyst, ACS Appl. Mater. Interfaces 13 (2021) 47511–47519, https://doi.org/10.1021/ACSAMI.1C11888.
[120] E.C. Su, B.S. Huang, M.Y. Wey, Green route for hydrogen evolution from real electroplating waste liquids induced by a solar light responsive photocatalyst, ACS Sustain. Chem. Eng. 5 (2017) 2146–2153, https://doi.org/10.1021/ACSSUSCHEMENG.6B01999.
[121] J. Wang, Z. Wang, P. Qu, Q. Xu, J. Zheng, S. Jia, J. Chen, Z. Zhu, A 2D/1D TiO2 nanosheet/CdS nanorods heterostructure with enhanced photocatalytic water splitting performance for H2 evolution, Int. J. Hydrog. Energy 43 (2018) 7388–7396, https://doi.org/10.1016/J.IJHYDENE.2018.02.191.
[122] J. Hu, C. Chen, Y. Zheng, G. Zhang, C. Guo, C.M. Li, Spatially separating redox centers on Z-scheme ZnIn2 S4 /BiVO4 hierarchical heterostructure for highly efficient photocatalytic hydrogen evolution, Small 16 (2020), https://doi.org/10.1002/SMLL.202002988.
[123] H.H. El-Maghrabi, A. Barhoum, A.A. Nada, Y.M. Moustafa, S.M. Seliman, A. M. Youssef, M. Bechelany, Synthesis of mesoporous core-shell CdS@TiO2 (0D and 1D) photocatalysts for solar-driven hydrogen fuel production, J. Photochem. Photobiol. A Chem. 351 (2018) 261–270, https://doi.org/10.1016/J.JPHOTOCHEM.2017.10.048.
[124] M. Yuan, W.H. Zhou, D.X. Kou, Z.J. Zhou, Y.N. Meng, S.X. Wu, Cu2ZnSnS4 decorated CdS nanorods for enhanced visible-light-driven photocatalytic hydrogen production, Int. J. Hydrog. Energy 43 (2018) 20408–20416, https://doi.org/10.1016/J.IJHYDENE.2018.09.161.
[125] X. Hu, J. Song, J. Luo, H. Zhang, Z. Sun, C. Li, S. Zheng, Q. Liu, Single-atomic Pt sites anchored on defective TiO2 nanosheets as a superior photocatalyst for hydrogen evolution, J. Energy Chem. 62 (2021) 1–10, https://doi.org/10.1016/J.JECHEM.2021.03.003.
[126] D. Zabelin, A. Zabelina, A. Tulupova, R. Elashnikov, Z. Kolska, V. Svorcik, O. Lyutakov, A surface plasmon polariton-triggered Z-scheme for overall water splitting and solely light-induced hydrogen generation, J. Mater. Chem. A Mater. 10 (2022) 13829–13838, https://doi.org/10.1039/D2TA02365B.
[127] X. Wang, X. Zheng, H. Han, Y. Fan, S. Zhang, S. Meng, S. Chen, Photocatalytic hydrogen evolution from biomass (glucose solution) on Au/CdS nanorods with Au3+ self-reduction, J. Solid State Chem. 289 (2020) 121495, https://doi.org/10.1016/J.JSSC.2020.121495.
[128] J. Zhang, D. Wang, R. Chen, X. Zhu, D. Ye, Y. Yang, Q. Liao, Insight into synergistic enhancement of photothermal catalytic hydrogen production by plasmonic Au-NP/TiO2 in the presence of glycerol, ECM 277 (2023) 116626, https://doi.org/10.1016/J.ENCONMAN.2022.116626.
[129] L. Li, R. Zhang, Y. Lin, D. Wang, T. Xie, Plasmon-enhanced bulk charge separation via morphological and interfacial engineering in Au@carbon dots@CdS hybrid, Chem. Eng. J. 453 (2023) 139970, https://doi.org/10.1016/J.CEJ.2022.139970.
[130] C. Hu, C. Tai, W. Zhang, Q. Lu, M. Wei, C. Si, E. Guo, Y. Pang, Plasmonic Au functionalized 3D SrTiO3/TiO2 hollow nanosphere enables efficient solar water splitting, J. Alloys Compd. 930 (2023) 167449, https://doi.org/10.1016/J.JALLCOM.2022.167449.
[131] I. Ahmad, S. Shukrullah, M.Y. Naz, H.N. Bhatti, N.R. Khalid, S. Ullah, Rational design of ZnO–CuO–Au S-scheme heterojunctions for photocatalytic hydrogen production under visible light, Int. J. Hydrog. Energy 48 (2023) 12683–12698, https://doi.org/10.1016/J.IJHYDENE.2022.11.289.
[132] X. Li, G. Lv, W. Ma, S. Li, J. Yang, R. Zhang, J. Zhang, Photocatalytic H2 evolution by AgNP@PSi/SiNS composite derived from diamond-wire sawing silicon waste, Sol. Energy Mater. Sol. Cells 236 (2022) 111495, https://doi.org/10.1016/J.SOLMAT.2021.111495.
[133] P.C. Nethravathi, M.V. Manjula, S. Devaraja, M. Sakar, D. Suresh, Eco-friendly preparation of Bi2O3, Ag-Bi2O3 and Ag-Bi2O3-rGO nanomaterials and their photocatalytic H2 evolution, dye degradation, nitrite sensing and biological applications, J. Photochem. Photobiol. A Chem. 435 (2023) 114295, https://doi.org/10.1016/J.JPHOTOCHEM.2022.114295.
[134] L. Zhao, M. Tang, F. Wang, X. Qiu, Efficient Cu/CeO2 composites for hydrogen production from photothermal methanol steam reforming: the utility of synergism of photo and thermal catalysis, Fuel 331 (2023) 125748, https://doi.org/10.1016/J.FUEL.2022.125748.
[135] Q. Wang, S. Zhu, S. Zhao, C. Li, R. Wang, D. Cao, G. Liu, Construction of Bi-assisted modified CdS/TiO2 nanotube arrays with ternary S-scheme heterojunction for photocatalytic wastewater treatment and hydrogen production, Fuel 322 (2022) 124163, https://doi.org/10.1016/J.FUEL.2022.124163.
[136] A. Petala, D.I. Kondarides, Photocatalytic hydrogen production over mixed Cd-Zn sulfide catalysts promoted with nickel or nickel phosphide, Catal. Today 355 (2020) 851–859, https://doi.org/10.1016/J.CATTOD.2019.03.036.
[137] Y. Wei, J. Xiong, W. Li, R.H. Kollarigowda, G. Cheng, Achieving photocatalytic hydrogen production from alkaline solution upon a designed mesoporous TiO2–Ni hybrid employing commonly used paper as a sacrificial electron donor, Inorg. Chem. Front. 5 (2018) 2709–2717, https://doi.org/10.1039/C8QI00621K.
[138] C. Cheng, J. Zhang, R. Zeng, F. Xing, C. Huang, Schottky barrier tuning via surface plasmon and vacancies for enhanced photocatalytic H2 evolution in seawater, Appl. Catal. B 310 (2022) 121321, https://doi.org/10.1016/J.APCATB.2022.121321.
[139] R. Jiang, B. Li, C. Fang, J. Wang, Metal/semiconductor hybrid nanostructures for plasmon-enhanced applications, Adv. Mater. 26 (2014) 5274–5309, https://doi.org/10.1002/ADMA.201400203.
[140] H. Van Dang, Y.H. Wang, J.C.S. Wu, Z-scheme photocatalyst Pt/GaP-TiO2-SiO2: Rh for the separated H2 evolution from photocatalytic seawater splitting, Appl. Catal. B 296 (2021) 120339, https://doi.org/10.1016/J.APCATB.2021.120339.
[141] Y. Liu, X. Zhang, Y. Wang, C. Xie, Y. Zhao, Y. Song, P. Yang, Deposition of CdS and au nanoparticles on TiO2(B) spheres towards superior photocatalytic performance, Int. J. Hydrog. Energy 44 (2019) 17697–17708, https://doi.org/10.1016/J.IJHYDENE.2019.04.273.
[142] M.V. Pavliuk, A.B. Fernandes, M. Abdellah, D.L.A. Fernandes, C.O. Machado, I. Rocha, Y. Hattori, C. Paun, E.L. Bastos, J. Sá, Nano-hybrid plasmonic photocatalyst for hydrogen production at 20% efficiency, Sci. Rep. 7 (1) (2017) 1–9, https://doi.org/10.1038/s41598-017-09261-7.
[143] G.K. Sukhadeve, H. Bandewar, S.Y. Janbandhu, J.R. Jayaramaiah, R.S. Gedam, Photocatalytic hydrogen production, dye degradation, and antimicrobial activity by Ag-Fe co-doped TiO2 nanoparticles, J. Mol. Liq. 369 (2023) 120948, https://doi.org/10.1016/J.MOLLIQ.2022.120948.
[144] H. An, M. Li, R. Liu, Z. Gao, Z. Yin, Design of AgxAu1−x alloy/ZnIn2S4 system with tunable spectral response and Schottky barrier height for visible-light-driven hydrogen evolution, Chem. Eng. J. 382 (2020) 122953, https://doi.org/10.1016/J.CEJ.2019.122953.
[145] T. Muhammad, Triphenylphosphine Ruthenium Photocatalyst for Hydrogen Production, US12364977B1, 2024.
[146] J. Low, J. Yu, M. Jaroniec, S. Wageh, A.A. Al-Ghamdi, Heterojunction photocatalysts, Adv. Mater. 29 (2017) 1601694, https://doi.org/10.1002/ADMA.201601694.
[147] W. Chen, R.Q. Yan, J.Q. Zhu, G.B. Huang, Z. Chen, Highly efficient visible-light-driven photocatalytic hydrogen evolution by all-solid-state Z-scheme CdS/QDs/ZnIn2S4 architectures with MoS2 quantum dots as solid-state electron mediator, Appl. Surf. Sci. 504 (2020) 144406, https://doi.org/10.1016/J.APSUSC.2019.144406.
[148] D. Salazar-Marín, G. Oza, J.A.D. Real, A. Cervantes-Uribe, H. Pérez-Vidal, M. K. Kesarla, J.G.T. Torres, S. Godavarthi, Distinguishing between type II and S-scheme heterojunction materials: a comprehensive review, Appl. Surf. Sci. Adv. 19 (2024) 100536, https://doi.org/10.1016/J.APSADV.2023.100536.
[149] J. Li, H. Yuan, W. Zhang, B. Jin, Q. Feng, J. Huang, Z. Jiao, Advances in Z-scheme semiconductor photocatalysts for the photoelectrochemical applications: a review, Carbon Energy 4 (2022) 294–331, https://doi.org/10.1002/CEY2.179.
[150] Q. Xu, L. Zhang, B. Cheng, J. Fan, J. Yu, S-scheme heterojunction photocatalyst, Chem 6 (2020) 1543–1559, https://doi.org/10.1016/J.CHEMPR.2020.06.010.
[151] J. Low, B. Cheng, J. Yu, Surface modification and enhanced photocatalytic CO2 reduction performance of TiO2: a review, Appl. Surf. Sci. 392 (2017) 658–686, https://doi.org/10.1016/J.APSUSC.2016.09.093.
[152] D. Huang, X. Yan, M. Yan, G. Zeng, C. Zhou, J. Wan, M. Cheng, W. Xue, Graphitic carbon nitride-based heterojunction photoactive nanocomposites: applications and mechanism insight, ACS Appl. Mater. Interfaces 10 (2018) 21035–21055, https://doi.org/10.1021/ACSAMI.8B03620.
[153] W. Jones, D.J. Martin, A. Caravaca, A.M. Beale, M. Bowker, T. Maschmeyer, G. Hartley, A. Masters, A comparison of photocatalytic reforming reactions of methanol and triethanolamine with Pd supported on titania and graphitic carbon nitride, Appl. Catal. B 240 (2019) 373–379, https://doi.org/10.1016/j.apcatb.2017.01.042.
[154] R. Shen, J. Xie, H. Zhang, A. Zhang, X. Chen, X. Li, Enhanced solar fuel H2 generation over g-C3N4 nanosheet photocatalysts by the synergetic effect of noble metal-free Co2P cocatalyst and the environmental phosphorylation strategy, ACS Sustain. Chem. Eng. 6 (2018) 816–826, https://doi.org/10.1021/acssuschemeng.7b03169.
[155] Z. Sun, M. Zhu, M. Fujitsuka, A. Wang, C. Shi, T. Majima, Phase effect of NixPy hybridized with g-C3N4 for photocatalytic hydrogen generation, ACS Appl. Mater. Interfaces 9 (2017) 30583–30590, https://doi.org/10.1021/acsami.7b06386.
[156] T. Wu, P. Wang, J. Qian, Y. Ao, C. Wang, J. Hou, Noble-metal-free nickel phosphide modified CdS/C3N4 nanorods for dramatically enhanced photocatalytic hydrogen evolution under visible light irradiation, Dalton Trans. 46 (2017) 13793–13801, https://doi.org/10.1039/c7dt02929b.
[157] Y.J. Yuan, Y. Yang, Z. Li, D. Chen, S. Wu, G. Fang, W. Bai, M. Ding, L.X. Yang, D. P. Cao, Z.T. Yu, Z.G. Zou, Promoting charge separation in g-C3N4/graphene/

MoS2 photocatalysts by two-dimensional nanojunction for enhanced photocatalytic H2 production, ACS Appl. Energy Mater. 1 (2018) 1400–1407, https://doi.org/10.1021/acsaem.8b00030.
[158] A.E. Hassan, A.M. Elewa, M.S.A. Hussien, A.F.M. EL-Mahdy, I.M.A. Mekhemer, I. S. Yahia, T.A. Mohamed, H.H. Chou, Z. Wen, Designing of covalent organic framework/2D g-C3N4 heterostructure using a simple method for enhanced photocatalytic hydrogen production, J. Colloid Interface Sci. 653 (2024) 1650–1661, https://doi.org/10.1016/j.jcis.2023.10.010.
[159] Y.H. Lai, P.W. Yeh, M.J. Jhong, P.C. Chuang, Solar-driven hydrogen evolution in alkaline seawater over earth-abundant g-C3N4/CuFeO2 heterojunction photocatalyst using microplastic as a feedstock, Chem. Eng. J. 475 (2023), https://doi.org/10.1016/j.cej.2023.146413.
[160] A. Sherryna, M. Tahir, Z.Y. Zakaria, Well-structured V2C MXenes coupled g-C3N4 2D/2D nanohybrids for proficient charge separation with the role of triethanolamine (TEOA) as a protective barrier of g-C3N4 for stimulating photocatalytic H2 production, Int. J. Hydrog. Energy (2023), https://doi.org/10.1016/j.ijhydene.2023.09.234.
[161] A.V. Zhurenok, K.O. Potapenko, D.V. Markovskaya, N.D. Sidorenko, S. V. Cherepanova, E.Y. Gerasimov, A.A. Saraev, E.A. Kozlova, Br- and I-modified g-C3N4 photocatalysts prepared via novel two-stage technique for hydrogen evolution and photocurrent generation, Int. J. Hydrog. Energy (2023), https://doi.org/10.1016/j.ijhydene.2023.09.195.
[162] S. Xu, M. Li, Y. Wang, Z. Jin, Enhanced photocatalytic hydrogen evolution over coal-based carbon quantum dots modified CoMoO4/g-C3N4, Int. J. Hydrog. Energy (2023), https://doi.org/10.1016/j.ijhydene.2023.09.260.
[163] S. Chen, Y. Peng, B. Lu, Catalysis of Hydrogen Evolution Reaction Using Ruthenium Ion Complexed Carbon Nitride Materials, US20230295816A1, 2023.
[164] J. Huang, T. Xiao, L. Feng, L. Cao, M. Niu, Q. Liu, X. Zhang, V-Ni2P/g-C3N4 Photocatalyst and its Preparation Method and Application Thereof, US11618011, 2022.
[165] W. Fuxian, L. Qiong, K, Rb Co-Doped C3N4 Photocatalyst and Application in Preparation of Acetaldehyde by Synergistic Photocatalytic CO2 Reduction and Ethanol Oxidation, CN116099563A, 2023.
[166] T.Y. Huang, Z. Yang, S.Y. Yang, Z.H. Dai, Y.J. Liu, J.H. Liao, G.Y. Zhong, Z.J. Xie, Y.P. Fang, S.S. Zhang, Construction of 2D/2D Ti3C2Tx MXene/CdS heterojunction with photothermal effect for efficient photocatalytic hydrogen production, J. Mater. Sci. Technol. 171 (2024) 1–9, https://doi.org/10.1016/j.jmst.2023.07.010.
[167] M. Cai, X. Zha, Z. Zhuo, J. Bai, Q. Wang, Q. Cheng, Y. Wei, S. Sun, Enhanced photocatalytic hydrogen production of ZnIn2S4 by using surface-engineered Ti3C2Tx MXene as a cocatalyst, Materials 16 (2023), https://doi.org/10.3390/ma16062168.
[168] P. Tian, X. He, L. Zhao, W. Li, W. Fang, H. Chen, F. Zhang, Z. Huang, H. Wang, Enhanced charge transfer for efficient photocatalytic H2 evolution over UiO-66-NH2 with annealed Ti3C2Tx MXenes, Int. J. Hydrog. Energy 44 (2019) 788–800, https://doi.org/10.1016/j.ijhydene.2018.11.016.
[169] P. Tian, X. He, L. Zhao, W. Li, W. Fang, H. Chen, F. Zhang, Z. Huang, H. Wang, Ti3C2 nanosheets modified Zr-MOFs with Schottky junction for boosting photocatalytic HER performance, Sol. Energy 188 (2019) 750–759, https://doi.org/10.1016/j.solener.2019.06.060.
[170] Y. Wang, X. Wang, Y. Ji, R. Bian, J. Li, X. Zhang, J. Tian, Q. Yang, F. Shi, Ti3C2 MXene coupled with CdS nanoflowers as 2D/3D heterostructures for enhanced photocatalytic hydrogen production activity, Int. J. Hydrog. Energy 47 (2022) 22045–22053, https://doi.org/10.1016/j.ijhydene.2022.05.014.
[171] Y. Zhuang, Y. Liu, X. Meng, Fabrication of TiO2 nanofibers/MXene Ti3C2 nanocomposites for photocatalytic H2 evolution by electrostatic self-assembly, Appl. Surf. Sci. 496 (2019), https://doi.org/10.1016/j.apsusc.2019.143647.
[172] Y. Li, L. Ding, Y. Guo, Z. Liang, H. Cui, J. Tian, Boosting the photocatalytic ability of g-C3N4 for hydrogen production by Ti3C2 MXene quantum dots, ACS Appl. Mater. Interfaces 11 (2019) 41440–41447, https://doi.org/10.1021/acsami.9b14985.
[173] T. Su, Z.D. Hood, M. Naguib, L. Bai, S. Luo, C.M. Rouleau, I.N. Ivanov, H. Ji, Z. Qin, Z. Wu, Monolayer Ti3C2 Tx as an effective co-catalyst for enhanced photocatalytic hydrogen production over TiO2, ACS Appl. Energy Mater. 2 (2019) 4640–4651, https://doi.org/10.1021/acsaem.8b02268.
[174] L. Cheng, Q. Chen, J. Li, H. Liu, Boosting the photocatalytic activity of CdLa2S4 for hydrogen production using Ti3C2 MXene as a co-catalyst, Appl. Catal. B 267 (2020), https://doi.org/10.1016/j.apcatb.2019.118379.
[175] Y. Li, Z. Yin, G. Ji, Z. Liang, Y. Xue, Y. Guo, J. Tian, X. Wang, H. Cui, 2D/2D/2D heterojunction of Ti3C2 MXene/MoS2 nanosheets/TiO2 nanosheets with exposed (001) facets toward enhanced photocatalytic hydrogen production activity, Appl. Catal. B 246 (2019) 12–20, https://doi.org/10.1016/j.apcatb.2019.01.051.
[176] R. Xiao, C. Zhao, Z. Zou, Z. Chen, L. Tian, H. Xu, H. Tang, Q. Liu, Z. Lin, X. Yang, In situ fabrication of 1D CdS nanorod/2D Ti3C2 MXene nanosheet Schottky heterojunction toward enhanced photocatalytic hydrogen evolution, Appl. Catal. B 268 (2020), https://doi.org/10.1016/j.apcatb.2019.118382.
[177] Y. Li, L. Ding, S. Yin, Z. Liang, Y. Xue, X. Wang, H. Cui, J. Tian, Photocatalytic H2 evolution on TiO2 assembled with Ti3C2 MXene and metallic 1T-WS2 as co-catalysts, Nano Lett. 12 (2020), https://doi.org/10.1007/s40820-019-0339-0.
[178] T. Liu, X. Wang, W. Liu, C. Xing, Y. Xiong, J. Tian, Growing one-dimensional Cd0.9Zn0.1S nanorods on two-dimensional Ti3C2 MXene nanosheets for superior photocatalytic hydrogen production performance, Appl. Surf. Sci. 626 (2023), https://doi.org/10.1016/j.apsusc.2023.157212.
[179] J. Li, H. Peng, B. Luo, J. Cao, L. Ma, D. Jing, The enhanced photocatalytic and photothermal effects of Ti3C2 Mxene quantum dot/macroscopic porous graphitic carbon nitride heterojunction for hydrogen production, J. Colloid Interface Sci. 641 (2023) 309–318, https://doi.org/10.1016/j.jcis.2023.03.015.
[180] Y. Li, L. Ding, Z. Liang, Y. Xue, H. Cui, J. Tian, Synergetic effect of defects rich MoS2 and Ti3C2 MXene as cocatalysts for enhanced photocatalytic H2 production activity of TiO2, Chem. Eng. J. 383 (2020), https://doi.org/10.1016/j.cej.2019.123178.
[181] J. Ran, G. Gao, F.T. Li, T.Y. Ma, A. Du, S.Z. Qiao, Ti3C2 MXene co-catalyst on metal sulfide photo-absorbers for enhanced visible-light photocatalytic hydrogen production, Nat. Commun. 8 (2017), https://doi.org/10.1038/ncomms13907.
[182] C. Wu, W. Huang, H. Liu, K. Lv, Q. Li, Insight into synergistic effect of Ti3C2 MXene and MoS2 on anti-photocorrosion and photocatalytic of CdS for hydrogen production, Appl. Catal. B 330 (2023), https://doi.org/10.1016/j.apcatb.2023.122653.
[183] P. Lin, J. Shen, X. Yu, Q. Liu, D. Li, H. Tang, Construction of Ti3C2 MXene/O-doped g-C3N4 2D-2D Schottky-junction for enhanced photocatalytic hydrogen evolution, Ceram. Int. 45 (2019) 24656–24663, https://doi.org/10.1016/j.ceramint.2019.08.203.
[184] P. Yanhua, G. Yanan, Z. Dongsheng, Preparation Method and Application of Ti3C2-MXene/ZnIn2S4 Composite Photocatalyst, CN113070074A, 2021.
[185] L. Futian, Z. Jiahui, L. Kui, TiO2-Ti3C2-CoSx Nanocrystal Photocatalyst and Preparation Method Thereof, CN109433237A, 2019.
[186] W. Junqi, L. Xiangjun, H. Guang, S. Weiqiang, Y. Yihong, Z. Shuai, M. Jingjing, W. Miao, Method for Producing Hydrogen Through Photocatalysis, CN118894490A, 2024.
[187] W. Junqi, L. Xiangjun, H. Guang, Y. Yihong, S. Weiqiang, M. Jinging, Z. Shuai, W. Miao, Ti3C2Tx/CdS Material for Hydrogen Production Through Photocatalytic Reforming of Biomass and Preparation Method of Ti3C2Tx/CdS Material, CN118904373A, 2024.
[188] L.C. Chen, C.Y. Teng, C.Y. Lin, H.Y. Chang, S.J. Chen, H. Teng, Architecting nitrogen functionalities on graphene oxide photocatalysts for boosting hydrogen production in water decomposition process, Adv. Energy Mater. 6 (2016), https://doi.org/10.1002/aenm.201600719.
[189] S.R. Shin, J.H. Park, K.H. Kim, K.M. Choi, J.K. Kang, Network of heterogeneous catalyst arrays on the nitrogen-doped graphene for synergistic solar energy harvesting of hydrogen from water, Chem. Mater. 28 (2016) 7725–7730, https://doi.org/10.1021/acs.chemmater.6b02780.
[190] M. Bowker, P.R. Davies, L.S. Al-Mazroai, Photocatalytic reforming of glycerol over gold and palladium as an alternative fuel source, Catal. Lett. 128 (2009) 253–255, https://doi.org/10.1007/s10562-008-9781-1.
[191] J. Zhang, Y. Zhao, X. Guo, C. Chen, C.L. Dong, R.S. Liu, C.P. Han, Y. Li, Y. Gogotsi, G. Wang, Single platinum atoms immobilized on an MXene as an efficient catalyst for the hydrogen evolution reaction, Nat. Catal. 1 (2018) 985–992, https://doi.org/10.1038/s41929-018-0195-1.
[192] X. An, W. Wang, J. Wang, H. Duan, J. Shi, X. Yu, The synergetic effects of Ti3C2 MXene and Pt as co-catalysts for highly efficient photocatalytic hydrogen evolution over g-C3N4, Phys. Chem. Chem. Phys. 20 (2018) 11405–11411, https://doi.org/10.1039/c8cp01123k.
[193] S. Jinwen, Cheng Cheng, M. Liuhao, G. Liejin, Graphite Phase Carbon Nitride and Preparation Method Thereof Produces Hydrogen Photochemical Catalyst and its Application, CN110127635B, 2019.
[194] T. Isimja, M. Aloufi, H. Idriss, Methods of Producing a Nanocomposite Heterojunction Photocatalyst, WO2019021189A1, 2019.
[195] Y. Xuefeng, Y. Na, W. Min, W. Jiahong, Ternary Composite Photocatalyst As Well as Preparation Method and Application, CN113522327A, 2021.
[196] W. Yuan, L. Cheng, Y. An, H. Wu, N. Yao, X. Fan, X. Guo, MXene nanofibers as highly active catalysts for hydrogen evolution reaction, ACS Sustain. Chem. Eng. 6 (2018) 8976–8982, https://doi.org/10.1021/acssuschemeng.8b01348.
[197] Y. Li, S. Yang, Z. Liang, Y. Xue, H. Cui, J. Tian, 1T-MoS2 nanopatch/Ti3C2 MXene/TiO2 nanosheet hybrids for efficient photocatalytic hydrogen evolution, Mater. Chem. Front. 3 (2019) 2673–2680, https://doi.org/10.1039/c9qm00608g.
[198] C. Peng, P. Wei, X. Li, Y. Liu, Y. Cao, H. Wang, H. Yu, F. Peng, L. Zhang, B. Zhang, K. Lv, High efficiency photocatalytic hydrogen production over ternary Cu/TiO2@Ti3C2Tx enabled by low-work-function 2D titanium carbide, Nano Energy 53 (2018) 97–107, https://doi.org/10.1016/j.nanoen.2018.08.040.
[199] H. Martínez-García, D. Salazar-Marín, V. Collins-Martínez, J.G. Torres-Torres, M. K. Kesarla, O.A. Jaramillo-Quintero, N. Hernández-Como, G. Oza, F. Ortiz-Chi, J. A. Diaz-Real, S. Godavarthi, Rationally designed C3N4/ TiO2 (anatase/brookite) heterojunction for enhanced photocatalytic hydrogen generation under visible light, Ceram. Int. (2023), https://doi.org/10.1016/j.ceramint.2023.08.084.
[200] G. Rongfeng, C. Xianhu, T. Yaxi, Z. Wenhui, Y. Xiuli, S. Rong, Sodium-boron Double-doped Nano-layered Graphite-like Phase Carbon Nitride and Preparation Method and Application, CN111215118B, 2022.
[201] T. Mian, Yicheng, J. Fulong, S. Xiaojia, D. Mali, Klaus, Aijun, Y. Gaodeng, Smith, Tantalum Nitride Doped With One or More Metals, a Catalyst, Methods for Water Splitting Using the Catalyst, and Methods, TW202302447A, 2023.
[202] Y. Li, L. Ding, S. Yin, Z. Liang, Y. Xue, X. Wang, H. Cui, J. Tian, Photocatalytic H2 evolution on TiO2 assembled with Ti3C2 MXene and metallic 1T-WS2 as co-catalysts, Nano Lett. 12 (2020), https://doi.org/10.1007/s40820-019-0339-0.
[203] L. Tie, S. Yang, C. Yu, H. Chen, Y. Liu, S. Dong, J. Sun, J. Sun, In situ decoration of ZnS nanoparticles with Ti 3 C 2 MXene nanosheets for efficient photocatalytic hydrogen evolution, J. Colloid Interface Sci. 545 (2019) 63–70, https://doi.org/10.1016/j.jcis.2019.03.014.
[204] S.A. Younis, E.E. Kwon, M. Qasim, K.H. Kim, T. Kim, D. Kukkar, X. Dou, I. Ali, Metal-organic framework as a photocatalyst: progress in modulation strategies

and environmental/energy applications, Prog. Energy Combust. Sci. 81 (2020) 100870, https://doi.org/10.1016/J.PECS.2020.100870.
[205] Y. Horiuchi, T. Toyao, M. Saito, K. Mochizuki, M. Iwata, H. Higashimura, M. Anpo, M. Matsuoka, Visible-light-promoted photocatalytic hydrogen production by using an amino-functionalized Ti(IV) metal-organic framework, J. Phys. Chem. C 116 (2012) 20848–20853, https://doi.org/10.1021/JP3046005.
[206] J. Wang, A.S. Cherevan, C. Hannecart, S. Naghdi, S.P. Nandan, T. Gupta, D. Eder, Ti-based MOFs: new insights on the impact of ligand composition and hole scavengers on stability, charge separation and photocatalytic hydrogen evolution, Appl. Catal. B 283 (2021) 119626, https://doi.org/10.1016/J.APCATB.2020.119626.
[207] W. Zhen, J. Ma, G. Lu, Small-sized Ni(1 1 1) particles in metal-organic frameworks with low over-potential for visible photocatalytic hydrogen generation, Appl. Catal. B 190 (2016) 12–25, https://doi.org/10.1016/J.APCATB.2016.02.061.
[208] M.A. Nasalevich, M. Van Der Veen, F. Kapteijn, J. Gascon, Metal–organic frameworks as heterogeneous photocatalysts: advantages and challenges, CrystEngComm 16 (2014) 4919–4926, https://doi.org/10.1039/C4CE00032C.
[209] A. De Vos, K. Hendrickx, P. Van Der Voort, V. Van Speybroeck, K. Lejaeghere, Missing linkers: an alternative pathway to UiO-66 electronic structure engineering, Chem. Mater. 29 (2017) 3006–3019, https://doi.org/10.1021/ACS.CHEMMATER.6B05444.
[210] C. Zhu, J. Hou, X. Wang, S. Wang, H. Xu, J. Hu, L. Jing, S. Wang, Optimizing ligand-to-metal charge transfer in metal–organic frameworks to enhance photocatalytic performance, Chem. Eng. J. 499 (2024), https://doi.org/10.1016/j.cej.2024.156527.
[211] X.P. Wu, L. Gagliardi, D.G. Truhlar, Cerium metal-organic framework for photocatalysis, J. Am. Chem. Soc. 140 (2018) 7904–7912, https://doi.org/10.1021/JACS.8B03613.
[212] G. Yang, J. Lv, Q. Yang, Q. Wang, Full-spectrum photocatalytic hydrogen production by MOFs materials-a minireview, Mater. Today Sustain. 31 (2025), https://doi.org/10.1016/j.mtsust.2025.101186.
[213] D. Shi, R. Zheng, M.-J. Sun, X. Cao, C. Hun-Xiao Sun, C.-J. Cui, C.-S. Liu, J. Zhao, Miao Du, D. Shi, C. Sun, C. Cui, C. Liu, M. Du, D.-J. Sun, D. Ao, R. Zheng, J. Zhao, Semiconductive copper(I)–organic frameworks for efficient light-driven hydrogen generation without additional photosensitizers and cocatalysts, Angew. Chem. Int. Ed. 56 (2017) 14637–14641, https://doi.org/10.1002/ANIE.201709869.
[214] G. Lan, Y.Y. Zhu, S.S. Veroneau, Z. Xu, D. Micheroni, W. Lin, Electron injection from photoexcited metal-organic framework ligands to Ru2 secondary building units for visible-light-driven hydrogen evolution, J. Am. Chem. Soc. 140 (2018) 5326–5329, https://doi.org/10.1021/JACS.8B01601.
[215] W.M. Liao, J.H. Zhang, Z. Wang, Y.L. Lu, S.Y. Yin, H.P. Wang, Y.N. Fan, M. Pan, C. Y. Su, Semiconductive amine-functionalized Co(II)-MOF for visible-light-driven hydrogen evolution and CO2 reduction, Inorg. Chem. 57 (2018) 11436–11442, https://doi.org/10.1021/ACS.INORGCHEM.8B01265.
[216] S. Afzal, W.A. Daoud, S.J. Langford, Photostable self-cleaning cotton by a copper (II) porphyrin/TiO2 visible-light photocatalytic system, ACS Appl. Mater. Interfaces 5 (2013) 4753–4759, https://doi.org/10.1021/AM400002K.
[217] H. Zhang, Q. Li, B. Li, B. Weng, Z. Tian, J. Yang, J. Hofkens, F. Lai, T. Liu, Atomically dispersed Pt sites on porous metal–organic frameworks to enable dual reaction mechanisms for enhanced photocatalytic hydrogen conversion, J. Catal. 407 (2022) 1–9, https://doi.org/10.1016/J.JCAT.2022.01.017.
[218] X. Wang, X. Zhang, W. Zhou, L. Liu, J. Ye, D. Wang, An ultrathin porphyrin-based metal-organic framework for efficient photocatalytic hydrogen evolution under visible light, Nano Energy 62 (2019) 250–258, https://doi.org/10.1016/J.NANOEN.2019.05.023.
[219] H. Li, X. Liu, Y. He, H. Feng, Y. Zhang, C. Liu, Z. Wu, 2D porphyrin-based MOFs with highly dispersed Pt nanoparticles via in-situ partial reduction strategy from porphyrin embedded with single-atom Pt for enhancing photocatalytic hydrogen production, Fuel 338 (2023) 127369, https://doi.org/10.1016/J.FUEL.2022.127369.
[220] Y. Tang, M. Chen, C. Zhang, H. Li, Y. He, X. Lai, L. Tao, J. Jing, X. Liu, 2D photosensitive porphyrin-based MOFs integrated with a Pd cocatalyst with fast charge transfer for efficient photocatalytic hydrogen evolution, Catal. Sci. Technol. 13 (2023) 5326–5332, https://doi.org/10.1039/D3CY00705G.
[221] E. Pena, J. Becerra, V.N. Gopalakrishnan, T.O. Do, Facile one-pot synthesis of plasmonic gold nanoparticles decorated porphyrin-metal organic framework for photocatalytic hydrogen evolution, Mol. Catal. 548 (2023) 113470, https://doi.org/10.1016/J.MCAT.2023.113470.
[222] S. Kyriakos, S. Berend, K. Stavroula, I.P. Chritopher, N. Ngoc Tu, Photocatalytic system comprising a titanium-based Mof, EP 3424594 (2019) A1.
[223] L. Xingyan, F. Huan, T. Yu, C. Mingzuo, X. Yonggang, T. Xiangguo, Preparation Method and Application of Porphyrin-metal Organic Framework Material, CN111804341A, 2022.
[224] Z. Lian, Z. Li, F. Wu, Y. Zhong, Y. Liu, W. Wang, J. Zi, W. Yang, Photogenerated hole traps in metal-organic-framework photocatalysts for visible-light-driven hydrogen evolution, Commun. Chem. 5 (1) (2022) 1–8, https://doi.org/10.1038/s42004-022-00713-4.
[225] H. Li, X. Liu, Y. He, H. Feng, Y. Zhang, C. Liu, Z. Wu, 2D porphyrin-based MOFs with highly dispersed Pt nanoparticles via in-situ partial reduction strategy from porphyrin embedded with single-atom Pt for enhancing photocatalytic hydrogen production, Fuel 338 (2023) 127369, https://doi.org/10.1016/J.FUEL.2022.127369.
[226] B. Mishra, A. Alam, A. Chakraborty, B. Kumbhakar, S. Ghosh, P. Pachfule, A. Thomas, Covalent organic frameworks for photocatalysis, Adv. Mater. (2024), https://doi.org/10.1002/adma.202413118.
[227] Z. Liang, R. Shen, Y.H. Ng, Y. Fu, T. Ma, P. Zhang, Y. Li, X. Li, Covalent organic frameworks: fundamentals, mechanisms, modification, and applications in photocatalysis, Chem. Catal. 2 (2022) 2157–2228, https://doi.org/10.1016/j.checat.2022.06.006.
[228] Y. Wang, W. Hao, H. Liu, R. Chen, Q. Pan, Z. Li, Y. Zhao, Facile construction of fully sp2-carbon conjugated two-dimensional covalent organic frameworks containing benzobisthiazole units, Nat. Commun. 13 (2022) 100, https://doi.org/10.1038/s41467-021-27573-1.
[229] H. Yu, J. Zhang, X. Yan, C. Wu, X. Zhu, B. Li, T. Li, Q. Guo, J. Gao, M. Hu, J. Yang, Donor–acceptor covalent organic framework hollow submicrospheres with a hierarchical pore structure for visible-light-driven H2 evolution, J. Mater. Chem. A 10 (2022) 11010–11018, https://doi.org/10.1039/D2TA01058E.
[230] Z. Zhao, X. Chen, B. Li, S. Zhao, L. Niu, Z. Zhang, Y. Chen, Spatial regulation of acceptor units in olefin-linked COFs toward highly efficient photocatalytic H2 evolution, Adv. Sci. 9 (2022) 2203832, https://doi.org/10.1002/advs.202203832.
[231] W. Chen, L. Wang, D. Mo, F. He, Z. Wen, X. Wu, H. Xu, L. Chen, Modulating benzothiadiazole-based covalent organic frameworks via halogenation for enhanced photocatalytic water splitting, Angew. Chem. Int. Ed. 59 (2020) 16902–16909, https://doi.org/10.1002/anie.202006925.
[232] C. Mo, M. Yang, F. Sun, J. Jian, L. Zhong, Z. Fang, J. Feng, D. Yu, Alkene-linked covalent organic frameworks boosting photocatalytic hydrogen evolution by efficient charge separation and transfer in the presence of sacrificial electron donors, Adv. Sci. 7 (2020) 1902988, https://doi.org/10.1002/advs.201902988.
[233] S. Ma, T. Deng, Z. Li, Z. Zhang, J. Jia, Q. Li, G. Wu, H. Xia, S.W. Yang, Photocatalytic hydrogen production on a sp2-carbon-linked covalent organic framework, Angew. Chem. Int. Ed. 61 (2022), https://doi.org/10.1002/anie.202208919.
[234] T. He, W. Zhen, Y. Chen, Y. Guo, Z. Li, N. Huang, Z. Li, R. Liu, Y. Liu, X. Lian, C. Xue, T.C. Sum, W. Chen, D. Jiang, Integrated interfacial design of covalent organic framework photocatalysts to promote hydrogen evolution from water, Nat. Commun. 14 (2023) 329, https://doi.org/10.1038/s41467-023-35999-y.
[235] R. Shen, X. Li, C. Qin, P. Zhang, X. Li, Efficient photocatalytic hydrogen evolution by modulating excitonic effects in Ni-intercalated covalent organic frameworks, Adv. Energy Mater. 13 (2023) 2203695, https://doi.org/10.1002/aenm.202203695.
[236] W. Xinchen, C. Xiong, C. Xiaowen, L. Zhipeng, H. Siyu, Pyrenyl Covalent Organic Framework Polymer Photocatalyst, Preparation Method Thereof and Application of Pyrenyl Covalent Organic Framework Polymer Photocatalyst in Hydrogen Production by Photocatalytic Decomposition of Water, CN116217849A, 2023.
[237] H. Li, J. Wang, Defect-rich Covalent Organic Framework Material, Preparation Method Thereof and Application Thereof in Photocatalytic Hydrogen Evolution, CN113896851B, 2022.
[238] X. Xinguo, W. Yan, D. Pengyu, Z. Aicaijun, C. Ting, Method for Preparing Monatomic Pt-Embedded Covalent Organic Framework Photocatalyst and Application, CN114534783A, 2023.
[239] Y. Zhou, Q. Yue, G. Li, J. Wang, Preparation Method of Covalent Organic Framework and Application of Covalent Organic Framework in Photocatalytic Seawater Hydrogen Evolution, CN115850625A, 2023.
[240] C. Dai, B. Liu, Conjugated polymers for visible-light-driven photocatalysis, Energy Environ. Sci. 13 (2020) 24–52, https://doi.org/10.1039/C9EE01935A.
[241] H. Zhang, W. Wei, K.A.I. Zhang, Emerging conjugated polymers for heterogeneous photocatalytic chemical transformation, Chem. Commun. 59 (2023) 9167–9181, https://doi.org/10.1039/D3CC02081A.
[242] L. Liu, M.Y. Gao, H. Yang, X. Wang, X. Li, A.I. Cooper, Linear conjugated polymers for solar-driven hydrogen peroxide production: the importance of catalyst stability, J. Am. Chem. Soc. 143 (2021) 19287–19293, https://doi.org/10.1021/jacs.1c09979.
[243] C. Yang, B.C. Ma, L. Zhang, S. Lin, S. Ghasimi, K. Landfester, K.A.I. Zhang, X. Wang, Molecular engineering of conjugated polybenzothiadiazoles for enhanced hydrogen production by photosynthesis, Angew. Chem. Int. Ed. 55 (2016) 9202–9206, https://doi.org/10.1002/anie.201603532.
[244] P. Dong, A. Zhang, J. Pan, K. Gao, Z. Wang, X. Xi, An all-organic S-scheme heterojunction containing donor–acceptor type conjugated polymer and C3N4 nanosheets assembled via π–π interaction for photocatalytic H2 generation, Appl. Surf. Sci. 615 (2023) 156414, https://doi.org/10.1016/j.apsusc.2023.156414.
[245] R.S. Sprick, B. Bonillo, R. Clowes, P. Guiglion, N.J. Brownbill, B.J. Slater, F. Blanc, M.A. Zwijnenburg, D.J. Adams, A.I. Cooper, Visible-light-driven hydrogen evolution using Planarized conjugated polymer Photocatalysts, Angew. Chem. Int. Ed. 55 (2016) 1792–1796, https://doi.org/10.1002/anie.201510542.
[246] M. Sachs, R.S. Sprick, D. Pearce, S.A.J. Hillman, A. Monti, A.A.Y. Guilbert, N. J. Brownbill, S. Dimitrov, X. Shi, F. Blanc, M.A. Zwijnenburg, J. Nelson, J. R. Durrant, A.I. Cooper, Understanding structure-activity relationships in linear polymer photocatalysts for hydrogen evolution, Nat. Commun. 9 (2018) 4968, https://doi.org/10.1038/s41467-018-07420-6.
[247] R. Li, X. Zhang, C. Zhang, J. Lu, J.-C. Wang, C.-X. Cui, X. Yang, F. Huang, J.-X. Jiang, Y. Zhang, Adenine-functionalized conjugated polymer as an efficient photocatalyst for hydrogen evolution from water, Int. J. Hydrog. Energy 47 (2022) 29771–29780, https://doi.org/10.1016/j.ijhydene.2022.06.296.
[248] Z. Li, Z. Jiao, B. Liu, G. Yue, J. Wang, Y. Tian, Halogenated Aromatic Linear Conjugated Polymer Photocatalytic Material As Well as Preparation Method and Application Thereof, 2022.
[249] J. Kosco, M. Bidwell, H. Cha, C.T. Howells, J.R. Durrant, I. McCulloch, Record Photocatalytic Hydrogen Evolution From Organic Semiconductor Heterojunction Nanoparticles, 2022.

[250] H. Song, S. Luo, H. Huang, B. Deng, J. Ye, Solar-driven hydrogen production: recent advances, challenges, and future perspectives, ACS Energy Lett. 7 (2022) 1043–1065, https://doi.org/10.1021/acsenergylett.1c02591.
[251] N. Fajrina, M. Tahir, A critical review in strategies to improve photocatalytic water splitting towards hydrogen production, Int. J. Hydrog. Energy 44 (2019) 540–577, https://doi.org/10.1016/j.ijhydene.2018.10.200.
[252] T. Hisatomi, K. Domen, Reaction systems for solar hydrogen production via water splitting with particulate semiconductor photocatalysts, Nat. Catal. 2 (2019) 387–399, https://doi.org/10.1038/s41929-019-0242-6.
[253] W.-J. Ong, L.-L. Tan, Y.H. Ng, S.-T. Yong, S.-P. Chai, Graphitic carbon nitride (g-C3N4)-based Photocatalysts for artificial photosynthesis and environmental remediation: are we a step closer to achieving sustainability? Chem. Rev. 116 (2016) 7159–7329, https://doi.org/10.1021/acs.chemrev.6b00075.
[254] S.N. Malik, V. Pugalenthi, A.N. Vaidya, P.C. Ghosh, S.N. Mudliar, Kinetics of Nano-catalysed Dark Fermentative Hydrogen Production From Distillery Wastewater, Energy Procedia, Elsevier Ltd, in, 2014, pp. 417–430, https://doi.org/10.1016/j.egypro.2014.07.284.
[255] S.S. Tak, O. Shetye, O. Muley, H. Jaiswal, S.N. Malik, Emerging technologies for hydrogen production from wastewater, Int. J. Hydrog. Energy 47 (2022) 37282–37301, https://doi.org/10.1016/j.ijhydene.2022.06.225.
[256] M.Z. Khan, A.S. Nizami, M. Rehan, O.K.M. Ouda, S. Sultana, I.M. Ismail, K. Shahzad, Microbial electrolysis cells for hydrogen production and urban wastewater treatment: a case study of Saudi Arabia, Appl. Energy 185 (2017) 410–420, https://doi.org/10.1016/j.apenergy.2016.11.005.
[257] Q. Wang, S. Zhu, S. Zhao, C. Li, R. Wang, D. Cao, G. Liu, Construction of Bi-assisted modified CdS/TiO2 nanotube arrays with ternary S-scheme heterojunction for photocatalytic wastewater treatment and hydrogen production, Fuel 322 (2022), https://doi.org/10.1016/j.fuel.2022.124163.
[258] S. Zhang, L. Wang, C. Liu, J. Luo, J. Crittenden, X. Liu, T. Cai, J. Yuan, Y. Pei, Y. Liu, Photocatalytic wastewater purification with simultaneous hydrogen production using MoS2 QD-decorated hierarchical assembly of ZnIn2S4 on reduced graphene oxide photocatalyst, Water Res. 121 (2017) 11–19, https://doi.org/10.1016/j.watres.2017.05.013.
[259] Z. Wei, M. Xu, J. Liu, W. Guo, Z. Jiang, W. Shangguan, Simultaneous Visible-light-induced Hydrogen Production Enhance-ment and Antibiotic Wastewater Degradation Using MoS 2 @Zn x Cd 1-x S: Solid-Solution-assisted Photocatalysis. http://www.sciencedirect.com/science/journal/18722067, 2020.
[260] Z. Qu, J. Wang, J. Tang, X. Shu, X. Liu, Z. Zhang, J. Wang, Carbon quantum dots/KNbO3 hybrid composites with enhanced visible-light driven photocatalytic activity toward dye waste-water degradation and hydrogen production, Mol. Catal. 445 (2018) 1–11, https://doi.org/10.1016/j.mcat.2017.11.002.
[261] G. Iervolino, V. Vaiano, D. Sannino, L. Rizzo, A. Galluzzi, M. Polichetti, G. Pepe, P. Campiglia, Hydrogen production from glucose degradation in water and wastewater treated by Ru-LaFeO3/Fe2O3 magnetic particles photocatalysis and heterogeneous photo-Fenton, Int. J. Hydrog. Energy 43 (2018) 2184–2196, https://doi.org/10.1016/j.ijhydene.2017.12.071.
[262] M. Nasr, A. Tawfik, S. Ookawara, M. Suzuki, Cost and Economic Analysis of Hydrogen and Methane Production From Starch Wastewater Industry Using Up-flow Anaerobic Staged Reactor, 2013, https://doi.org/10.13140/RG.2.1.1271.6640.
[263] S.Y. Arzate Salgado, R.M. Ramírez Zamora, R. Zanella, J. Peral, S. Malato, M. I. Maldonado, Photocatalytic hydrogen production in a solar pilot plant using a Au/TiO2 photo catalyst, Int. J. Hydrog. Energy 41 (2016) 11933–11940, https://doi.org/10.1016/j.ijhydene.2016.05.039.
[264] C.Y. Toe, J. Pan, J. Scott, R. Amal, Identifying key design criteria for large-scale photocatalytic hydrogen generation from engineering and economic perspectives, ACS ES&T Eng. 2 (2022) 1130–1143, https://doi.org/10.1021/acsestengg.2c00030.
[265] Z. Wang, Y. Gao, D. Zhao, W. Yu, W. Chen, M. Zhang, CN213314911U Photocatalytic Reactor With High Light Energy Utilization Rate, 2021.
[266] L.Y. Guo, CN1307416C Multichannel Rapid Evaluating Device for Photolysis Hydrogen Making Catalyst Performance, 2007.
[267] S. Yang, J. Li, X. Qu, Z. Huang, Z. Liu, Q. Li, X. Zhang, J. Wu, G. Meng, CN219596606U Internal Irradiation Type Photocatalytic Hydrogen Production Reactor, 2023.
[268] M. Shaghaghi, H. Sargazi, A. Bazargan, M. Bellardita, Photocatalytic reactor types and configurations, in: Photocatalytic Water and Wastewater Treatment, IWA Publishing, 2022, pp. 73–110, https://doi.org/10.2166/9781789061932_0073.
[269] O. Sacco, V. Vaiano, D. Sannino, Main parameters influencing the design of photocatalytic reactors for wastewater treatment: a mini review, J. Chem. Technol. Biotechnol. 95 (2020) 2608–2618, https://doi.org/10.1002/jctb.6488.
[270] D. Wang, M.A. Mueses, J.A.C. Márquez, F. Machuca-Martínez, I. Grčić, R. Peralta Muniz Moreira, G. Li Puma, Engineering and modeling perspectives on photocatalytic reactors for water treatment, Water Res. 202 (2021), https://doi.org/10.1016/j.watres.2021.117421.
[271] P. Pichat, Photocatalysis and Water Purification: From Fundamentals to Recent Applications, 2013, https://doi.org/10.1002/9783527645404.
[272] R.G. Nair, P.J. Bharadwaj, S.K. Samdarshi, Design Improvement and Performance Evaluation of Solar Photocatalytic Reactor for Industrial Effluent Treatment, 2015, https://doi.org/10.1016/j.ecoenv.2015.07.036.
[273] H. Nishiyama, T. Yamada, M. Nakabayashi, Y. Maehara, M. Yamaguchi, Y. Kuromiya, Y. Nagatsuma, H. Tokudome, S. Akiyama, T. Watanabe, R. Narushima, S. Okunaka, N. Shibata, T. Takata, T. Hisatomi, K. Domen, Photocatalytic solar hydrogen production from water on a 100-m 2 scale, Nature 304 (598) (2021), https://doi.org/10.1038/s41586-021-03907-3.
[274] D. Fattoruso, A. Puga, Photocatalytic Panel Reactor for the Anaerobic Photoreforming of Waste Aqueous Effluents and the Production of Hydrogen as Co-product, WO2023012057A1, 2023.
[275] M. Baojun, S. Xudong, System for Photocatalytic Hydrogen Production, CN216155478U, 2022.
[276] Y. Ren, L. Zhao, D. Jing, L. Guo, Investigation and modeling of CPC based tubular photocatalytic reactor for scaled-up hydrogen production, Int. J. Hydrog. Energy 41 (2016) 16019–16031, https://doi.org/10.1016/j.ijhydene.2016.04.225.
[277] E.B. Agyekum, C. Nutakor, A.M. Agwa, S. Kamel, A critical review of renewable hydrogen production methods: factors affecting their scale-up and its role in future energy generation, Membranes (Basel). 12 (2022), https://doi.org/10.3390/membranes12020173.
[278] B. Wang, W. Wang, D. Xia, G. Huang, L. Ye, CN108103519A Apparatus and Method for Photocatalytic Degradation and Hydrogen Production by Using Natural Magnetic Ore, 2018.
[279] C. Li, M. Yang, Z. Jiang, T. Liu, CN103861542A Reaction Device for Preparing Hydrogen Through Solar Photocatalysis, 2014.
[280] S.Y. Arzate Salgado, R.M. Ramírez Zamora, R. Zanella, J. Peral, S. Malato, M. I. Maldonado, Photocatalytic hydrogen production in a solar pilot plant using a Au/TiO2 photo catalyst, Int. J. Hydrog. Energy 41 (2016) 11933–11940, https://doi.org/10.1016/j.ijhydene.2016.05.039.
[281] M.I. Maldonado, A. López-Martín, G. Colón, J. Peral, J.I. Martínez-Costa, S. Malato, Solar pilot plant scale hydrogen generation by irradiation of Cu/TiO2 composites in presence of sacrificial electron donors, Appl. Catal. B 229 (2018) 15–23, https://doi.org/10.1016/j.apcatb.2018.02.005.
[282] S.K. Lakhera, A. Rajan, R. T.P, N. Bernaurdshaw, A review on particulate photocatalytic hydrogen production system: progress made in achieving high energy conversion efficiency and key challenges ahead, Renew. Sust. Energ. Rev. 152 (2021), https://doi.org/10.1016/j.rser.2021.111694.
[283] Y. Chen, R. Li, W. Zheng, H. Zhu, H. Xia, CN111453696A Concentrating Fixed-film Solar Photocatalytic Hydrogen Production Device, 2020.
[284] L. Guo, Z. Yanwei, CN1817789A System for Producing Hydrogen in Light-catalytic Decomposed Water With Double Beds, 2006.
[285] S. Mu Jin, Kang, H. Zhu, K. Zou, M. Gao, CN102285638A, Visible Light Catalytic Hydrogen Production Reactor, 2011.
[286] L. Lin, T. Hisatomi, S. Chen, T. Takata, K. Domen, Visible-light-driven photocatalytic water splitting: recent progress and challenges, Trends Chem. 2 (2020) 813–824, https://doi.org/10.1016/j.trechm.2020.06.006.
[287] Q. Jia, D. Duan, X. Zhang, Mikishina, Y. Li, Y. Ren, CN116239078A, Device and Method for Producing Hydrogen by Photolysis of Water, 2023.
[288] G. Liejin, J. Dengwei, Z. Xianghui, X. Chanjuan, Z. Ximin, CN100515924C Optical Catalytic Hydrogen Production System by Directly Utilizing Solar Energy to Decompose Water, 2009.
[289] P. Dong, L. Zhang, C. Wang, J. Gao, J. Tan, CN116358171A Secondary Reflection Condensation System and Application Thereof in Photocatalytic Hydrogen Production Reactor, 2023.
[290] C. Acar, I. Dincer, G.F. Naterer, Review of photocatalytic water-splitting methods for sustainable hydrogen production, Int. J. Energy Res. 40 (2016) 1449–1473, https://doi.org/10.1002/ER.3549.
[291] L. Yang, X. Li, G. Zhang, P. Cui, X. Wang, X. Jiang, J. Zhao, Y. Luo, J. Jiang, Combining photocatalytic hydrogen generation and capsule storage in graphene based sandwich structures, Nature Communications 2017 8:1 8 (2017) 1–7. doi: https://doi.org/10.1038/ncomms16049.
[292] R. Moradi, K.M. Groth, Hydrogen storage and delivery: review of the state of the art technologies and risk and reliability analysis, Int. J. Hydrog. Energy 44 (2019) 12254–12269, https://doi.org/10.1016/J.IJHYDENE.2019.03.041.
[293] Y. Wang, P. Ran, Y. Chen, CN111874864A Solar Photocatalytic Hydrogen Production System Capable of Safely Separating Hydrogen, 2020.
[294] J. Yang, X. Zhang, X. Mi, Y. Wang, CN115818566A Photocatalytic Hydrogen Production Device, 2023.
[295] Y. Yan, Z. Yaqian, Concentrating Photocatalytic Hydrogen Production Cogeneration System, CN116647181A, 2023.
[296] T. Masuda, R. Tomizawa, K. Okumura, T. Hasegawa, Hydrogen Gas Production Equipment Using Photocatalyst, JP2023094488A, 2025.
[297] R.A. Chiverton, Photocatalytic Generation of Hydrogen, WO2020039205A1, 2019.
[298] B. Ma, X. Song, CN216155478U System for Photocatalytic Hydrogen Production, 2022.
[299] M.G. Kholief, A.E.L. Hesham, F.S. Hashem, F.M. Mohamed, Synthesis and utilization of titanium dioxide nano particle (TiO2NPs) for photocatalytic degradation of organics, Sci. Rep. 14 (2024), https://doi.org/10.1038/s41598-024-53617-9.
[300] S.N. Saeedi, M.H. Rasoulifard, M.S.S. Dorraji, H. Douroudgari, N. Sehati, Enhanced photocatalytic degradation of organic pollutants using a TiO2–clay nanocomposite in a rotary photoreactor with experimental and theoretical insights, Sci. Rep. 15 (2025), https://doi.org/10.1038/s41598-025-22099-8.
[301] T. Dong, H.Y.M. Cheung, J.H.K. Man, Z. Zheng, I.M.C. Lo, Recent advances in oxidant-involved photoelectrochemical systems for sustainable wastewater treatment: mechanisms, applications, and perspectives, Npj Mater. Sustain. 3 (2025) 41, https://doi.org/10.1038/s44296-025-00084-6.
[302] T. Ahasan, P. Xu, H. Wang, Dual-function photocatalysis in the visible spectrum: Ag-G-TiO2 for simultaneous dye wastewater degradation and hydrogen production, Catalysts 14 (2024), https://doi.org/10.3390/catal14080530.
[303] I.Y. Qudsieh, M.A. Ali, I.M. Maafa, Effect of water matrix on photocatalytic degradation of organic pollutants in water: a literature review, Rev. Chem. Eng. 41 (2025) 539–573, https://doi.org/10.1515/revce-2024-0093.

[304] M.M. Pituco, P.H. Marrocos, S. Méndez, R. Montes, R. Rodil, F.C. Moreira, V.J. P. Vilar, Ozone injection system based on NETmix technology for quaternary treatment of urban wastewater, J. Environ. Chem. Eng. 13 (2025), https://doi.org/10.1016/j.jece.2025.115465.
[305] A. Kumar, P. Sharma, G. Sharma, P. Dhiman, G.T. Mola, M. Farghali, A. K. Rashwan, M. Nasr, A.I. Osman, T. Wang, Simultaneous hydrogen production and photocatalytic pollutant removal: a review, Environ. Chem. Lett. 22 (2024) 2405–2424, https://doi.org/10.1007/s10311-024-01756-w.
[306] A. Rioja-Cabanillas, D. Valdesueiro, P. Fernández-Ibáñez, J.A. Byrne, Hydrogen from wastewater by photocatalytic and photoelectrochemical treatment, J. Phys. Energy 3 (2021), https://doi.org/10.1088/2515-7655/abceab.
[307] A.R. de Olivera, C.S. Santos, I.F. Mena, M.A. Montiel, R. Montes, J.B. Quintana, R. Rodil, A.I. Gomes, F.C. Moreira, J. Gäbler, L. Schäfer, C. Sáez, M.A. Rodrigo, V. J.P. Vilar, Integration of a 3D-printed electrochemical reactor with a tubular membrane photoreactor to promote sulfate-based advanced oxidation processes, Chem. Eng. J. 500 (2024), https://doi.org/10.1016/j.cej.2024.156900.
[308] N.S. Ali, K.R. Kalash, A.N. Ahmed, T.M. Albayati, Performance of a solar photocatalysis reactor as pretreatment for wastewater via UV, UV/TiO2, and UV/H2O2 to control membrane fouling, Sci. Rep. 12 (2022), https://doi.org/10.1038/s41598-022-20984-0.
[309] D.F.S. Morais, J.C.B. Lopes, M.M. Dias, V.J.P. Vilar, F.C. Moreira, e–NETmix: a pioneering electrochemical flow reactor with enhanced mass transfer, Chem. Eng. J. 481 (2024), https://doi.org/10.1016/j.cej.2023.148244.
[310] F. Hönig, G.D. Rupakula, D. Duque-Gonzalez, M. Ebert, U. Blum, Enhancing the levelized cost of hydrogen with the usage of the byproduct oxygen in a wastewater treatment plant, Energies (Basel) 16 (2023), https://doi.org/10.3390/en16124829.
[311] D. Jing, A.A. Mohammed, A. Kadi, S. Elmirzaev, M.O. Al-Khafaji, M. Marefati, Wastewater treatment to improve energy and water nexus with hydrogen fuel production option: techno-economic and process analysis, Process. Saf. Environ. Prot. 172 (2023) 437–450, https://doi.org/10.1016/j.psep.2023.02.032.
[312] H. Barghash, A. Al Farsi, K.E. Okedu, B.M. Al-Wahaibi, Cost benefit analysis for green hydrogen production from treated effluent: the case study of Oman, Front. Bioeng. Biotechnol. 10 (2022), https://doi.org/10.3389/fbioe.2022.1046556.
[313] C. Cameron, S. McLoone, D.D. Furszyfer Del Rio, D. Rooney, A. Foley, A techno-economic analysis of a co-located wastewater treatment and hydrogen facility, J. Clean. Prod. 421 (2023), https://doi.org/10.1016/j.jclepro.2023.138468.
[314] X. Zhang, M. Schwarze, R. Schomäcker, R. van de Krol, F.F. Abdi, Life cycle net energy assessment of sustainable H2 production and hydrogenation of chemicals in a coupled photoelectrochemical device, Nat. Commun. 14 (2023), https://doi.org/10.1038/s41467-023-36574-1.
[315] M.R. Shaner, H.A. Atwater, N.S. Lewis, E.W. McFarland, A comparative technoeconomic analysis of renewable hydrogen production using solar energy, Energy Environ. Sci. 9 (2016) 2354–2371, https://doi.org/10.1039/c5ee02573g.
[316] A. Grimm, W.A. de Jong, G.J. Kramer, Renewable hydrogen production: a techno-economic comparison of photoelectrochemical cells and photovoltaic-electrolysis, Int. J. Hydrog. Energy 45 (2020) 22545–22555, https://doi.org/10.1016/j.ijhydene.2020.06.092.
[317] V. Prasad, F. Khalid, Solar to sustainability (S2S): a comparative life cycle assessment of hydrogen production with a focus on a photoelectrochemical anion exchange membrane reactor, RSC Sustainability 3 (2025) 4651–4666, https://doi.org/10.1039/d5su00330j.
[318] S. Collins, Y. Acevedo, D.V. Esposito, R. Bala Chandran, S. Ardo, B.D. James, H. Breunig, Levelized cost and carbon intensity of solar hydrogen production via water splitting using a scalable and intrinsically safe photocatalytic Z-scheme raceway system, Energy Environ. Sci. 18 (2025) 6690–6700, https://doi.org/10.1039/d4ee05889e.
[319] S.A.M. Ahmed, P. Nagababu, S. Rayalu, Advancements in solar-powered hydrogen production: a review of concentrated solar power electrolysis, photoelectrochemical, and PV-based electrolysis, Discov. Electrochem. 2 (2025) 68, https://doi.org/10.1007/s44373-025-00080-4.
[320] I. Holmes-Gentle, S. Tembhurne, C. Suter, S. Haussener, Kilowatt-scale solar hydrogen production system using a concentrated integrated photoelectrochemical device, Nat. Energy 8 (2023) 586–596, https://doi.org/10.1038/s41560-023-01247-2.
[321] P. Li, D. Kowalczyk, J. Liessem, M.M. Elnagar, D. Mitoraj, R. Beranek, D. Ziegenbalg, Optimizing reaction conditions for the light-driven hydrogen evolution in a loop photoreactor, Beilstein J. Org. Chem. 20 (2024) 74–91, https://doi.org/10.3762/bjoc.20.9.
[322] S. Ragab, M.R. Elkatory, M.A. Hassaan, A. El Nemr, Experimental, predictive and RSM studies of H2 production using Ag-La-CaTiO3 for water-splitting under visible light, Sci. Rep. 14 (2024), https://doi.org/10.1038/s41598-024-51219-z.
[323] H. Sheng, J. Wang, J. Huang, Z. Li, G. Ren, L. Zhang, L. Yu, M. Zhao, X. Li, G. Li, N. Wang, C. Shen, G. Lu, Strong synergy between gold nanoparticles and cobalt porphyrin induces highly efficient photocatalytic hydrogen evolution, Nat. Commun. 14 (2023), https://doi.org/10.1038/s41467-023-37271-9.
[324] I. Vamvasakis, E.K. Andreou, G.S. Armatas, Mesoporous dual-semiconductor ZnS/CdS nanocomposites as efficient visible light photocatalysts for hydrogen generation, Nanomaterials 13 (2023), https://doi.org/10.3390/nano13172426.
[325] M.M. Atilano-Camino, A. García-González, D.S. Olivo-Alanís, R.B. García-Reyes, Photoreforming of fermentation byproducts by TiO2 and Pt/TiO2 to enhance hydrogen production: insight into a real perspective, J. Environ. Chem. Eng. 12 (2024), https://doi.org/10.1016/j.jece.2024.112017.
[326] M.T.A. Iapichino, R. Fiorenza, V. Patamia, G. Floresta, A. Gulino, M. Condorelli, G. Impellizzeri, G. Compagnini, S. Sciré, H2 production by solar photoreforming of plastic materials using SiC-g-C3N4composites, Catal. Commun. 187 (2024), https://doi.org/10.1016/j.catcom.2024.106850.
[327] C. Shi, Y. An, G. Gao, J. Xue, H. Algadi, Z. Huang, Z. Guo, Insights into selective glucose photoreforming for coproduction of hydrogen and organic acid over biochar-based heterojunction photocatalyst cadmium sulfide/titania/biochar, ACS Sustain. Chem. Eng. 12 (2024) 2538–2549, https://doi.org/10.1021/acssuschemeng.3c04835.
[328] M. Umair, A. Ruiz-Aguirre, I. Berruti, S.M. Rodríguez, L. Palmisano, V. Loddo, M. Bellardita, Biomass derivatives photoreforming in pilot plant scale to obtain H2 under green conditions by using ball milling Cu2O-TiO2 P25 photocatalysts, Chem. Eng. J. 504 (2025), https://doi.org/10.1016/j.cej.2024.158585.
[329] S. Belda-Marco, P. Ayala, S.N. Myakala, D. Eder, M.Á. Lillo-Ródenas, A. Cherevan, M.C. Román-Martínez, Production of H2 and organic acids by cellulose photoreforming with TiO2-bimetallic(CuNi) co-catalysts: metal loading and photodeposition sequence effects, Environ. Res. 271 (2025), https://doi.org/10.1016/j.envres.2025.121141.
[330] L.C. Valencia-Valero, K.A. Simbaña, J.E. Eleraky, M. Hapońska, A. Puga, Demonstration of hydrogen production from food industry wastewaters by solar photoreforming: from the laboratory to outdoors operation in panel reactors, Chem. Eng. J. 510 (2025), https://doi.org/10.1016/j.cej.2025.161636.
[331] M. Muscetta, G. Russo, R. Andreozzi, R. Marotta, G. Palmisano, G. Policastro, M. Race, L. Clarizia, I. Di Somma, Photocatalytic hydrogen production from formic acid over waste derived Au-based catalysts, Sep. Purif. Technol. 377 (2025), https://doi.org/10.1016/j.seppur.2025.134231.
[332] P.P. Falara, M. Antoniadou, A. Zourou, E. Sakellis, K.V. Kordatos, Carbon dot-titanium dioxide (CD/TiO2) nanocomposites: reusable photocatalyst for sustainable H2 production via photoreforming of green organic compounds, Coatings 14 (2024), https://doi.org/10.3390/coatings14010131.
[333] M.C. Herrera-Beurnio, F.J. López-Tenllado, J. Hidalgo-Carrillo, J. Martín-Gómez, R. Estévez, F.J. Urbano, A. Marinas, Glycerol photoreforming for photocatalytic hydrogen production on binary and ternary Pt-g-C3N4-TiO2 systems: a comparative study, Catal. Today 430 (2024), https://doi.org/10.1016/j.cattod.2024.114548.
[334] J.G. Villachica-Llamosas, A. Ruiz-Aguirre, G. Colón, J. Peral, S. Malato, CuO–TiO2 pilot-plant system performance for solar photocatalytic hydrogen production, Int. J. Hydrog. Energy 51 (2024) 1069–1077, https://doi.org/10.1016/j.ijhydene.2023.07.149.
[335] Z. Yin, H. Chen, Q. Wang, Z. Wang, G. Yu, B. Tang, M. Zhang, K. Li, Z. Zhang, Q. Luo, T. Hu, B. Lv, Construction of an interface interaction in a g-C3N4/CdS/NiS for photoreforming of plastic and clean hydrogen regeneration, J. Colloid Interface Sci. 675 (2024) 218–225, https://doi.org/10.1016/j.jcis.2024.06.214.
[336] J. Hu, X. Li, J. Qu, X. Yang, Y. Cai, T. Yang, F. Yang, C.M. Li, Bifunctional honeycomb hierarchical structured 3D/3D ReS2/ZnIn2S4-Sv heterojunction for efficient photocatalytic H2-evolution integrated with biomass oxidation, Chem. Eng. J. 453 (2023), https://doi.org/10.1016/J.CEJ.2022.139957.
[337] Y. Yang, D. Li, J. Cai, H. Wang, C. Guo, S. Wen, W. Li, T. Wang, D. Liu, Y. Yang, D. Li, J. Cai, H. Wang, C. Guo, S. Wen, W. Li, T. Wang, D. Liu, Enhanced photocatalytic hydrogen evolution from organic ternary heterojunction nanoparticles featuring a compact alloy-like phase, Adv. Funct. Mater. 33 (2023) 2209643, https://doi.org/10.1002/ADFM.202209643.
[338] X. Zhang, X. Ma, Y. Ye, C. Guo, X. Xu, J. Zhou, B. Wang, Enhanced photocatalytic hydrogen evolution with a mixed-valence iron metal-organic framework, Chem. Eng. J. 456 (2023) 140939, https://doi.org/10.1016/J.CEJ.2022.140939.
[339] H. Li, X. Liu, Y. He, H. Feng, Y. Zhang, C. Liu, Z. Wu, 2D porphyrin-based MOFs with highly dispersed Pt nanoparticles via in-situ partial reduction strategy from porphyrin embedded with single-atom Pt for enhancing photocatalytic hydrogen production, Fuel 338 (2023) 127369, https://doi.org/10.1016/J.FUEL.2022.127369.
[340] Y. Tang, M. Chen, C. Zhang, H. Li, Y. He, X. Lai, L. Tao, J. Jing, X. Liu, 2D photosensitive porphyrin-based MOFs integrated with a Pd cocatalyst with fast charge transfer for efficient photocatalytic hydrogen evolution, Catal. Sci. Technol. 13 (2023) 5326–5332, https://doi.org/10.1039/D3CY00705G.
[341] L. Liu, S. Du, Y. Xiao, X. Guo, S. Jin, G. Shao, F. Zhang, Saturated Ti-coordinated {001} facets-dependent photocatalytic water reduction over NH2-MIL-125(Ti) sheets: observation and unraveling of facets effect, Appl. Catal. B 338 (2023) 123094, https://doi.org/10.1016/j.apcatb.2023.123094.
[342] T. He, W. Zhen, Y. Chen, Y. Guo, Z. Li, N. Huang, Z. Li, R. Liu, Y. Liu, X. Lian, C. Xue, T.C. Sum, W. Chen, D. Jiang, Integrated interfacial design of covalent organic framework photocatalysts to promote hydrogen evolution from water, Nat. Commun. 14 (1) (2023) 1–11, https://doi.org/10.1038/s41467-023-35999-y.
[343] W. Zhou, Q.W. Deng, H.J. He, L. Yang, T.Y. Liu, X. Wang, D.Y. Zheng, Z. Ben Dai, L. Sun, C. Liu, H. Wu, Z. Li, W.Q. Deng, Heterogenization of Salen metal molecular catalysts in covalent organic frameworks for photocatalytic hydrogen evolution, Angew. Chem. Int. Ed. 62 (2023), https://doi.org/10.1002/ANIE.202214143.
[344] R. Shen, X. Li, C. Qin, P. Zhang, X. Li, Efficient photocatalytic hydrogen evolution by modulating excitonic effects in Ni-intercalated covalent organic frameworks, Adv. Energy Mater. 13 (2023) 2203695, https://doi.org/10.1002/AENM.202203695.
[345] Z. Li, T. Deng, S. Ma, Z. Zhang, G. Wu, J. Wang, Q. Li, H. Xia, S.W. Yang, X. Liu, Three-component donor−π−acceptor covalent−organic frameworks for boosting photocatalytic hydrogen evolution, J. Am. Chem. Soc. 145 (2023) 8364–8374, https://doi.org/10.1021/JACS.2C11893.
[346] S. Bao, Q. Tan, S. Wang, J. Guo, K. Lv, S.A.C. Carabineiro, L. Wen, TpBD COF@ZnIn2S4 nanosheets: a novel S-scheme heterojunction with enhanced

photoreactivity for hydrogen production, Appl. Catal. B 330 (2023) 122624, https://doi.org/10.1016/J.APCATB.2023.122624.
[347] X. Chi, Q. Chen, Z.-A. Lan, X. Zhang, X. Chen, X. Wang, Structure–property relationship of cyano-functionalized conjugated polymers for photocatalytic hydrogen production, Chem. Eur. J. 29 (2023) e202202734, https://doi.org/10.1002/chem.202202734.
[348] H. Gu, H. Zhang, X. Wang, Q. Li, S. Chang, Y. Huang, L. Gao, Y. Cui, R. Liu, W. L. Dai, Robust construction of CdSe nanorods@Ti3C2 MXene nanosheet for superior photocatalytic H2 evolution, Appl. Catal. B 328 (2023), https://doi.org/10.1016/j.apcatb.2023.122537.
[349] C. Zhang, H. Li, Y. Zhang, Y. Wang, Q. Liang, M. Zhou, S. Xu, Z. Li, Bifunctional synergistic S-scheme Mn0.25Cd0.75S/honeycomb-like g-C3N4 heterojunction for efficient photocatalytic H2 evolution integrated with amoxicillin degradation, Chem. Eng. J. 476 (2023), https://doi.org/10.1016/j.cej.2023.146494.
[350] W. Peng, L. Xiaolei, F.U. Hui, H. Baibiao, W. Zeyan, L. Yuanyuan, Z. Zhaoke, C. Hefeng, Z. Qianqian, Z. Xiaoyang, System and Method for Realizing Pure Water Decomposition by Photocatalysis-Electrocatalysis Coupled Iodine Cycle, CN116216633A, 2023.
[351] L.U. Yanhong, W. Xi, Y.E. Zhantong, Z. Suling, Z. Shengyan, Composite Photocatalyst, Preparation Method Thereof and Hydrogen Production Method, CN119303603A, 2024.
[352] J. Yi, Z. Hongshuai, X. Lixin, BN/CdS Photocatalyst, Preparation Method Thereof and Application of BN/CdS Photocatalyst in Photocatalytic Hydrogen Production, CN119733542A, 2025.
[353] W. Hongmei, G. Qiqi, G. Liping, C. Shijin, L. Zhufeng, Bimetal Sulfide-based Photocatalyst, Preparation Method and Application Thereof in Hydrogen Production Coupling Plastic Degradationg, CN119771447A, 2025.
[354] L.I. Yanqiu, C. Zhenqian, Z. Zhen, X. Wang, Z. Peng, CdS@ MoS2 Photocatalyst, Preparation Method Thereof and Application of CdS@ MoS2 Photocatalyst in Biomass Reforming Hydrogen Production, CN119327487A, 2025.
[355] J. Yi, Z. Hongshuai, X. Lixin, Indium Zinc Sulfide-based Composite Catalyst, Preparation Method Thereof and Application of Indium Zinc Sulfide-based Composite Catalyst in Photocatalytic Hydrogen Production, CN119733531A, 2025.
[356] N. Xiaowei, Y. Zexi, H. Jiayi, L. Xing, Y. Ting, Q. Yitong, Q. Nana, J. Zhang, Preparation Method of Composite Photocatalytic Hydrogen Production Material MoO3/CuO, CN117463354A, 2023.
[357] L. Guigao, T. Qingshan, J. Wei, Application of CdS-Ru Photocatalyst in Hydrogen Production Through Photocatalytic Reforming of Biomass, CN118002153A, 2024.
[358] H. Wenwen, S. Wangwang, J. Fang, Z. Tao, L. Menglong, Preparation Method of NiS-Coated MOF-808 Composite Material for Photocatalytic Hydrogen Production, CN117427690A, 2023.
[359] Y.E. Jianfeng, W.U. Jin, Y.E. Xiaozhou, Y. Wang, Modified ZnO Photocatalyst and Application Thereof in Photocatalytic Hydrogen Production, CN118807814A, 2024.
[360] Z. Liyi, L. Yanchu, C. Yu, Metal Organic Framework Material, Ligand Thereof and Application of Metal Organic Framework Material in Photocatalytic Hydrogen Production, CN116425996A, 2023.
[361] A. Yang, J. Weiyi, W. Lingling, L. Xinling, P. Huan, MOF TiO2-NiO Material for Producing Hydrogen through Efficient Water Photolysis As Well as Preparation Method and Application of MOF TiO2-NiO Material, CN114950439A, 2022.
[362] P. Yunhong, W. Tiejun, L. Wenting, L. Jianxian, Z.-C. Ziyu, Z. Baofang, MIL-68 (in) Derived Heterojunction Catalyst With Hollow Structure As Well as Preparation Method and Application of MIL-68 (in) Derived Heterojunction Catalyst, CN117065767A, 2023.
[363] X. Xinguo, W. Yan, D. Pengyu, Z.-A. Caijun, C. Ting, Method for Preparing Photocatalyst With Monatomic Pt Embedded Into Covalent Organic Framework and Application of Photocatalyst, CN114534783A, 2022.
[364] L. Liuyi, L. Chentao, W. Lanshun, Y. Yan, Biphenyl Covalent Organic Framework Copper-loaded Material, Preparation Method Thereof and Application Thereof in Photocatalytic Hydrogen Production, CN113856763A, 2021.
[365] H. Qing, H. Feini, W. Haozhen, Triazinyl Covalent Organic Framework Material for Producing Hydrogen by Efficiently Decomposing Water With Visible Light and Preparation Method of Triazinyl Covalent Organic Framework Material, CN116425935A, 2023.
[366] L. Liuyi, C. Yanlei, Y. Yan, Preparation of Benzotrithienyl Covalent Organic Photocatalytic Material Connected with Dipyridyl Group and Application of Benzotrithienyl Covalent Organic Photocatalytic Material in Photocatalytic Full-Decomposition of Water, CN115646545A, 2023.
[367] S. Yaorong, H. Peigang, Preparation Method of g-C3N4-based P-N Homojunction Photocatalyst and Preparation Method of Hydrogen, CN112354553B, 2023.